

# LONG-TERM SPECTROSCOPIC SURVEY OF THE PLEIADES CLUSTER: THE BINARY POPULATION

GUILLERMO TORRES, DAVID W. LATHAM, AND SAMUEL N. QUINN

Center for Astrophysics | Harvard & Smithsonian, 60 Garden St., Cambridge, MA 02138, USA; gtorres@cfa.harvard.edu

*Accepted for publication in The Astrophysical Journal*

## ABSTRACT

We present the results of a spectroscopic monitoring program of the Pleiades region aimed at completing the census of spectroscopic binaries in the cluster, extending it to longer periods than previously reachable. We gathered 6104 spectra of 377 stars between 1981 and 2021, and merged our radial velocities with 1151 measurements from an independent survey by others started three years earlier. With the combined data spanning more than 43 yr we have determined orbits for some 30 new binary and multiple systems, more than doubling the number previously known in the Pleiades. The longest period is 36.5 yr. A dozen additional objects display long-term trends in their velocities, implying even longer periods. We examine the collection of orbital elements for cluster members, and find that the shape of the incompleteness-corrected distribution of periods (up to  $10^4$  days) is similar to that of solar-type binaries in the field, while that of the eccentricities is different. The mass-ratio distribution is consistent with being flat. The binary frequency in the Pleiades for periods up to  $10^4$  days is  $25 \pm 3\%$ , after corrections for undetected binaries, which is nearly double that of the field up to the same period. The total binary frequency including known astrometric binaries is at least 57%. We estimate the internal radial velocity dispersion in the cluster to be  $0.48 \pm 0.04 \text{ km s}^{-1}$ . We revisit the determination of the tidal circularization period, and confirm its value to be  $7.2 \pm 1.0$  days, with an improved precision compared to an earlier estimate.

## 1. INTRODUCTION

Radial velocity (RV) studies of stars in the Pleiades cluster have been carried out for well over a century, predating the classical proper motion studies that were central to establishing the cluster's membership (e.g., Trumpler 1921; Hertzsprung 1947; Artyukhina 1969). The earliest attempt to measure radial velocities in the Pleiades seems to be that of Pickering (1896), who reported only briefly that observations with an objective prism suggested the relative motions of the seven brightest members in the group probably do not exceed  $30 \text{ km s}^{-1}$ . Other, more successful efforts in the first few years of the 20th century include those of Adams (1904), Jung (1914), and Hartmann (1914). Since then, numerous investigations of increasing measurement precision have been made to establish the mean velocity of the cluster and its internal dispersion, to aid in revealing its structure, and to search for spectroscopic binaries. Radial-velocity studies addressing one or more these issues include those by Frost et al. (1926), Smith & Struve (1944), Abt et al. (1965), Pearce & Hill (1975), Liu et al. (1991), Morse et al. (1991), and Mermilliod et al. (2009), among others.

Naturally, the earlier studies focused on the brighter stars in the Pleiades, which are of spectral type B. Those happen to be the more difficult objects because their spectral lines are usually broadened due to rapid rotation, resulting in poor velocity precision. Velocities for later-type stars of spectral type A and F only began to appear with the work of Smith & Struve (1944), which, like most subsequent programs, ran for only one or two years or gathered relatively few observations per star. It is not surprising, then, that no spectroscopic binaries in the Pleiades were known until the late 1950's, when the first one was discovered: the double-lined system HD 23642 (Pearce 1958; Abt 1958), which is now

known to be eclipsing (Miles 1999; Torres 2003). More extensive studies designed to look for spectroscopic binaries among the B, A, and F stars were undertaken by Abt et al. (1965) and Pearce & Hill (1975). Altogether they reported spectroscopic orbits for eight objects, although unfortunately five of them have been shown to be spurious (see Torres 2020) and two others are non-members. The challenging history of binary discovery in the Pleiades up to that time is attributable to the difficulty of the measurements, as even stars as late as mid F can still rotate quite rapidly in the cluster, up to  $100 \text{ km s}^{-1}$  in some cases. One other spectroscopic binary, HD 23631, was reported by Conti (1968), and is a metallic-line star, so its rotation is relatively slow.

Significant progress came with the long-term observing program carried out by J. C. Mermilliod and collaborators (Rosvick et al. 1992; Mermilliod et al. 1992a, 1997; Raboud & Mermilliod 1998; Mermilliod et al. 2009), which ran for 20 years between the beginning of 1978 and the end of 1997. This study used the northern CORAVEL instrument (Baranne et al. 1979) on the Swiss 1m telescope at the Haute-Provence Observatory (France), and observed some 270 stars of spectral type F5–K0, complementing earlier efforts that had focused on the hotter objects.<sup>1</sup> The CORAVEL program led to the discovery and characterization of about a dozen new spectroscopic binaries with orbital periods up to about two years.

An independent, long-term radial-velocity monitoring program at the Center for Astrophysics (CfA) has been running for 39 years, beginning in 1982, and is ripe for analysis. It is the subject of this paper. It overlaps sub-

<sup>1</sup> A second CORAVEL instrument was installed on the Danish 1.54m telescope at La Silla Observatory (Chile), but was not used to observe the Pleiades. All references to CORAVEL in this paper will be understood hereafter to refer to the northern instrument.

stantially both in time and in the sample of targets with the CORAVEL effort, but continued for more than 20 years after the end of those observations. It was designed to complete the census of short-period binaries in the Pleiades that may have been missed by earlier studies, and to extend the coverage to much longer orbital periods, reaching into the regime in which some of them could be spatially resolved by imaging techniques. This could enable dynamical mass measurements that are exceedingly rare in the cluster. The sample of stars observed at the CfA is also larger (roughly 380 objects) and covers a wider range of spectral types than earlier studies, from mid-B to early M. As we report below, the survey more than doubles the number of known spectroscopic binaries in the cluster with orbital solutions, several of them benefiting from the addition of the CORAVEL velocities, which are of similar precision as ours. Indeed, the combined CfA and CORAVEL data sets, which span more than 43 years, permit a more comprehensive study of the binary population in the Pleiades, including a re-determination of the binary frequency, the distribution of orbital elements, the internal velocity dispersion in the cluster, and a more robust determination of the tidal circularization period. In this work we will therefore merge the two samples together, with the goal of addressing all of these issues.

Most of the early-type stars of spectral type B and A on the CfA observing list are rotating too rapidly for the standard cross-correlation techniques that we apply in this work to yield meaningful RVs. For this reason, results for 33 of those stars based on a different methodology for measuring velocities have been published separately (Torres 2020), and include the discovery of three new spectroscopic binaries with orbital solutions reported in that work. Nevertheless, these early-type stars are part of the original sample, so they will be included in portions of the analysis in this paper, which we have organized as follows.

In Section 2 we describe the CfA sample and how it was assembled, and discuss membership in the cluster. We also summarize the properties of the CORAVEL sample that we incorporate into the subsequent analysis. The spectroscopic observations and techniques for radial velocity determination are described in Section 3, and in Section 4 we present our effective temperature and projected rotational velocity estimates for all stars. The derivation of orbital elements for the spectroscopic binaries and the discussion of a few triple systems is found in Section 5. It is followed by a description of systems that only show long-term trends, and additional binaries with orbital elements published by others (Sections 6 and 7). The next two sections discuss our criteria for radial velocity variability and our detection completeness. Then in Section 10 we analyze the distributions of orbital periods, eccentricities, and mass ratios for the binaries with orbits. With the larger number of binaries resulting from this work, Section 11 discusses the binary frequency in the cluster, comparing it with estimates in other populations. Astrometric binaries among the stars in our sample are reported in Section 12, and in Section 13 we use the collection of RVs to redetermine the mean velocity of the cluster, and for a detailed study of the internal velocity dispersion. Section 14 then revisits the eccentricity versus log period diagram in the Pleiades, which

is a powerful indicator of the effectiveness of tidal forces in binaries. The prospects for mass determinations for the binaries in the Pleiades using astrometric information that will be available at the conclusion of the Gaia mission are discussed in Section 15. We summarize our findings in Section 16.

## 2. SAMPLE SELECTION

The list of targets for the CfA survey of the Pleiades area was drawn initially from an unpublished catalog of proper motion members and suspected members assembled by John Stauffer and Charles Prosser at the Center for Astrophysics, which was in turn compiled from various classical sources (Hertzsprung 1947; Artyukhina 1969; Haro et al. 1982; van Leeuwen et al. 1986). This list evolved over time to include more confirmed members from other sources (Jones 1981; Stauffer et al. 1991; Prosser et al. 1991; Stauffer et al. 2007; Kamai et al. 2014) in order to improve completeness down to about  $V = 14$ , which was considered the practical limit given the telescopes available for this work. Brighter stars of spectral type B that are typically rotating very rapidly were added later, when it was realized that the more advanced instrumentation described below that we began using in 2009 would allow meaningful velocities to be determined. The final sample of 377 stars covers the spectral type range from mid B to early M, and an area of roughly  $10^\circ \times 10^\circ$  on the sky. While we cannot claim completeness down to  $V = 14$  because our sample relies on a number of external sources of candidate members consulted over the years, we are not aware of any selection biases against stars of a specific spectral type (i.e., mass). We list all targets in Table 1, with SIMBAD identifiers, coordinates, and other information extracted from the Gaia EDR3 catalog (Fabricius et al. 2020). The 33 early-type stars whose velocities have been reported in a separate publication are flagged with a “b” in the table.

### 2.1. Membership

The original selection of the stars in the CfA sample (including the early-type stars) was based largely on proper motion and other information to establish membership, but was made without the benefit of the much more precise astrometry now available from the Gaia mission. We therefore expected that a reevaluation at this time would reveal that a subset of our targets are not actual cluster members. This is borne out by the velocity measurements presented later, which deviate significantly in a number of cases from the cluster’s mean velocity of about  $5.7 \text{ km s}^{-1}$ . For a better assessment of whether our stars belong to the Pleiades, we initially relied on the list of probable members from the Gaia team (Gaia Collaboration et al. 2018b), which was assembled from parallax and proper motion information from the second data release (DR2), but without making use of radial velocities. As with any membership list, there is always the possibility that it is both contaminated and incomplete to some degree.<sup>2</sup> We find that 229 of our

<sup>2</sup> A detailed investigation of Pleiades membership based on the more recent early third data release (EDR3) of Gaia (Fabricius et al. 2020) has not yet been made as of this writing, and is outside the scope of this paper. However, we do not expect it to be radically different from DR2, as the proper motions and parallaxes are quite similar, only more precise in EDR3.

**Table 1**  
List of Objects in the Pleiades Region Observed Spectroscopically at the CfA.

	Name	R.A. (degree)	Dec. (degree)	Gaia ID	$G$ (mag)	$\pi_{\text{Gaia}}$ (mas)	$\mu_{\alpha} \cos \delta$ (mas yr $^{-1}$ )	$\mu_{\delta}$ (mas yr $^{-1}$ )	Mem
1	AK III-31	51.88537	+25.89995	117280133627745280	9.05	$13.737 \pm 0.021$	$+16.513 \pm 0.023$	$-29.410 \pm 0.020$	NM
2	PELS 121	51.92529	+23.80351	68711956249760768	10.13	$5.237 \pm 0.015$	$+4.479 \pm 0.016$	$-35.678 \pm 0.013$	NM
3	PELS 1	52.06861	+22.64106	61842035801405824	10.41	$2.281 \pm 0.049$	$+15.006 \pm 0.050$	$-24.159 \pm 0.042$	NM
4	AK III-59	52.16877	+25.60767	69221506874062720	11.51	$6.334 \pm 0.020$	$+24.659 \pm 0.025$	$-28.865 \pm 0.018$	NM
5	AK III-79	52.35599	+25.65215	69595035885590144	9.33	$7.318 \pm 0.017$	$+31.053 \pm 0.019$	$-26.596 \pm 0.016$	NM
6	AK III-158	52.80562	+26.43951	69659730977217792	9.12	$10.624 \pm 0.021$	$+15.011 \pm 0.025$	$-50.421 \pm 0.017$	NM
7	AK III-153	52.81658	+25.25526	69335619861034752	8.09	$7.617 \pm 0.033$	$+22.625 \pm 0.037$	$-46.757 \pm 0.025$	b

**Note.** — ICRS coordinates, source identifiers,  $G$ -band magnitudes, parallaxes, and proper motion components are extracted from the Gaia EDR3 catalog. Objects that are not considered members of the cluster are indicated with “NM” in the last column (see Section 2.1). Early-type stars in the group of 33 with spectroscopic results reported previously (Torres 2020) are indicated with a “b” in the last column. (This table is available in its entirety in machine-readable form.)

377 stars are included in that list. Two of them (HII 5 and HCG 258) have high-quality astrometry and no indication that they are binaries, but their radial velocities are several  $\text{km s}^{-1}$  lower than the cluster mean, and their parallax and p.m. are at the very edges of the distributions for the cluster. We have therefore chosen to consider them as non-members.

Conversely, 148 of our targets have no entries in the Gaia membership list, and this includes such well known bona fide members in our sample as Electra (HII 468), Taygeta (HII 563), and Maia (HII 785). The explanation for these particular cases is that their extreme brightness has seriously impacted the precision of their astrometry, and kept them off the Gaia list. For about half of the 148 stars missing in that list, the astrometry and/or our radial velocity measurements clearly indicate they are non-members. Of the remaining half, six have no parallax or p.m. measurements in the Gaia EDR3 catalog, but their RVs are consistent with membership, so we have tentatively retained them as members. For many of the others the parallax or p.m. deviations are such that the choice is not clear, although there is reason to believe their astrometry may be compromised, causing them to have been excluded as members in the Gaia team’s analysis. For example, a quantity known as the renormalized unit weight error (RUWE) is advocated as a robust statistical indicator of the quality of the astrometric fit, with values in the range 1–1.4 generally being considered acceptable (see, e.g., Lindegren 2018). Taking the RUWE values from Gaia EDR3, we find a median of  $\text{RUWE} = 1.72$  for the stars in our sample that are not in the Gaia membership list, versus 1.08 for the ones that are. One possible reason for the inflated RUWE values is unrecognized binarity, and in fact we have found that several dozen of the stars not on the list of Gaia members are either spectroscopic binaries, many with long orbital periods, or else they have close visual companions. We give these stars the benefit of the doubt, and do not exclude them as members if their radial velocity is within  $2 \text{ km s}^{-1}$  of the expected value. Most of the other missing objects have astrometry consistent with membership, once we allow for the observed trend between the parallaxes and the p.m. components illustrated in Figure 6 of Gao (2019). That trend is the result of Gaia being able to resolve the depth of the cluster along the line of sight (the depth is slightly less than 1/10 of its distance).

All in all, we flagged 68 of the objects in the CfA sample as non-members, and consider another four to be

doubtful, but still possible members (MT 41, HII 1653, TRU S177, and AK V-198). This leaves 309 stars out of our original sample of 377 that we consider to be members or possible members. The non-members and doubtful members are marked as such in Table 1. The location of the members in the color-magnitude diagram of the cluster is shown in Figure 1, along with a 125 Myr solar-metallicity model isochrone from the PARSEC 1.2S series (Chen et al. 2014). The bottom panel shows the distribution of estimated stellar masses.

The CORAVEL program in the Pleiades observed a total of about 270 stars, and included many objects in the outer regions of the cluster that had previously been proposed as possible members, but which had never been observed spectroscopically. Not surprisingly, a good fraction of those turned out to be non-members based on the CORAVEL radial velocities or other information, and we have verified those assessments using the parallaxes and proper motions now available from Gaia EDR3. A total of 178 CORAVEL objects remain as members, of which all but two (PELS 30 and PELS 39) were also observed at the CfA. For completeness, we have chosen to add these two objects to our sample for the analysis of the binary population in the cluster in later sections of the paper.

### 3. OBSERVATIONS

Spectroscopic monitoring of the Pleiades region at the CfA began in December of 1981, and was carried out with four instrument/telescope combinations. From that initial date until February of 2009, spectra were gathered with three nearly identical copies of the Digital Speedometer (Latham 1992a). They were attached to the 1.5m Tillinghast reflector at the Fred L. Whipple Observatory on Mount Hopkins (AZ), the now closed 1.5m Wyeth reflector at the Oak Ridge Observatory (MA), and the 4.5m-equivalent MMT also on Mount Hopkins, before its conversion to a monolithic 6.5m telescope. The Digital Speedometers had a resolving power of  $R \approx 35,000$ , and were equipped with photon-counting Reticon detectors that limited the recorded output to a single echelle order about  $45 \text{ \AA}$  wide, centered on the Mg Ib triplet near  $5187 \text{ \AA}$ . The signal-to-noise ratios (S/N) of the 2441 usable spectra obtained at the three telescopes range from 5 to about 100 per resolution element of  $8.5 \text{ km s}^{-1}$ , although at the higher levels the limitation is systematics in the flatfield corrections rather than photon noise. Reduction procedures have been described by Latham (1985, 1992a).

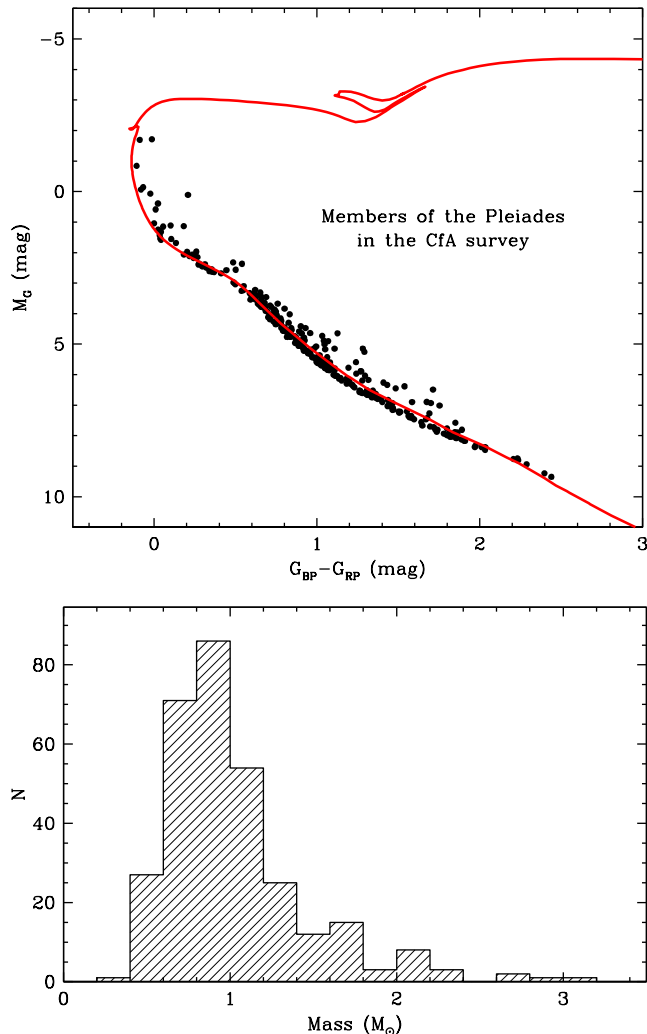


**Figure 1.** *Top:* Absolute  $G$ -band magnitude as a function of  $G_{BP} - G_{RP}$  color from the Gaia EDR3 catalog for the Pleiades members in our sample. Also shown is a 125 Myr isochrone from the PARSEC 1.2S series of Chen et al. (2014) for solar metallicity ( $Z = 0.0152$  in these models). Interstellar extinction has been applied to the isochrone based on an assumed average reddening of  $E(B - V) = 0.04$ . The  $M_G$  values rely on the individual parallax of each star. *Bottom:* Histogram of stellar masses, estimated from the  $G_{BP} - G_{RP}$  colors and the same isochrone as above.

The stability of the velocity zero-point of each of these three instruments was monitored by taking sky exposures at dusk and dawn, and applying small velocity corrections to the raw velocities from run to run that were typically smaller than  $2 \text{ km s}^{-1}$  (see Latham 1992a). With these corrections the velocities from the three telescopes were placed on the same native CfA system, which is slightly offset from the IAU system by  $0.14 \text{ km s}^{-1}$  (Stefanik et al. 1999), as determined from observations of minor planets in the solar system. To remove this shift, a correction of  $+0.14 \text{ km s}^{-1}$  has been added to all our raw velocities from the Digital Speedometers.

Beginning in October of 2009, further observations were collected with the Tillinghast Reflector Echelle Spectrograph (TRES; Fűrész 2008; Szentgyorgyi & Fűrész 2007) on the 1.5m Tillinghast reflector. This is a modern, bench-mounted, fiber-fed spectrograph delivering a resolving power of  $R \approx 44,000$ , with a CCD detector that records 51 echelle orders between

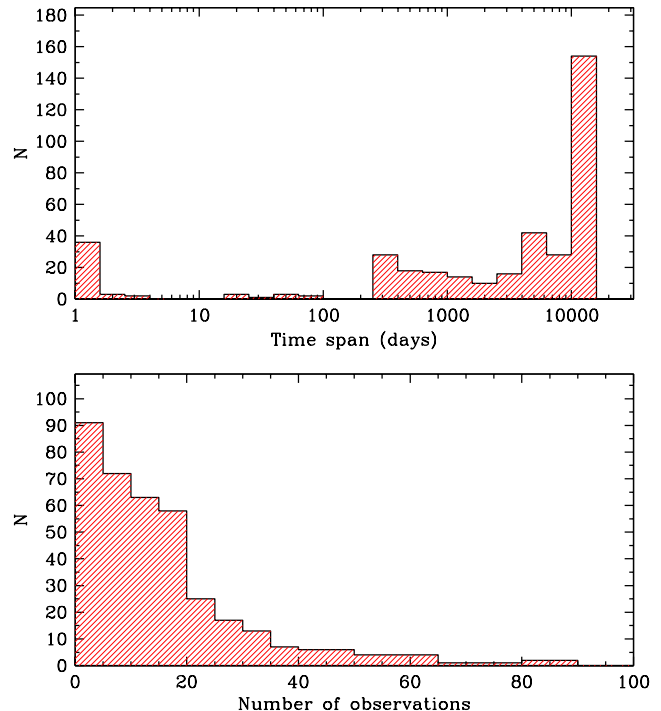


**Figure 2.** Histograms of the time span and number of spectra per object for the 377 targets in the CfA survey of the Pleiades. 3800–9100 Å. We gathered 3663 spectra with this instrument through the end of the 2020/2021 observing season, with S/N ranging between 5 and 500 per resolution element of  $6.8 \text{ km s}^{-1}$ . Reductions were performed with a dedicated pipeline (see Buchhave et al. 2012). Observations of IAU standard stars were made each run to monitor changes in the velocity zero-point of TRES. This was done by cross-correlating the spectra of each standard against a high-S/N observation of the same star. Observations of asteroids were then used to translate the raw TRES velocities to an absolute system, as done with the Digital Speedometers.

The distribution of the time span and number of observations for each target are seen in Figure 2. About 40% of our stars have observations that span 30 yr or more, and for 60% of the sample the coverage exceeds 10 yr.

### 3.1. Radial Velocities

Radial velocities for all except the early-type stars treated separately were obtained by cross-correlation using the XCSAO task running under IRAF.<sup>3</sup> This procedure also reports an internal RV error estimate for each measurement that is a function of the properties of the cross-correlation peak (see Kurtz & Mink 1998). For the TRES instrument, we used only the order centered on the Mg Ib triplet so as to match the spectral region of the Digital Speedometers. Templates were taken from a pre-computed library of calculated spectra based on model atmospheres by R. L. Kurucz, and a line list tuned to better match real stars (see Nordström et al. 1994; Latham et al. 2002). The templates are available over wide ranges in effective temperature ( $T_{\text{eff}}$ ), rota-

<sup>3</sup> IRAF is distributed by the National Optical Astronomy Observatory, which is operated by the Association of Universities for Research in Astronomy (AURA) under a cooperative agreement with the National Science Foundation.



tional broadening ( $V_{\text{rot}}$ ), metallicity ( $[m/H]$ ), and surface gravity ( $\log g$ ). Gaussian broadening was applied to match the resolution of each instrument. The optimal synthetic template for each star was derived as described by Torres et al. (2002). Briefly, this involved running grids of correlations over wide intervals for the template parameters, and selecting the ones providing the largest cross-correlation coefficient averaged over all exposures. We assumed  $[m/H] = 0.0$ , as the composition of the Pleiades is very near solar (e.g., Taylor 2008; Soderblom et al. 2009; Schuler et al. 2010; Netopil et al. 2016), and  $\log g = 4.5$ , which is appropriate for the vast majority of our stars.

Velocities for double-lined binaries were measured with TODCOR (Zucker & Mazeh 1994), a two-dimensional cross-correlation technique that uses two templates, one for each component. There is one triple-lined object in our sample (HII 1338), and for this target we used TRICOR, which is an extension of TODCOR to three dimensions (Zucker et al. 1995). The selection of templates for double- and triple-lined systems followed the general procedure described before. TODCOR and TRICOR also yield the light ratios among the components, which we report below in Section 5.

Because of the limited number of lines in the narrow spectral region recorded with the Digital Speedometers (45 Å), systematic errors in the velocities for double-lined binaries can occur as lines of the components shift in and out of the window in opposite directions at different orbital phases. Experience has shown that the effect can be several  $\text{km s}^{-1}$  in some cases, but is negligible for TRES, which has more than twice the spectral coverage (100 Å). We corrected these velocity errors by performing numerical simulations, as described by Latham et al. (1996). See also Torres et al. (1997).

For single-lined objects with sharp lines and spectral type similar to the Sun, typical internal velocity precisions reported by XCSAO are about  $0.5 \text{ km s}^{-1}$  for the Digital Speedometers, and  $\sim 0.15 \text{ km s}^{-1}$  for TRES using the Mg Ib order and the templates described above. We note that TRES is capable of significantly better velocity precision for certain applications such as exoplanet follow-up, in which absolute velocities are typically not needed. One can then take advantage of the full wavelength coverage afforded by the instrument, by cross-correlating multiple echelle orders against a spectrum of the same star used as a template, to measure relative velocities. For the present work, however, we require absolute velocities, so we have chosen to use synthetic templates and the single Mg Ib order, which is rich in RV information. This is sufficient for our purposes, given that we expect many of the Pleiades stars to exhibit activity-driven apparent variations of at least many tens of  $\text{m s}^{-1}$  by virtue of the young age of the cluster. Moreover, rapid rotation is also common among these stars, which will further degrade the precision. Figure 3 shows how the errors increase as the stars rotate more rapidly, reaching  $3\text{--}4 \text{ km s}^{-1}$  at  $V_{\text{rot}} \approx 100 \text{ km s}^{-1}$ .

Individual heliocentric radial velocities on the IAU system are listed for all single-lined objects in Table 2,<sup>4</sup>

<sup>4</sup> We exclude from this table the velocities for HII 2147, which were published separately by Torres et al. (2020), as well as those for the 33 rapidly-rotating stars reported by Torres (2020).

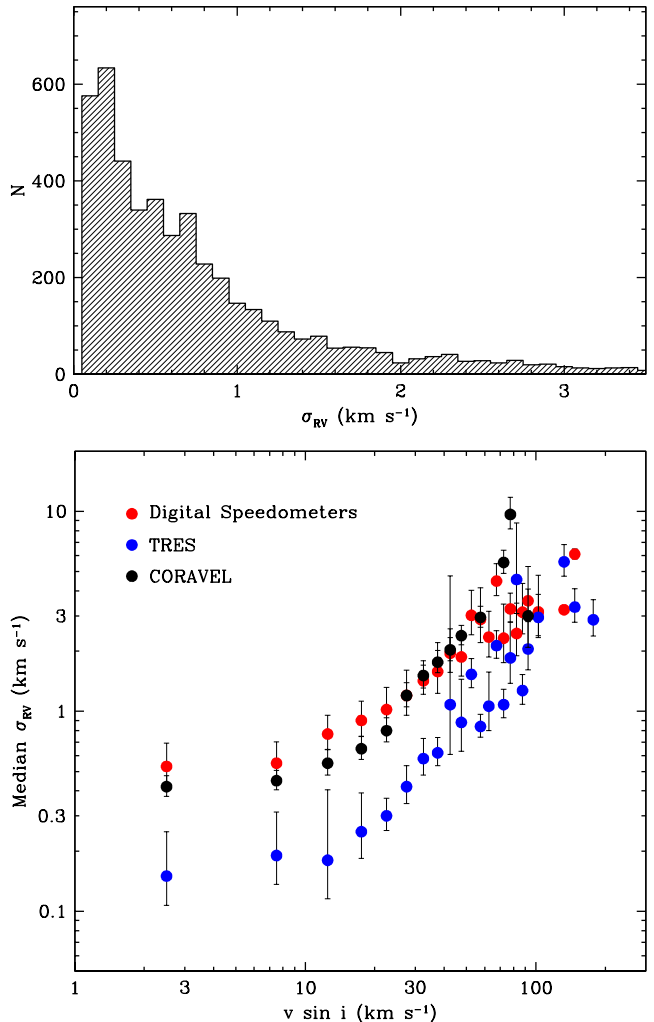


**Figure 3.** *Top:* Distribution of the individual internal radial velocity uncertainties for stars with single-lined spectra observed at the CfA, as reported by the IRAF task XCSAO. *Bottom:* Radial velocity precision for the Digital Speedometers, TRES, and CORAVEL as a function of rotational broadening (see Section 4), in bins of  $5 \text{ km s}^{-1}$ . The points show the median of each bin, with error bars calculated as half of the interquartile range.

and for double-lined binaries (SB2s) in Table 3. The latter table incorporates the corrections for systematics mentioned above for all velocity measurements from the Digital Speedometers. Both tables also list the RV uncertainties, and the S/N of each exposure. Statistics for the 377 objects in the sample are presented in Table 4, and include the time span, the number of observations from the Digital Speedometers and TRES, the weighted average velocity and corresponding uncertainty (including the CORAVEL measurements; see below), and other information described later.

As indicated before, the CORAVEL observations have similar uncertainties as ours (see Figure 3), and several of the binary orbital solutions presented below in Section 5 are helped by including those velocities. Most of those measurements appeared in original form in a series of papers over a period of seven years (Rosvick et al. 1992; Mermilliod et al. 1992a, 1997; Raboud & Mermilliod 1998), and the final catalog of Pleiades velocities from the CORAVEL team that included additional measurements was published later by

**Table 2**

CfA Radial Velocity Measurements for Single-lined Objects.

Name	HJD (2,400,000+)	RV (km s <sup>-1</sup> )	S/N	Inst
PELS 121	52497.8622	5.67 ± 0.50	11	1
PELS 121	52529.8427	6.32 ± 0.75	11	1
PELS 121	52583.7015	5.59 ± 0.52	10	1
PELS 121	56672.6857	5.60 ± 0.09	54	2
PELS 121	56977.8214	5.60 ± 0.13	40	2

**Note.** — The heliocentric radial velocities are on the reference frame of the minor planets in the Solar System (see Stefanik et al. 1999). Signal-to-noise ratios in the S/N column are per resolution element. Codes in the Inst column are 1 for the Digital Speedometers and 2 for TRES. HII 2147 and rapidly-rotating early type stars are not included, as their velocities have been published separately by Torres et al. (2020) and Torres (2020), respectively. (This table is available in its entirety in machine-readable form.)

**Table 3**

CfA Radial Velocity Measurements for Double-lined Objects.

Name	HJD (2,400,000+)	RV <sub>1</sub> (km s <sup>-1</sup> )	RV <sub>2</sub> (km s <sup>-1</sup> )	S/N	Inst
AK III-31	45695.6647	48.32 ± 1.31	-66.64 ± 15.84	9	1
AK III-31	45711.6059	-7.39 ± 1.49	20.72 ± 18.11	8	1
AK III-31	45757.4924	-47.10 ± 1.15	98.40 ± 13.93	10	1
AK III-31	52879.8425	-11.59 ± 0.85	25.42 ± 10.33	14	1
AK III-31	52921.8160	52.62 ± 0.85	-78.92 ± 10.33	14	1

**Note.** — The heliocentric radial velocities are on the reference frame of the minor planets in the Solar System (see Stefanik et al. 1999). Signal-to-noise ratios in the S/N column are per resolution element. Codes in the Inst column are 1 for the Digital Speedometers and 2 for TRES. (This table is available in its entirety in machine-readable form.)

Mermilliod et al. (2009). The first three of the original sources described how they adjusted the RV measurements for zero-point differences to place them on the reference frame defined by Mayor & Maurice (1985), which corresponds to the faint IAU standard system ( $V > 4.3$ ; see Stefanik et al. 1999). The study of Raboud & Mermilliod (1998) did not specify the zero-point, but indicated that the entire CORAVEL data set was in the process of being recalibrated for zero-point errors and color effects. By the time of the publication by Mermilliod et al. (2009), the recalibration had been completed and the full set of Pleiades velocities was placed on the system defined by Udry et al. (1999), based on more precise observations of IAU standards with a different instrument (ELODIE; Baranne et al. 1996). The velocities of Mermilliod et al. (2009) supersede and sometimes augment those in the original sources, and are systematically higher by 0.3–0.5 km s<sup>-1</sup>. The total number of CORAVEL measurements incorporated into our analysis in this paper is 1151. When added to our own 6104 observations from TRES and the Digital Speedometers, this brings the total number of individual radial-velocity epochs to 7255.

A comparison between the mean CORAVEL and CfA velocities for 129 stars in common that are not known to be binaries, and have 3 or more measurements in each data set, indicates a systematic difference of only  $\text{CORAVEL} - \text{CfA} = +0.031 \pm 0.041$  km s<sup>-1</sup>, with a standard deviation of 0.46 km s<sup>-1</sup> (see Figure 4). There is

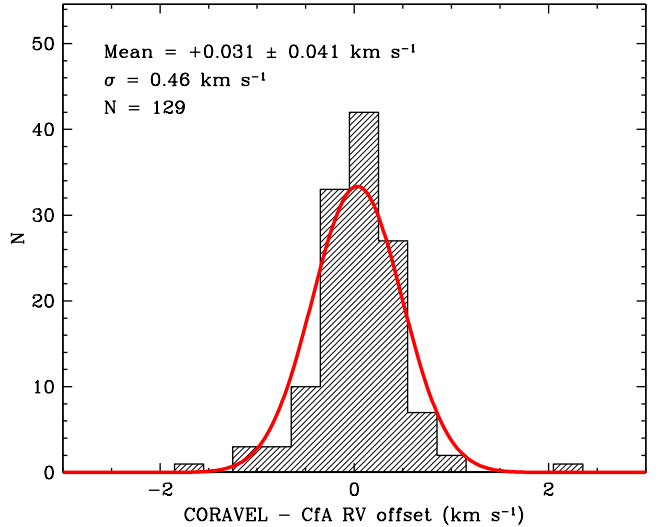


**Figure 4.** Differences between the weighted mean velocities from CORAVEL and CfA for 129 stars in common that are not known to be binaries, and have 3 or more measurements each. Two outliers greater than 4 km s<sup>-1</sup> in absolute value have been removed, as they may be previously unrecognized binaries. The curve represents a Gaussian fit.

no significant dependence of the differences on either effective temperature or rotational velocity. Given the excellent agreement in the zero-points, we proceed below to combine the data with no further adjustments. The number of CORAVEL observations for each star is indicated in Table 4.

#### 4. EFFECTIVE TEMPERATURES AND ROTATIONAL VELOCITIES

In the process of selecting the best synthetic template for the cross-correlations, we made an estimate of the effective temperature and projected rotational velocity of each star to a finer resolution than the sampling of our library of templates, which is 250 K in temperature and is variable in  $V_{\text{rot}}$  (smaller steps for slow rotators, increasing for fast rotators). We did this by interpolating among neighboring templates independently for the spectra from the Digital Speedometers and TRES, and found excellent agreement. In general we have adopted the TRES results on account of the higher quality and greater wavelength coverage of those observations. We report these measurements in Table 5, for both the single-lined and double-lined objects. The uncertainties are based on the scatter of the individual spectra, with an adopted floor of 100 K in temperature and 2 km s<sup>-1</sup> in the rotational velocity when it is below our spectral resolution. For completeness, we include the rotational velocities for the early-type stars reproduced from the work of Torres (2020). In a few cases (HII 1284, HII 1876, and TRU S194) we have been able to estimate the temperatures of those rapidly rotating objects using the techniques in this paper.

Until now we have been referring to our estimates of the projected rotational velocity as  $V_{\text{rot}}$ , rather than  $v \sin i$ . We note that strictly speaking the measurements include other sources of line broadening aside from rotation, such as macroturbulence ( $\zeta_{\text{RT}}$ ), which we do not attempt to account for. Our synthetic spectra were calculated with a value of  $\zeta_{\text{RT}} = 2$  km s<sup>-1</sup>, which should be representative of solar-type and cooler stars. Earlier-

**Table 4**  
Radial Velocity Statistics for Objects in the Pleiades Region Observed Spectroscopically at the CfA.

	Name	Time Span (days)	$N_{\text{DS}}$	$N_{\text{TRES}}$	$N_{\text{COR}}$	Mean $RV$ ( $\text{km s}^{-1}$ )	$P(\chi^2)$	$e/i$	Flags
1*	AK III-31	13481	65	1	27	$13.72 \pm 4.67$	0.00000	75.938	NM, SB2
2	PELS 121	12846	3	8	4	$5.56 \pm 0.14$	0.92131	0.269	NM
3	PELS 1	0	1	0	0	$-60.38 \pm 2.69$	...	...	NM
4	AK III-59	8740	2	7	3	$5.14 \pm 0.17$	0.27167	0.441	NM
5*	AK III-79	6877	6	0	0	$10.35 \pm 1.91$	0.06339	1.123	NM
6	AK III-158	20	4	0	0	$-5.01 \pm 2.67$	0.64266	0.564	NM

**Note.** — The columns give the time span of the CfA observations followed by the number of radial velocity measurements from the Digital Speedometers, TRES, and CORAVEL, and the weighted mean  $RV$  including the CORAVEL measurements, when available. For objects with more than one measurement we then list the  $\chi^2$  probability and the  $e/i$  metric for velocity variability, described in Section 8. The last column indicates non-members (NM), and known binaries with spectroscopic orbits (SB1, SB2, SB3), astrometric orbits (AST), or long-term trends (L), as reported in Sections 5, 6, and 7. Early-type stars with spectroscopic results published previously (Torres 2020) are included for completeness, and are flagged with a “b” in the last column. Stars with notes of interest given in the Appendix are indicated with an asterisk following the running number before the name. (This table is available in its entirety in machine-readable form.)

**Table 5**  
Effective Temperatures and Projected Rotational Velocities.

	Name	$T_{\text{eff}}$ (K)	$v \sin i$ ( $\text{km s}^{-1}$ )	$T_{\text{eff}}$ (K)	$v \sin i$ ( $\text{km s}^{-1}$ )
		Primary		Secondary	
1	AK III-31	$5770 \pm 100$	$10 \pm 2$	4250*	6*
2	PELS 121	$6120 \pm 100$	$4 \pm 2$	...	...
3	PELS 1	$8350 \pm 150$	$31 \pm 3$	...	...
4	AK III-59	$5330 \pm 100$	$3 \pm 2$	...	...
5	AK III-79	$6530 \pm 300$	$73 \pm 4$	...	...

**Note.** — Quantities flagged with an asterisk were adopted based on external information. Tertiary parameters adopted for HII 1338 are  $T_{\text{eff}} = 5250$  K and  $v \sin i = 0$   $\text{km s}^{-1}$ . The temperature determination for the Am secondary of HII 1431 used  $[\text{Fe}/\text{H}] = +0.5$ . Rotational velocities for rapidly-rotating early type stars are reproduced from the work of Torres (2020). Parameters for the secondary of HII 2147 are from Torres et al. (2020). (This table is available in its entirety in machine-readable form.)

type stars, on the other hand, are expected to have larger values, but they are also rotating more rapidly, so that rotation ends up being the dominant broadening mechanism. Additionally, the parameter  $V_{\text{rot}}$  used for the library of synthetic templates is the equatorial velocity for a model star viewed equator-on. There may be systematic differences with  $v \sin i$  as rotation increases and stars are viewed more pole-on. For example, gravity darkening is not included. For our sample, we do not expect these differences to be significant given the reduced precision of the measurements for rapid rotators, so for the remainder of the paper we will use the more familiar notation  $v \sin i$  for all our rotational velocity estimates. Figure 5 shows the distribution of  $T_{\text{eff}}$  and  $v \sin i$  for the CfA sample. Objects reported previously by Torres (2020) are excluded from this figure, as they generally have no temperature estimates. Objects hotter than about 6000 K tend to rotate more rapidly, although a number of cooler objects can have very large  $v \sin i$  values as well. These are sometimes referred to as ultrafast rotators (see, e.g., Soderblom et al. 1993).

## 5. ORBITAL SOLUTIONS FOR SPECTROSCOPIC BINARIES

### 5.1. Single- and Double-lined Binaries

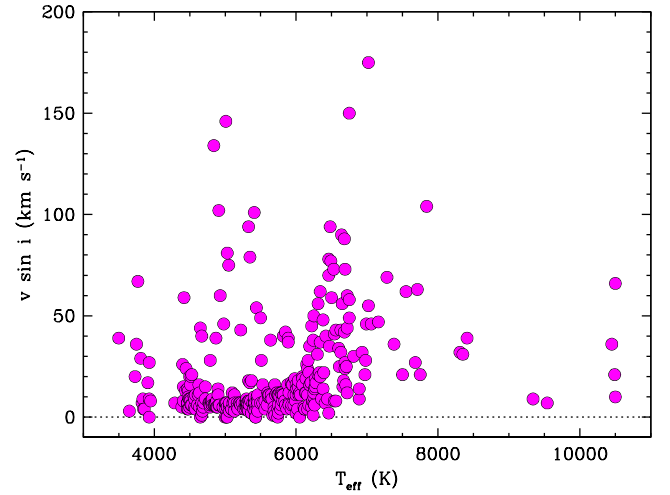


**Figure 5.** Effective temperatures and projected rotational velocities for all objects in the CfA survey with single-lined spectra.

The combination of our radial velocity measurements with those of Mermilliod et al. (2009) has allowed us to discover many new spectroscopic binaries in our sample. For the single-lined systems (SB1) we performed weighted least-squares orbital solutions solving for the standard elements  $P$  (orbital period),  $\gamma$  (center-of-mass velocity),  $K_1$  (primary velocity semiamplitude),  $e$  and  $\omega_1$  (eccentricity and argument of periastron for the primary), and  $T_0$  (a reference time of periastron passage, for eccentric orbits, or a time of maximum primary velocity, for circular orbits). Orbits were assumed to be circular when initial solutions solving for  $e$  gave a value that was not statistically significant. Relative weights for the observations were taken to be inversely proportional to  $\sigma_{\text{RV}}^2$ , where  $\sigma_{\text{RV}}$  is the formal error of the measurement. As those uncertainties can sometimes be underestimated (or overestimated), we solved simultaneously for a multiplicative scale factor  $F$  for the uncertainties in order to achieve reduced  $\chi^2$  values near unity. The orbital elements are collected in Table 6, and include the derived quantities  $f(M)$  (the standard mass function), the coefficient of  $M_2 \sin i$  (the minimum secondary mass), and  $a_1 \sin i$  (the projected linear semimajor axis of the primary). The number of observations, the standard deviation of the residuals, and the error scaling factor are

listed as well, and non-members are flagged at the end of each line.

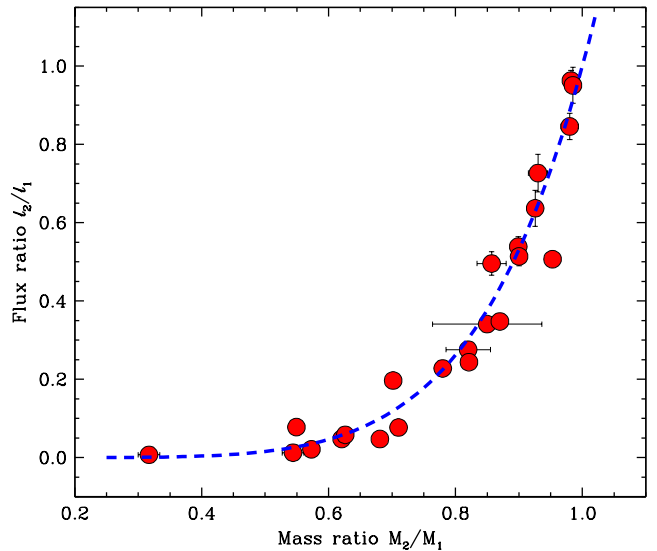
For double-lined binaries we proceeded in a similar fashion, solving for the additional parameter  $K_2$  representing the velocity semiamplitude of the secondary. As the secondary velocities are typically poorer than those of the primary because the secondaries are fainter, we allowed separate scaling factors for the two stars. The orbital elements are presented in Table 7. Derived properties are listed separately in Table 8. They include the minimum masses  $M_1 \sin^3 i$  and  $M_2 \sin^3 i$ , the mass ratio  $q \equiv M_2/M_1$ , the individual projected semimajor axes  $a_1 \sin i$  and  $a_2 \sin i$ , and the total projected semimajor axis  $a \sin i$  in units of the solar radius. In some cases there can be a systematic offset between the primary and secondary velocities caused, e.g., by a mismatch between the properties of the real stars and the templates used for the components. If not accounted for, this can bias the velocity semiamplitudes, or possibly the center-of-mass velocity of the binary. Most commonly this mismatch will occur for the secondary, as we are sometimes unable to determine its temperature or rotational velocity independently from our spectra, and had to adopt educated guesses based on models or other observables. Therefore, we have added as a free parameter a velocity offset  $\Delta RV$  that we solved for simultaneously with the other elements. These offsets are listed in the table as well, when they are different from zero by more than twice their uncertainty.

Table 8 reports also the flux ratios determined with TODCOR, which correspond to the mean wavelength of our observations ( $\approx 5187 \text{ \AA}$ ). We expect a strong correlation between the flux ratios and the mass ratios for the double-lined binaries, resulting from the theoretical mass-luminosity relation. This trend is illustrated in Figure 6. The bolometric mass-luminosity relation on the main sequence is often approximated as a power law ( $L \propto M^\alpha$ ), although the exponent depends on the mass range ( $\alpha \sim 3-4$ ). The value of  $\alpha$  has been shown to be larger when considering fluxes over a discrete bandpass (e.g., Goldberg et al. 2002), and indeed the PARSEC 1.2S isochrone invoked earlier for the Pleiades predicts a slope for the mass-luminosity relation that is  $\sim 6$  in a bandpass near our spectral window, for masses between  $0.5$  and  $1.5 M_\odot$ . This  $\alpha = 6$  relation converted to the linear scale of the measurements is shown as a dashed line in the figure, and is seen to match the empirical relation well.

The error scaling factors  $F$  from our orbital solutions for the SB1s and SB2s are fairly close to unity in most cases, indicating that our internal uncertainties (and those from the CORAVEL) are quite realistic. Their distribution is shown in Figure 7. Graphical representations of the orbital solutions for each SB1 and SB2 are presented at the end of the paper in Figures 20–23, and notes for some of the systems with features of interest are given in the Appendix.

## 5.2. Spectroscopic Triple Systems

Two of the objects with variable velocity in our sample are hierarchical spectroscopic triple systems, discussed here. Several others are spectroscopic binaries with outer astrometric companions.



**Figure 6.** Flux ratios as a function of the mass ratios for the double-lined binaries in the sample. The dashed line corresponds to a power law with an exponent of  $\alpha = 6$ , represented here on the linear scale of the observations.

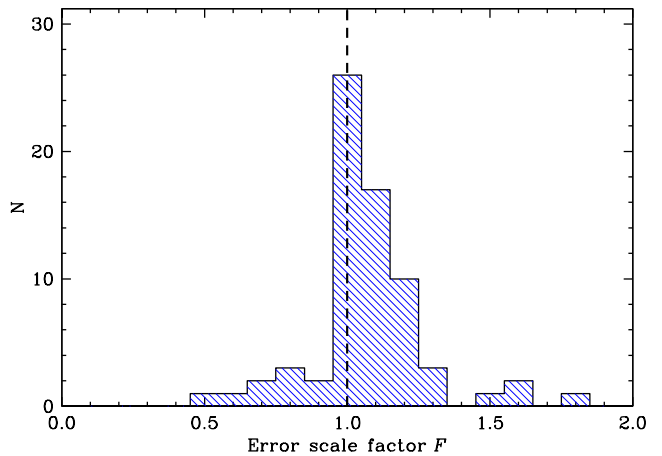


**Figure 7.** Histogram of the error scaling factors for SB1s and SB2s (see the text), showing that the internal errors from CfA and the northern CORAVEL are realistic.

### 5.2.1. HII 1338

This object was reported as a double-lined spectroscopic binary by several authors on the basis of one or a few observations (Abt 1970; Liu et al. 1991; Soderblom et al. 1993). A spectroscopic orbit with a period of 7.75 days was first presented by Raboud & Mermilliod (1998), although as far as we are aware the original velocities were never published (and do not appear in the catalog of Mermilliod et al. 2009). Raboud & Mermilliod (1998) stated only that they obtained 25 and 21 measurements for the primary and secondary over a period of about two years (presumably sometime between 1978 and 1995), and noted that they saw hints of the presence of a third star at certain phases.

Our observations with the Digital Speedometers also reveal signs of the tertiary, and although we have been able to measure its velocity using TRICOR, the measurements are very poor due to the faintness of that component. We list them nonetheless in Table 9, along with those of the primary and secondary. The template used



**Table 6**  
Orbital Elements for the Single-lined Binaries in the Sample.

Name	$P$ (day)	$\gamma$ (km s <sup>-1</sup> )	$K_1$ (km s <sup>-1</sup> )	$e$	$\omega_1$ (degree)	$T_0$ (HJD) (2,400,000+)	$f(M)$ ( $M_\odot$ )	$M_2 \sin i$ ( $M_\odot$ )	$a_1 \sin i$ (10 <sup>6</sup> km)	$\sigma$ (km s <sup>-1</sup> ) $N_{\text{obs}}$	$F$
15 PELS 7	7322. 109.	2.898 0.048	2.168 0.044	0.506 0.013	203.4 2.1	57996. 23.	0.00496 0.00036	0.1705 0.0041	188.2 5.2	0.099 33	0.786 NM
26 AK II-346	6123. 123.	4.65 0.28	4.40 0.44	0.030 0.083	114. 160.	54024. 2754.	0.054 0.016	0.378 0.038	371. 37.	1.073 63	1.219
44 AK III-664	14.07286 0.00095	4.06 0.13	15.64 0.17	0.313 0.011	105.4 2.2	53383.133 0.067	0.00478 0.00016	0.1685 0.0019	2.875 0.033	0.512 24	1.349
74 HII 120	2940. 12.	6.818 0.041	2.426 0.057	0.303 0.026	238.6 4.4	56530. 37.	0.00377 0.00024	0.1556 0.0033	93.5 2.1	0.228 53	0.935
93 HII 233	1241.5 1.4	5.321 0.039	1.978 0.060	0.242 0.025	248.9 7.7	51856. 22.	0.000910 0.000080	0.0969 0.0029	32.77 0.97	0.277 64	0.991
98 HII 250	971.59 0.67	4.206 0.029	3.180 0.046	0.6613 0.0099	243.5 1.6	54910.3 2.3	0.001366 0.000050	0.1110 0.0014	31.87 0.39	0.175 51	1.014
133 HII 522	23.83746 0.00049	6.597 0.082	4.98 0.12	0.109 0.023	30. 13.	48736.23 0.83	0.000300 0.000022	0.0669 0.0016	1.623 0.039	0.451 42	1.079
144 HII 571	15.872245 0.000032	5.829 0.060	26.476 0.088	0.3281 0.0031	88.48 0.45	52084.074 0.020	0.02573 0.00021	0.29521 0.00080	5.459 0.015	0.322 89	1.608
158 HII 727	7271. 153.	6.08 0.20	8.6 1.7	0.832 0.039	146.2 3.2	51330. 159.	0.081 0.024	0.433 0.043	476. 49.	0.848 65	0.988
160 HII 745	1541.4 9.8	5.28 0.10	6.80 0.13	0.120 0.025	6. 12.	56509. 55.	0.0492 0.0030	0.3664 0.0074	143.1 3.0	0.688 62	0.730
201 TRU S93	1059.7 3.8	4.092 0.071	3.18 0.12	0.392 0.037	156.5 4.7	56204. 14.	0.00276 0.00027	0.1402 0.0046	42.7 1.4	0.390 56	1.032
233 HII 1407	953.08 0.90	5.285 0.088	7.76 0.11	0.322 0.011	262.2 2.2	55419.4 4.4	0.0392 0.0018	0.3398 0.0053	96.3 1.5	0.376 55	0.657
235 HII 1397	7.345274 0.000018	6.903 0.069	13.214 0.097	0 ...	... ...	49630.041 0.015	0.001756 0.000039	0.12065 0.00088	1.3347 0.0098	0.416 47	1.223
251 HII 1653	548.2 1.1	7.39 0.52	6.20 0.51	0 ...	... ...	55674.1 9.8	0.0135 0.0033	0.238 0.020	46.7 3.8	1.667 27	0.781
254 HII 1762	4017. 155.	6.29 0.38	10.48 0.49	0.468 0.039	350. 10.	58398. 65.	0.331 0.042	0.692 0.029	512. 28.	1.485 33	0.634
277 HII 2172	30.21296 0.00011	5.967 0.046	14.667 0.059	0.3294 0.0037	121.54 0.90	49574.579 0.062	0.008314 0.000096	0.20258 0.00078	5.753 0.022	0.332 75	1.162
282 HII 2284	807.39 0.45	5.705 0.015	3.617 0.024	0.4111 0.0061	54.6 1.2	56747.8 2.5	0.003000 0.000060	0.14422 0.00096	36.61 0.24	0.079 38	0.492
291 HII 2407	7.0504772 0.0000090	6.195 0.051	19.672 0.057	0 ...	... ...	52656.3988 0.0064	0.005561 0.000048	0.17717 0.00051	1.9072 0.0055	0.413 74	1.185
297 HII 2500	2391. 17.	5.628 0.094	6.32 0.13	0 ...	... ...	56290. 11.	0.0626 0.0040	0.3970 0.0084	207.8 4.8	0.586 48	1.010
328 HII 3104	1312.5 4.5	7.036 0.093	2.72 0.14	0.207 0.051	235. 21.	57554. 74.	0.00256 0.00038	0.1368 0.0067	48.0 2.4	0.295 22	0.799
330 HII 3097	780.38 0.14	5.549 0.042	4.537 0.082	0.777 0.010	29.8 1.3	51415.4 1.3	0.00188 0.00011	0.1235 0.0024	30.65 0.60	0.310 69	0.972
342 PELS 69	1327.5 1.3	7.66 0.10	4.96 0.13	0.436 0.029	232.3 3.5	55577.8 8.6	0.0122 0.0010	0.2302 0.0063	81.4 2.2	0.517 39	0.958 NM
348 AK IV-287	1808. 26.	4.59 0.29	4.75 0.43	0.229 0.064	20. 31.	57765. 151.	0.0185 0.0051	0.265 0.024	115. 11.	1.585 42	1.621

**Note.** — Uncertainties for the orbital elements and derived quantities are given in the second line for each system. The symbol  $T_0$  represents a reference time of periastron passage for eccentric orbits, and a time of maximum primary velocity for circular orbits.  $M_2 \sin i$  is the coefficient of the minimum secondary mass multiplying the factor  $(M_1 + M_2)^{2/3}$ . The first line of the last column ( $F$ ) represents the scale factor applied to the internal RV uncertainties to produce a reduced  $\chi^2$  of unity. Non-members are indicated with “NM” in the second line of the last column. For AK II-346 and HII 1762, the orbits reported are for the secondary component; the primary is not seen in our spectra.

**Table 7**  
Orbital Elements for the Double-lined Binaries in the Sample.

Name	$P$ (day)	$\gamma$ (km s <sup>-1</sup> )	$K_1$ (km s <sup>-1</sup> )	$K_2$ (km s <sup>-1</sup> )	$e$	$\omega_1$ (degree)	$T_0$ (HJD) (2,400,000+)	$\Delta_{\text{CfA}}$ (km s <sup>-1</sup> )	$\Delta_{\text{COR}}$ (km s <sup>-1</sup> )	
1 AK III-31	5.0043210 0.0000090	5.511 0.056	54.774 0.065	87.45 0.73	0 ...	... ...	53131.5598 0.0019	... ...	... ...	NM
21 AK III-419	34.321476 0.000067	3.811 0.033	38.87 0.20	43.18 0.22	0.6493 0.0022	345.18 0.16	53996.096 0.010	... ...	... ...	
81 HII 164	268.704 0.056	4.968 0.086	9.830 0.070	30.9 1.7	0.2505 0.0072	73.7 2.8	52933.9 1.6	2.9 1.4	... ...	
86 HII 173	481.25 0.10	5.216 0.076	15.99 0.12	16.79 0.15	0.0986 0.0067	214.0 3.9	48399.4 5.4	... ...	... ...	
89 HII 177	2278.3 1.2	10.724 0.030	9.073 0.066	10.092 0.059	0.4900 0.0036	331.45 0.57	54258.7 2.9	... ...	... ...	NM
112 HII 320	757.01 0.22	5.759 0.059	12.248 0.065	14.30 0.38	0.3064 0.0049	284.8 1.1	52047.4 2.2	... ...	... ...	
119 PELS 38	17.285878 0.000069	6.910 0.026	19.078 0.025	33.30 0.69	0.0811 0.0018	132.7 1.5	55314.946 0.068	... ...	... ...	
145 HII 605	20.79762 0.00012	5.08 0.12	42.27 0.12	68.09 0.72	0.4318 0.0026	287.62 0.51	52405.746 0.020	-1.38 0.60	... ...	
165 HII 761	3.3072926 0.0000025	5.349 0.073	51.477 0.080	75.60 0.77	0 ...	... ...	52392.7804 0.0015	... ...	... ...	
180 AK I-2-288	17.46668 0.00013	4.568 0.040	18.548 0.069	21.32 0.10	0.2010 0.0030	325.91 0.91	55197.296 0.044	... ...	... ...	
204 HII 1117	26.02712 0.00010	7.424 0.099	13.30 0.15	13.57 0.15	0.5745 0.0062	136.95 0.90	49112.755 0.030	0.42 0.20	-0.08 0.16	
227 HII 1338	7.757171 0.000072	3.14 0.14	58.45 0.22	63.15 0.25	0.0344 0.0032	297.1 5.8	53459.92 0.12	... ...	... ...	
228 HII 1348	94.805 0.012	6.367 0.022	20.163 0.054	25.85 0.33	0.5543 0.0017	82.20 0.32	56452.796 0.068	... ...	... ...	
234 HII 1392	767.04 0.25	5.78 0.24	23.65 0.32	25.42 0.28	0.8206 0.0075	221.7 1.0	57386.28 0.24	1.09 0.37	... ...	
237 HII 1431	2.461127 0.000015	6.29 0.20	100.07 0.23	142.60 0.28	0 ...	... ...	52969.43596 0.00092	1.74 0.31	... ...	
290 HII 2406	33.006290 0.000049	6.065 0.036	25.801 0.033	47.4 1.5	0.5109 0.0011	218.29 0.21	57815.0878 0.0096	... ...	... ...	
299 HII 2507	16.726227 0.000040	6.428 0.020	39.358 0.023	71.651 0.079	0 ...	... ...	54799.3046 0.0037	0.428 0.075	... ...	
300 HCG 384	542.11 0.27	5.75 0.11	15.06 0.23	18.36 0.78	0.6624 0.0080	167.3 1.2	57624.31 0.79	... ...	... ...	
351 DH 794	5.694369 0.000042	7.426 0.057	40.200 0.084	56.60 0.67	0.0119 0.0021	201.4 7.9	58470.71 0.12	... ...	... ...	
356 HCG 489	3.108737 0.000012	6.619 0.086	76.29 0.16	77.44 0.22	0 ...	... ...	57190.40052 0.00075	... ...	... ...	
358 HCG 495	8.57662 0.00053	7.61 0.31	53.06 0.42	54.01 0.52	0.1368 0.0071	272.4 2.6	57190.015 0.060	2.90 0.51	... ...	
359 AK V-151	3079. 25.	14.97 0.21	10.1 1.0	11.83 0.23	0.301 0.019	247.1 3.9	54181. 32.	... ...	... ...	NM
366 AK V-198	176.364 0.011	7.858 0.068	14.599 0.043	17.779 0.081	0.2182 0.0054	329.0 1.4	54750.00 0.54	-0.62 0.15	... ...	

**Note.** — Uncertainties for the orbital elements are given in the second line for each system. The symbol  $T_0$  represents a reference time of periastron passage for eccentric orbits, and a time of maximum primary velocity for circular orbits. Primary/secondary velocity offsets for CfA and the CORAVEL are listed under  $\Delta_{\text{CfA}}$  and  $\Delta_{\text{COR}}$ . Non-members are indicated with “NM” in the last column.

**Table 8**  
Derived Properties for the Double-lined Binaries in the Sample.

Name	$M_1 \sin^3 i$ ( $M_\odot$ )	$M_2 \sin^3 i$ ( $M_\odot$ )	$a_1 \sin i$ ( $10^6$ km)	$a_2 \sin i$ ( $10^6$ km)	$a_{\text{tot}} \sin i$ ( $R_\odot$ )	$q$	$\sigma_1$ (km s $^{-1}$ ) $N_1$	$\sigma_2$ (km s $^{-1}$ ) $N_2$	$F$	$\ell_2/\ell_1$	
1 AK III-31	0.917 0.017	0.5745 0.0060	3.7692 0.0045	6.018 0.050	14.068 0.072	0.6263 0.0053	0.431 66	5.095 66	1.044 1.005	0.0583 0.0089	NM
21 AK III-419	0.4546 0.0039	0.4093 0.0035	13.951 0.047	15.497 0.050	42.33 0.12	0.9003 0.0031	0.396 77	0.387 77	1.016 1.070	0.514 0.024	
81 HII 164	1.30 0.18	0.413 0.034	35.16 0.26	110.6 5.9	209.6 8.5	0.318 0.017	0.369 55	6.951 32	1.048 1.081	0.0076 0.0040	
86 HII 173	0.886 0.018	0.844 0.015	105.31 0.78	110.6 1.0	310.3 1.9	0.953 0.011	0.813 80	1.041 74	1.210 1.192	0.507 0.013	
89 HII 177	0.5796 0.0087	0.5211 0.0086	247.8 1.8	275.6 1.7	752.3 3.9	0.8990 0.0081	0.405 90	0.362 90	1.030 1.002	0.539 0.025	NM
112 HII 320	0.682 0.040	0.584 0.020	121.36 0.77	141.7 3.8	378.1 5.9	0.857 0.023	0.243 46	1.207 23	1.065 1.137	0.496 0.030	
119 PELS 38	0.1620 0.0076	0.0928 0.0025	4.5198 0.0059	7.89 0.16	17.84 0.24	0.573 0.012	0.092 36	2.939 31	0.991 1.027	0.0213 0.0066	
145 HII 605	1.311 0.032	0.814 0.012	10.902 0.035	17.57 0.19	40.92 0.28	0.6207 0.0068	0.553 42	3.343 42	1.058 1.057	0.0478 0.0039	
165 HII 761	0.4183 0.0093	0.2849 0.0035	2.3411 0.0037	3.438 0.035	8.307 0.051	0.6809 0.0070	0.469 48	4.554 48	1.029 1.028	0.0475 0.0055	
180 AK I-2-288	0.05764 0.00060	0.05015 0.00044	4.364 0.016	5.016 0.024	13.483 0.042	0.8700 0.0053	0.257 32	0.367 30	1.453 1.131	0.348 0.011	
204 HII 1117	0.01449 0.00034	0.01420 0.00034	3.897 0.041	3.975 0.041	11.315 0.085	0.980 0.014	0.836 84	0.838 85	1.305 1.188	0.846 0.034	
227 HII 1338	0.7491 0.0067	0.6933 0.0060	6.231 0.023	6.732 0.026	18.632 0.052	0.9256 0.0049	1.538 72	1.741 72	1.026 1.027	0.637 0.046	
228 HII 1348	0.3101 0.0083	0.2418 0.0036	21.878 0.046	28.05 0.35	71.77 0.51	0.7799 0.0098	0.090 22	0.902 22	1.093 1.196	0.228 0.015	
234 HII 1392	0.908 0.059	0.845 0.056	142.6 3.4	153.3 3.4	425.2 9.2	0.930 0.015	1.025 30	0.872 30	1.045 0.980	0.727 0.048	
237 HII 1431	2.1414 0.0099	1.5028 0.0072	3.3867 0.0078	4.8260 0.0094	11.805 0.018	0.7018 0.0021	1.308 49	1.569 49	1.034 1.034	0.197 0.010	
290 HII 2406	0.551 0.040	0.300 0.012	10.067 0.015	18.49 0.59	41.04 0.85	0.544 0.017	0.194 68	7.402 38	1.120 1.053	0.0126 0.0028	
299 HII 2507	1.5302 0.0040	0.8406 0.0015	9.0525 0.0052	16.480 0.018	36.700 0.028	0.54931 0.00067	0.143 59	0.519 59	1.034 0.991	0.078 0.003	
300 HCG 384	0.484 0.042	0.397 0.020	84.12 0.90	102.5 4.2	268.3 6.2	0.820 0.035	0.517 29	2.563 29	1.076 1.078	0.276 0.018	
351 DH 794	0.3129 0.0081	0.2222 0.0032	3.1476 0.0066	4.432 0.053	10.895 0.077	0.7103 0.0085	0.164 19	1.952 19	1.129 1.137	0.077 0.011	
356 HCG 489	0.5895 0.0035	0.5807 0.0030	3.2612 0.0070	3.3105 0.0092	9.446 0.017	0.9851 0.0034	0.433 19	0.581 19	0.907 1.256	0.951 0.046	
358 HCG 495	0.535 0.011	0.5255 0.0098	6.199 0.048	6.310 0.060	17.98 0.11	0.982 0.012	1.055 17	1.322 17	1.201 1.202	0.963 0.026	
359 AK V-151	1.57 0.16	1.33 0.26	406. 41.	477.6 8.7	1270. 62.	0.850 0.086	1.574 11	0.797 44	1.799 1.126	0.341 0.020	NM
366 AK V-198	0.3166 0.0032	0.2600 0.0021	34.55 0.10	42.08 0.19	110.15 0.33	0.8212 0.0043	0.236 45	0.451 44	1.211 1.038	0.244 0.010	

**Note.** — Uncertainties for the derived quantities are given in the second line for each system.  $M_2 \sin i$  is the coefficient of the minimum secondary mass multiplying the factor  $(M_1 + M_2)^{2/3}$ . The column with the  $F$  heading contains the scale factors applied to the internal RV uncertainties for the primary and secondary in order to produce a reduced  $\chi^2$  of unity. Non-members are indicated with “NM” in the last column.

for the tertiary has a temperature of 5250 K and no rotational broadening. The primary and secondary have a flux ratio of  $\ell_2/\ell_1 = 0.637 \pm 0.046$ , and between the tertiary and the primary the ratio is  $\ell_3/\ell_1 = 0.335 \pm 0.046$ .

The center-of-mass velocity of the SB2 is  $\gamma = 3.14 \pm 0.14 \text{ km s}^{-1}$  (see Table 7 and Figure 21), which deviates significantly from the cluster mean. On the other hand, the weighted mean of our 72 tertiary velocities, assuming they are constant, is  $7.15 \pm 0.94 \text{ km s}^{-1}$ , which is on the opposite side of the cluster mean, consistent with membership in the Pleiades if the tertiary and the SB2 are physically associated. Interestingly, Raboud & Mermilliod (1998) reported a rather different  $\gamma$  velocity for the SB2 of  $6.3 \pm 0.4 \text{ km s}^{-1}$ , and also that the tertiary velocities appeared to be close to the cluster mean, whereas our tertiary velocities are somewhat higher. All of this would be consistent with a hierarchical triple scenario in which the SB2's center of mass and the tertiary were closer in velocity to each other and to the cluster mean at the time of the CORAVEL observations, and farther apart when we observed the object a decade or two later. No significant trend is detected in the residuals of the primary or secondary in our observations, taken over a period of seven years, suggesting the outer period is much longer than that.

A visual companion to HII 1338 was detected by speckle interferometry in 2005 at a separation of  $0''.20$  (Mason et al. 2009), and again in 2010 by lunar occultations (Loader et al. 2012). At the distance to the Pleiades, the expected orbital period is of the order of a century. This visual companion may be the tertiary seen in our spectra. The previous data release (DR2) of the Gaia catalog listed a parallax and proper motion for HII 1338 that were inconsistent with membership in the cluster, but had very large uncertainties indicating that the astrometric solution was compromised. The latest data release (EDR3) no longer reports either a parallax or the proper motion, again suggesting difficulty with the astrometric solution, possibly caused by the visual companion.

### 5.2.2. HII 2027

Mermilliod et al. (1992a) recognized this as a triple system consisting of a single-lined spectroscopic binary with a period of 48.6 days (components Ba and Bb), accompanied by a brighter star (A) that was also visible in their cross-correlation profiles. They detected a drift in the center-of-mass velocity of the binary and a change in the other direction for the third star, indicating motion in a wide orbit supporting the physical association. Additional velocities for the two visible stars A and Ba were reported by Mermilliod et al. (2009). The total time span of the CORAVEL measurements is slightly over 19 years, from 1978 to 1997.

The CfA observations of HII 2027 were collected between 1982 and early 2021, extending the time baseline enough to permit a solution for the elements of the outer orbit for the first time. Radial velocities for components A and Ba were derived with TODCOR, and while experiments using TRICOR revealed hints of the secondary in the 48.6 day orbit (star Bb), we were not able to measure its velocities reliably. Our measured velocities for A and Ba are listed in Table 10. The flux ratio between components Ba and A is  $0.737 \pm 0.030$  at a mean wavelength

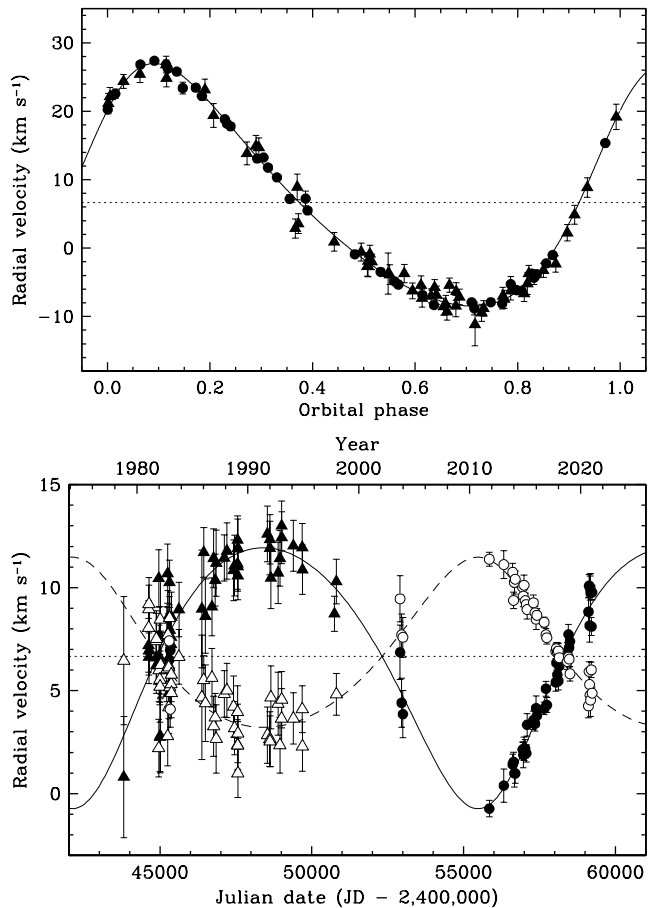


**Figure 8.** *Top:* Observations and inner 48.6 day orbit model of HII 2027. Motion in the outer orbit has been subtracted from the measured velocities of star Ba. Triangles represent CORAVEL measurements, and circles are for RVs from the CfA. The dotted line represents the center-of-mass velocity of the triple system. *Bottom:* Observations and model for the outer orbit, with motion in the inner orbit subtracted from the velocities of star Ba (open symbols). The point style is the same as in the top panel.

of  $5187 \text{ \AA}$ .

We combined the CORAVEL measurements with ours to solve for the inner and outer orbits simultaneously, assuming they are dynamically independent. Internal errors were adjusted separately for the primary and secondary to give reduced  $\chi^2$  values near unity. The CfA errors listed in Table 10 already include those adjustments; the adjustment factors for the CORAVEL measurements were 2.1 and 1.8. The elements are given in Table 11, and the orbits together with all observations are represented graphically in Figure 8. The outer orbit has a period of 36.5 yr, the longest in our survey of the Pleiades.

HII 2027 has a visual companion found with adaptive optics imaging in 1996 (Bouvier et al. 1997), with a current separation of  $0''.2$ . It corresponds to the inner 48.6 day binary.

### 5.3. Other Multiple Systems

Later in Section 12 we report known astrometric companions to our targets, and in some cases these additional objects have been found around systems that already have (closer) spectroscopic companions. Examples of such hierarchical triple systems are HII 102, HII 120, HII 571, HII 717, HII 1348, and possibly HII 745 and



**Table 9**  
Radial Velocity Measurements for the Triple-lined System HII 1338.

HJD (2,400,000+)	$RV_1$ (km s <sup>-1</sup> )	$RV_2$ (km s <sup>-1</sup> )	$RV_3$ (km s <sup>-1</sup> )	S/N	Inst
51920.6419	$-36.18 \pm 2.08$	$51.17 \pm 2.36$	$16.2 \pm 10.5$	27	1
51939.5019	$33.24 \pm 2.21$	$-26.69 \pm 2.50$	$1.5 \pm 11.1$	26	1
52508.8216	$15.74 \pm 1.62$	$-10.48 \pm 1.83$	$4.5 \pm 8.1$	35	1
52567.9234	$35.50 \pm 1.59$	$-31.95 \pm 1.80$	$21.9 \pm 8.0$	36	1
52603.7973	$-50.82 \pm 1.66$	$64.88 \pm 1.88$	$2.7 \pm 8.4$	34	1

**Note.** — The heliocentric radial velocities are on the reference frame of the minor planets in the Solar System (see Stefanik et al. 1999). Signal-to-noise ratios in the S/N column are per resolution element. Codes in the Inst column are 1 for the Digital Speedometers and 2 for TRES. (This table is available in its entirety in machine-readable form.)

**Table 10**  
Radial Velocity Measurements for the Double-lined Triple System HII 2027.

HJD (2,400,000+)	$RV_A$ (km s <sup>-1</sup> )	$RV_{Ba}$ (km s <sup>-1</sup> )	S/N	Inst.
45302.8342	$6.50 \pm 1.28$	$6.48 \pm 1.09$	10	1
45339.8090	$6.96 \pm 1.04$	$22.57 \pm 0.88$	12	1
52907.8553	$6.86 \pm 1.32$	$-4.18 \pm 1.12$	9	1
52958.6826	$4.41 \pm 1.19$	$-3.15 \pm 1.01$	10	1
53001.6534	$3.86 \pm 1.14$	$-7.54 \pm 0.97$	11	1

**Note.** — The heliocentric radial velocities are on the reference frame of the minor planets in the Solar System (see Stefanik et al. 1999). Signal-to-noise ratios in the S/N column are per resolution element. Codes in the Inst column are 1 for the Digital Speedometers and 2 for TRES. (This table is available in its entirety in machine-readable form.)

**Table 11**  
Orbital Elements for the Double-lined Triple System HII 2027.

Parameter	Value
$P_{AB}$ (days)	$13351 \pm 79$
$\gamma$ (km s <sup>-1</sup> )	$6.615 \pm 0.053$
$K_A$ (km s <sup>-1</sup> )	$6.22 \pm 0.24$
$K_B$ (km s <sup>-1</sup> )	$4.19 \pm 0.19$
$e_{AB}$	$0.174 \pm 0.021$
$\omega_A$ (degree)	$196.2 \pm 8.8$
$T_{AB}$ (HJD-2,400,000)	$42559 \pm 329$
$P_B$ (days)	$48.62538 \pm 0.00055$
$K_{Ba}$ (km s <sup>-1</sup> )	$17.736 \pm 0.094$
$e_B$	$0.2368 \pm 0.0051$
$\omega_{Ba}$ (degree)	$307.8 \pm 1.4$
$T_B$ (HJD-2,400,000)	$45867.54 \pm 0.21$
Derived quantities	
$M_A \sin^3 i_{AB}$ ( $M_\odot$ )	$0.599 \pm 0.070$
$M_B \sin^3 i_{AB}$ ( $M_\odot$ )	$0.891 \pm 0.098$
$a_A \sin i_{AB}$ (10 <sup>6</sup> km)	$1125 \pm 44$
$a_B \sin i_{AB}$ (10 <sup>6</sup> km)	$757 \pm 36$
$q \equiv M_B/M_A$	$1.487 \pm 0.060$
$f(M)$ ( $M_\odot$ ) for inner pair	$0.02578 \pm 0.00040$
$M_{Bb} \sin i_B$ ( $[M_{Ba} + M_{Bb}]^{2/3} M_\odot$ )	$0.2954 \pm 0.0015$
$a_{Ba} \sin i_B$ (10 <sup>6</sup> km)	$11.522 \pm 0.060$
$N_A$ (CfA / CORAVEL)	40 / 53
$N_{Ba}$ (CfA / CORAVEL)	40 / 52
Cycles covered for outer orbit	1.15

**Note.** — Subscripts “AB” correspond to the outer pair (A+B). Star Ba is the primary of the inner binary.

HCG 384, although the physical association of the tertiaries in the last two cases has not been confirmed. Additionally, HII 3197 is also a triple system in which the secondary and tertiary were both detected astrometrically. The 16'' pair HII 303 and HII 302 is another case, provided they are bound, in which the northern, brighter star (HII 303) has a closer 1''8 visual companion. More detailed information for all of these objects may be found in the Appendix.

Even higher multiplicity systems may also be present in our sample. Each component of the 5''7 visual pair HII 1392 and HII 1397 is in turn a spectroscopic binary (SB2 in the case of HII 1392), which would make this a hierarchical quadruple system, provided the visual components are physically bound. A more complex case is that of HII 2507, HII 2503, and HII 2500. The latter two objects are 3''3 and 10''1 from the first, respectively, and HII 2507 itself is an SB2, while HII 2500 is an SB1 and has another companion at 0''3 that is not the same as the spectroscopic one. Therefore, this could well be a sextuple system.

## 6. LONG-TERM TRENDS

More than a dozen objects in our sample exhibit long-term trends in their velocities indicating they are binaries, but the observations are insufficient to determine a period unambiguously. Most of them benefit greatly from the longer baseline that comes from including the CORAVEL observations. The time histories of these objects are shown in Figure 24 at the end of the paper.

In several cases (AK I-1-29, HII 727, HII 338, HII 717, HII 916) we have supplemented the CfA+CORAVEL observations with other measurements from the literature that help cover gaps or support the trends (Liu et al. 1991; Soderblom et al. 1993; Barrado y Navascués et al. 1998; White et al. 2007; Kunder et al. 2017).<sup>5</sup> For HII 727, the observations cover a single periastron passage, which causes some ambiguity in the period (see figure). Nevertheless, based on the distribution of the rest of our velocities including archival ones, we have derived a tentative orbit with a period of about 7200 days that is shown in Figure 21 and listed in Table 6.

## 7. OTHER PUBLISHED ORBITAL SOLUTIONS IN THE PLEIADES

Future studies of the binary population in the Pleiades may benefit from having the collection of all known bi-

<sup>5</sup> The Soderblom et al. (1993) and White et al. (2007) measurements have been adjusted as indicated by Torres (2020), to place them on the same zero-point as the CfA observations.

naries with orbital solutions in one place. With that in mind, we have supplemented our own discoveries with a compilation of all other orbits from the literature that we know of, presented in Table 12. All are considered members of the cluster.

The first four systems in the table are part of our original sample, but were published separately. They include three rapidly-rotating early-type stars from Torres (2020), and HII 2147 (Torres et al. 2020), which was spatially resolved with the technique of very long baseline interferometry (Melis et al. 2014) and yielded absolute masses for the components. Next we include the spectroscopic-interferometric binary Atlas (27 Tau, HII 2168; Zwahlen et al. 2004), and the Be shell star Pleione (28 Tau, HII 1180; Nemravová et al. 2010, their Solution 3), which has a period of 218 days. A second, tentative 35 yr long periodicity in the radial velocities for Pleione has been reported, but has not been confirmed to be due to orbital motion, and may simply reflect a periodicity in the shell episodes (see, e.g., Luthardt & Menchenkova 1994; Katahira et al. 1996). We do not include it in the table.

Also listed are the elements for two low-mass eclipsing binaries in the Pleiades uncovered by the Kepler/K2 mission (HCG 76 and MHO 9; David et al. 2016), and for the 30.2 yr astrometric binary HII 3197 (Schaefer et al. 2014), for which we have only a handful of radial velocity measurements over a period of less than 100 days.

Finally, we mention the interesting case of PPL 15, a 5.8 day double-lined spectroscopic binary in the Pleiades consisting of brown dwarfs (Basri & Martín 1999). The Gaia EDR3 catalog confirms it is a cluster member, although the parallax uncertainty is quite large.

## 8. RADIAL VELOCITY VARIABILITY

As stated earlier, for this work we rely on the merged CfA + CORAVEL data sets, and we will assume that any scatter in the velocities significantly in excess of the observational uncertainties is caused by a binary companion, or perhaps several. Note that because of the relatively young age of the Pleiades, some low-level variability is also to be expected from stellar activity, which is higher in the Pleiades than in the field, but is sometimes difficult to distinguish from changes due to orbital motion.

As a quantitative measure of the variability we adopted the  $e/i$  (external/internal) statistic, defined as the ratio of the standard deviation of the RVs to the measurement precision. This is a commonly used metric in many spectroscopic surveys (e.g., Mermilliod et al. 1992a; Hole et al. 2009; Geller et al. 2015). We calculated it as described in the second of those references, making use of the individual uncertainty of each measurement. The  $e/i$  values for the 377 stars in our sample are listed in Table 4, where we also specify the number of CORAVEL measurements for each target.

In Figure 9 we have sorted the  $e/i$  values in increasing order, and show them for all stars that are considered to be Pleiades members, and that have three or more observations. We include the two CORAVEL objects mentioned previously that were not observed at the CfA (PELS 30 and PELS 39). Targets that are known to be spectroscopic binaries are distinguished with different symbols from stars not previously flagged as binaries

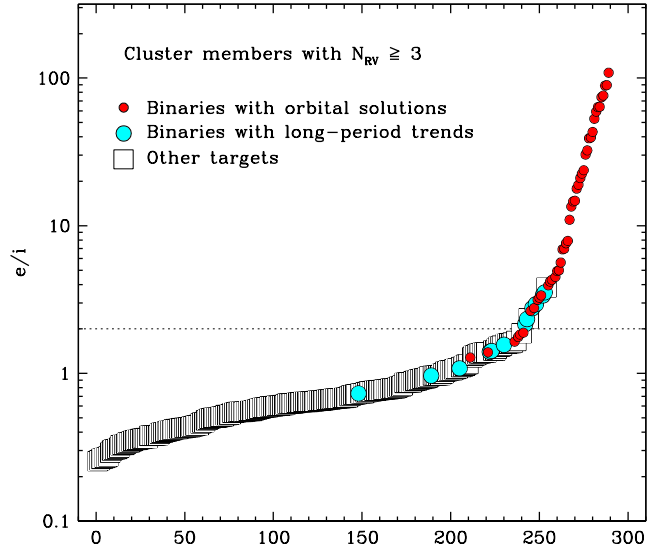


**Figure 9.** Values of  $e/i$  sorted in increasing order for Pleiades members in our sample, based on the merged CfA and CORAVEL data sets. Known binaries are marked as labeled, and the dotted line represents the adopted threshold for this work, above which stars are considered to be binaries.

(Table 4). The distribution shows a change in slope, or “knee”, at a value of  $e/i \approx 2$ . The vast majority of objects with larger values are known spectroscopic binaries reported in Sections 5, 6, and 7, with solved orbits or with long-term trends. We have therefore chosen to adopt this  $e/i$  value as our threshold for variability in the survey, and it is marked with a dotted line in the figure. A few of the binaries with solved orbits also appear below the line, along with several that have long-term trends. The latter have been identified mostly by visual inspection rather than by the scatter of the RVs. Not surprisingly, the binaries below the line tend to have small velocity amplitudes. We expect that a few other cases with smaller  $e/i$  values may also be long-period and/or low-amplitude binaries, but those are undetectable given the precision of our measurements.

Two objects not previously known to be binaries have  $e/i$  values larger than 2.0, and we therefore consider them to be velocity variables: AK I-2-121, and PELS 30. The first is rotating quite rapidly ( $v \sin i = 49 \text{ km s}^{-1}$ ), and the second was observed only with the CORAVEL, and has four measurements.

In addition to the  $e/i$  statistic, we have also computed the  $\chi^2$  value for each object along with its associated probability,  $P(\chi^2)$ . We include those probabilities in Table 4 as well, for readers who would like to use them to make their own selection of variables. We have found, however, that  $P(\chi^2)$  is much more sensitive to outliers than  $e/i$ , and for any reasonable probability threshold such as 0.01 or even 0.001, it leads to several dozen objects with low  $e/i$  values to be classified as variables, whereas visual inspection suggests they are most likely just more active. For this reason we have preferred to use the more conservative  $e/i$  statistic.

## 9. COMPLETENESS

While our sample contains several dozen confirmed spectroscopic binaries that have either computed orbits or obvious long-term trends, or that are revealed by their excess radial velocity scatter ( $e/i > 2$ ), we are likely to

**Table 12**  
Orbital Elements for Other Astrometric or Spectroscopic Pleiades Binaries Published Previously.

Name	$P$ (day)	$\gamma$ (km s <sup>-1</sup> )	$K_1$ (km s <sup>-1</sup> )	$K_2$ (km s <sup>-1</sup> )	$e$	$\omega_1$ (degree)	$T_0$ (HJD) (2,400,000+)	$a''$ (mas)	$i$ (degree)	$\Omega$ (degree)	Ref
HII 2147	6641 42	5.70 0.17	... ...	7.102 0.081	0.105 0.011	256.8 4.6	47284 107	62.32 0.45	75.78 0.46	141.80 0.19	1
TRU S26	71.8198 0.0084	3.94 0.78	21.1 1.3	... ...	0.284 0.048	111 11	58403.4 2.0	... ...	... ...	... ...	2
HII 563	3172.4 9.9	5.66 0.34	7.64 0.88	... ...	0.391 0.079	350 11	37784 82	... ...	... ...	... ...	2
TRU S194	3635 19	7.183 0.068	3.72 0.16	... ...	0.528 0.035	207.8 3.4	49190 47	... ...	... ...	... ...	2
HII 2168	290.984 0.079	... ...	26.55 1.41	36.89 0.22	0.2385 0.0063	151.9 2.2	50583.0 1.9	13.08 0.12	107.87 0.49	154.0 0.7	3
HII 1180	218.053 0.053	... ...	6.39 0.46	... ...	0.745 0.026	157.3 3.5	52039.73 0.73	... ...	... ...	... ...	4
HCG 76	32.7470 0.0013	5.31 0.17	26.75 0.30	29.19 0.29	0.1328 0.0043	30.8 3.2	57068.748 0.001	... ...	89.126 0.029	... ...	5
MHO 9	42.80 ...	4.6 1.3	16.4 3.0	39.3 6.8	0.406 0.056	132.0 9.8	57099.21943 0.00064	... ...	89.278 0.094	... ...	5
HII 3197	11106 99	... ...	... ...	... ...	0.5562 0.0018	221.51 0.29	55909.4 4.4	80.84 0.40	47.67 0.34	22.77 0.56	6
PPL 15	5.825 0.3	6.5 2.0	... ...	... ...	0.42 0.05	62 ...	50782.59 0.01	... ...	... ...	... ...	7

**Note.** —  $T_0$  is a reference time of primary eclipse for HCG 76 and MHO 9, and a time of periastron passage for the other systems. The last three elements are the angular semimajor axis ( $a''$ ), the inclination angle ( $i$ ), and the position angle of the ascending node ( $\Omega$ ). The second line for each system lists the  $1\sigma$  uncertainties. References in the last column are: (1) Torres et al. (2020); (2) Torres (2020); (3) Zwahlen et al. (2004); (4) Nemravová et al. (2010); (5) David et al. (2016); (6) Schaefer et al. (2014); and (7) Basri & Martín (1999).

have missed others because of our time sampling and the limited precision of our observations. This is surely the case for systems with low-mass companions, or for longer-period binaries, as not all our targets have been observed for the full duration of the survey. To estimate our completeness, we simulated a large number of binaries for each of our targets and used the same  $e/i$  criterion as above to decide when each synthetic binary would have been recovered. The number of recovered binaries divided by the number of simulations for each object then represents our completeness, or detection fraction.

We carried out these simulations for the 231 targets that have not previously been flagged as spectroscopic binaries, and that have three or more observations. Synthetic binaries were generated using the distributions of orbital elements for field stars, following the general procedure described by Geller et al. (2015). We sampled the orbital periods and mass ratios from the distributions of Raghavan et al. (2010) for solar-type binaries. For the eccentricities, those authors proposed a distribution that is flat up to at least  $e = 0.6$ , with a deficit of higher values possibly caused either by dynamical interactions or by a lack of measurements. Geller & Mathieu (2012) showed that a good representation of the entire set of eccentricities can be achieved with a Gaussian model having a mean of 0.39 and a standard deviation of 0.31. We adopted the latter function, and assumed circular orbits for periods shorter than the tidal circularization period, which is  $P_{\text{circ}} = 7.2$  days in the Pleiades (see Section 14). We also restricted the simulated binaries to configurations that are detached, as determined from the masses and radii adopted for the two components (see below). Our simulations accounted for the correla-

tion between the mass ratios and periods that is illustrated in Figure 17 of Raghavan et al. (2010) (see also Geller et al. 2015). Inclination angles were assumed to be distributed isotropically, and arguments of periastron and orbital phases were sampled from uniform distributions. Approximate primary masses and radii sufficient for this purpose were obtained from the PARSEC isochrone for the Pleiades shown in Figure 1, interpolated at the  $G_{\text{BP}} - G_{\text{RP}}$  color of each target as listed the Gaia EDR3 catalog. Secondary masses then followed from the mass ratios. Radii for the secondary components, which are also needed to compute the size of the Roche lobes and verify whether the configurations are detached, were assumed to scale with their masses. In generating binaries for any given object, we randomly perturbed the primary masses using a Gaussian distribution with a standard deviation of 50%, to account for possible systematic errors in the PARSEC model. With the primary and secondary masses known, we then calculated the velocity semiamplitudes, and predicted velocities at the actual times of observation for each star. Finally, we added Gaussian noise corresponding to the measured uncertainty at each epoch, and computed the  $e/i$  values. We repeated this for a population of  $10^5$  synthetic binaries for each target. Simulated systems resulting in  $e/i > 2$  were considered to be detectable, as with the real data.

We find that our survey is highly sensitive to binaries with orbital periods up to 100 days (97% completeness), and that we detect about 84% of the binaries with periods less than 1000 days, and 67% of the ones up to  $10^4$  days. We are increasingly less sensitive to longer periods, as shown in the left panel of Figure 10. Two of

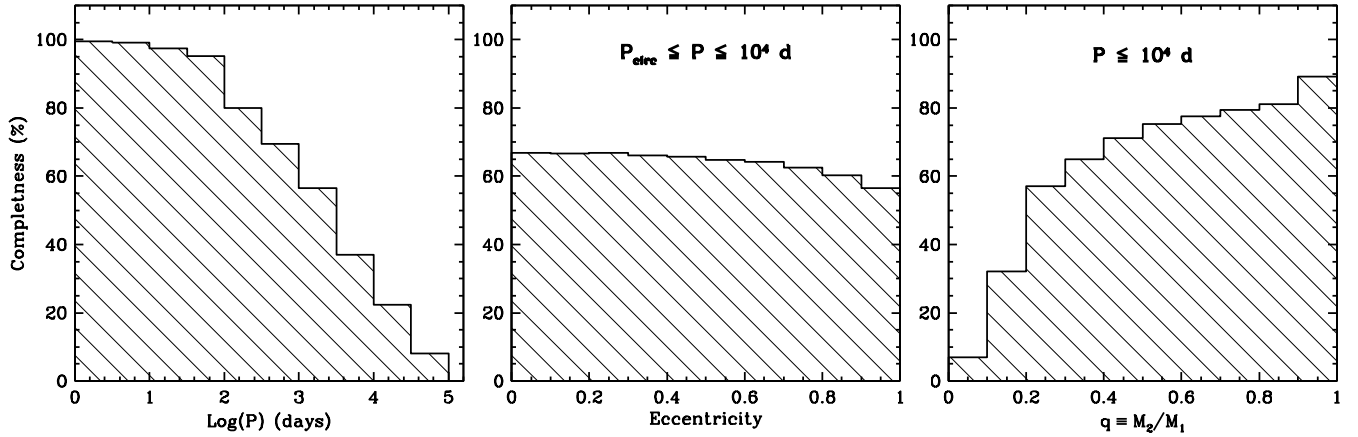


**Figure 10.** Completeness curves for the Pleiades binaries from our Monte Carlo simulations. The panels show our sensitivity as a function of orbital period, eccentricity (for periods  $P_{\text{circ}} \leq P \leq 10^4$  days), and mass ratio ( $P \leq 10^4$  days). See the text for an explanation of these ranges.

our targets have known orbital periods beyond  $10^4$  days. One is HII 3197, with  $P \approx 11,100$  days, but we do not include it in the statistical analysis below because its orbit was determined astrometrically, rather than from our RV measurements, which show little variation. The other long-period system is the hierarchical triple HII 2027, with  $P \approx 13,400$  days for its outer orbit. As a precaution we will exclude it as well, as the orbital elements may have suffered changes due to internal dynamics over the lifetime of the Pleiades, particularly for the inner pair. All other binaries have much shorter periods than this. Therefore, for the analysis of the distribution of orbital parameters below, we have chosen to restrict the study to binaries with periods less than  $10^4$  days.

Our completeness as a function of eccentricity out to periods of  $10^4$  days, shown also in Figure 10, is fairly flat and drops only slightly at the higher values. On the other hand, while we have good sensitivity to binaries with equal mass components (right panel), we miss many systems with low-mass secondaries, particularly below  $q = 0.2$ . Note that the completeness curves in each of these three parameters are not independent of each other. The orbital period has the largest impact on detectability, because shorter periods will typically lead to higher velocity amplitudes. The overall lower completeness in both eccentricity and mass ratio is caused in part by the longer-period binaries that are more difficult to detect, and that occur at all mass ratios and eccentricities.

## 10. DISTRIBUTION OF ORBITAL ELEMENTS

Armed with estimates of our ability to detect binaries with different properties, we now investigate the distributions of their orbital elements using the sample of 25 single-lined binaries in the Pleiades with known orbits, and 20 double-lined systems. As illustrated below, the majority of these binaries have primary components quite similar in mass to the Sun. Given the relatively small size of the sample, we refrain from dividing it up by mass, and will consider it as a single set of “solar-type” binaries for comparison with other populations.

### 10.1. Period Distribution

In Figure 11 (top) we show the distribution of orbital periods for the 45 systems in our Pleiades sample with  $P \leq 10^4$  days (i.e., excluding HII 3197 and HII 2027; see

above). The hatched histogram is the observed distribution, and the solid gray histogram includes the corrections for incompleteness described in the previous section. For reference, we show also with a dashed line the log-normal period distribution from Raghavan et al. (2010) for solar-type field stars, which we have normalized to the same number of binaries found in our sample up to  $10^4$  days. The field distribution is characterized by a mean period of  $\log P = 5.03$  and a standard deviation of  $\sigma_{\log P} = 2.28$ , with  $P$  in units of days.

The cumulative distribution of the observed periods is shown in the bottom panel, along with the corresponding distribution from Raghavan et al. (2010) transformed so that it reflects the same level of incompleteness as the observed distribution. We obtained this curve by multiplying the Gaussian model by our corresponding incompleteness function from Figure 10, and then integrating. An Anderson-Darling test on the two distributions gives a  $p$  value of 0.033, implying the shape of the cumulative distribution function of binary periods in the Pleiades up to  $10^4$  days is not statistically distinguishable from that of solar-type binaries in the field.

### 10.2. Eccentricity Distribution

The observed eccentricity distribution for the 40 binaries with periods between the circularization period (7.2 days) and  $10^4$  days is presented in Figure 12 (top). Also shown in gray is the corresponding histogram corrected for incompleteness, based on the results in Section 9. We indicate with a dashed line the eccentricity distribution proposed by Geller & Mathieu (2012) that we adopted for our simulations in Section 9, which is a Gaussian with a mean of  $e = 0.39$  and a standard deviation of  $\sigma_e = 0.31$ . The dotted line is for the flat distribution proposed originally by Raghavan et al. (2010). The corresponding cumulative distribution functions are shown in the bottom panel, where the filled circles represent the observed distribution. The two models have been modified in the same way as explained above for the period distribution, to include the same incompleteness as the observations. Anderson-Darling tests indicate the observed distribution is statistically distinct from both the Gaussian model and the flat model, with  $p$  values



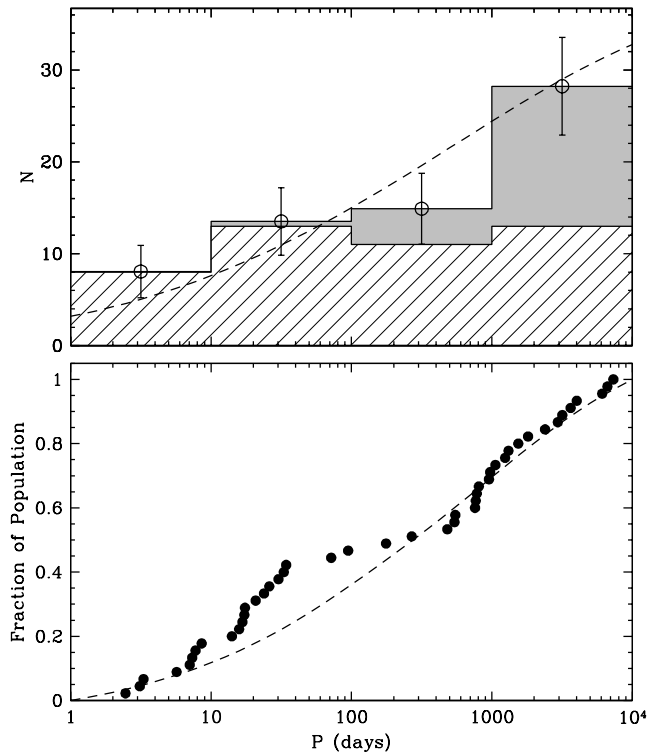


**Figure 11.** Observed period distribution for the Pleiades binaries in our survey with periods up to  $10^4$  days, shown as a hatched histogram in the top panel, and in cumulative distribution form in the bottom panel (filled circles). In the top panel, the solid gray histogram includes the corrections for incompleteness derived in Section 9. Error bars on the corrected distribution are from counting statistics. For reference, in both panels we show also the log-normal period distribution for field stars from Raghavan et al. (2010), normalized in the top panel so that the integral under the curve equals the number of binaries in the sample, after corrections for incompleteness.

under 0.001 in both cases.<sup>6</sup> While qualitatively similar eccentricity distributions as in the Pleiades are found in some older clusters such as M67 (4 Gyr; Geller et al. 2021) and NGC 188 (7 Gyr; Geller & Mathieu 2012), in the sense of peaking at small values and tailing off at high values, there may be differences in detail, as we find in the field. The Pleiades distribution is well represented by a Gaussian model with a mean of  $e = 0.16$  (smaller than found by Geller & Mathieu 2012) and  $\sigma_e = 0.37$ . This is shown with a solid line in the top panel of Figure 12.

### 10.3. Mass Ratio Distribution

The distribution of mass ratios in a population of binaries provides valuable constraints on their formation mechanisms (e.g., Bodenheimer et al. 1993; Bate & Bonnell 1997; Clarke 2001; Halbwachs et al. 2003), and on the dynamical evolution of star clusters to which the binaries belong (Hut et al. 1992; Benacquista & Downing 2013). A typical sample of binaries with known orbits will usually consist of both single-lined and double-lined systems. The ones that are double-lined provide a direct measure of  $q \equiv M_2/M_1$

<sup>6</sup> Strictly speaking, the flat model was proposed by Raghavan et al. (2010) to be a reasonable representation for field binaries only up to  $e = 0.6$ , beyond which they noted a deficit of eccentric systems. Even over this restricted range, the Anderson-Darling test indicates a rather significant difference with the observed distribution in the Pleiades ( $p = 0.0044$ ).

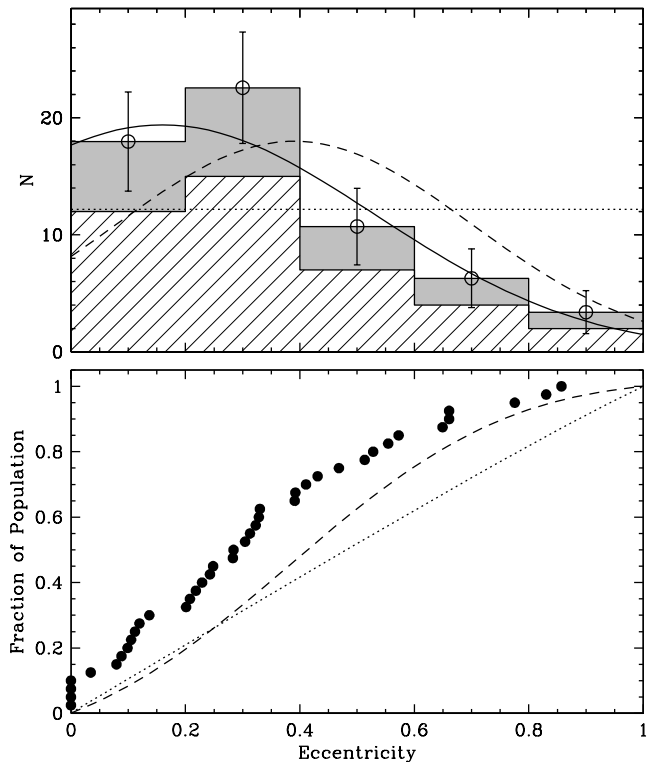


**Figure 12.** Observed eccentricity distribution for the Pleiades binaries with  $P_{\text{circ}} \leq P \leq 10^4$  days, shown in the same way as the periods in Figure 11. The dashed line in the top panel is the Gaussian model proposed by Geller & Mathieu (2012) for field binaries of solar type, and the dotted line represents the uniform distribution of Raghavan et al. (2010), both normalized to the same number of binaries in our sample. The solid line corresponds to a Gaussian fit to the Pleiades distribution, with a mean of  $e = 0.16$  and  $\sigma_e = 0.37$ . The bottom panel shows the corresponding cumulative distribution functions, where the two models have our observational incompleteness applied so that they can be compared directly with the observations.

from the ratio of the velocity semiamplitudes,  $K_1/K_2$ . For single-lined binaries, on the other hand, the information is more limited and comes only in the form of the mass function,  $f(M)$ , which requires both the primary mass and the orbital inclination to be known in order to calculate the mass ratio.

It is therefore common to apply statistical inversion techniques in order to infer the shape of the mass-ratio distribution for SB1s from the distribution of  $f(M)$ , or some function of  $f(M)$ , and to then add in the SB2s. Many such methods with varying degrees of sophistication have been developed (see, e.g., Lucy & Ricco 1979; Mazeh & Goldberg 1992; Heacox 1995; Halbwachs et al. 2003; Carquillat & Prieur 2007; Boffin 2010; Curé et al. 2015; Shahaf et al. 2017). A few of them are parametric in the sense of having to propose some a priori form for the mass-ratio distribution of SB1s, while others are not. A common assumption in all of these methods is that there is no other information on the masses except perhaps for a rough estimate of  $M_1$ , e.g., from a spectral type.

However, in a cluster such as the Pleiades with a known age and metallicity, this is not necessarily the case. Brightness measurements for the combined light of a binary contain useful information on the individual masses that can be extracted if the parallax is known,

and if there is no contaminating flux from other sources. The only other ingredient needed is a model isochrone for the cluster, such as the one shown in Figure 1. With these constraints and the dynamical information from the orbits, it is possible to estimate the mass ratio directly for each SB1, obviating the need for a statistical procedure. This is the approach we have chosen to follow here. For a somewhat similar application of this idea, see Goldberg & Mazeh (1994).

In addition to using the brightness measurements for each binary in the three Gaia bandpasses ( $G$ ,  $G_{BP}$ ,  $G_{RP}$ ), we also extracted the near-infrared  $JHK_S$  magnitudes from the 2MASS catalog (Cutri et al. 2003), which should be more sensitive to the light contribution from the secondaries because they are of later spectral type than the primaries. We corrected the magnitudes for extinction following Cardelli et al. (1989), assuming an average reddening for the cluster of  $E(B - V) = 0.04$  mag, and adjusted the magnitudes for the distance modulus of each SB1 using its parallax as listed by Gaia EDR3. For the comparison of these magnitudes with the predictions from the isochrone, we found it more convenient to use as a constraint the minimum secondary mass,  $M_2 \sin i = (2\pi G)^{-1/3} P^{1/3} \sqrt{1 - e^2} K_1 (M_1 + M_2)^{2/3}$ , as listed in Table 6, rather than the mass function. For each binary we then explored a range of  $M_1$  and  $\sin i$  values, and for each trial pair  $\{M_1, \sin i\}$  we solved for  $M_2$  using the equation above, requiring the mass ratio to be no larger than unity. If this last condition was not met during the iterations, we simply reversed the masses, as this does not affect the photometry for the combined light. This was continued until the  $\chi^2$  value between the six observed magnitudes and the model fluxes at  $\{M_1, M_2\}$  was minimized. We adopted the 2MASS uncertainties as given, but to be conservative and allow for errors in the model fluxes, we inflated the uncertainties for the Gaia magnitudes to 0.02 mag, as they are typically much smaller (often less than 0.001 mag).

The composition of our binary sample by mass is illustrated in Figure 13. The panels show the nominal primary and secondary values from the procedure described above, to which we have added the corresponding values for the SB2s from a similar exercise using the known mass ratios instead of the minimum secondary masses. The primary masses for the ensemble of binaries are seen to be concentrated around one solar mass.

To propagate uncertainties for the SB1s, we used a Monte Carlo procedure whereby we repeated the fits to the photometry 1000 times for each binary, perturbing the values of all measurements in each simulation. This was done by adding Gaussian noise to  $M_2 \sin i$  with a standard deviation equal to its uncertainty, and similarly for the magnitudes. We also added Gaussian noise to the reddening in the amount of 0.02 mag, to account for the fact that reddening is not uniform across the cluster (see Breger 1986; Taylor 2008). Finally, we broadened the individual mass distributions by perturbing each estimate by 20% of its value, to allow for further systematic errors in the model masses and to provide a degree of smoothing given the relatively small size of the SB1 sample. We then merged the resulting individual mass-ratio distributions for all binaries to construct the distribution for the ensemble.

Out of our sample of 25 SB1s, a search in the literature revealed that one of them, HII 2500, has a visual companion currently separated by  $0''.3$  that is 1.7 mag fainter in the  $K$  band (Bouvier et al. 1997), and which is not the secondary in the binary (see Section 5.3). As this third star is likely affecting the photometry and may therefore bias the mass estimates, we have chosen to remove it. Similarly, HII 563 has a companion about 1.6 mag fainter detected multiple times by the lunar occultation technique, which appears also to not be the secondary in the SB1 system (see Torres 2020). We have excluded it as well, leaving 23 objects in the sample with periods up to  $10^4$  days.

Given that these mass ratios are strictly model-dependent, one may ask to what extent systematic errors in the models might cause distortions in the true shape of the mass-ratio distribution. To investigate this, we used the sample of SB2s, and calculated the minimum secondary mass from the orbital elements as if the secondaries had not been detected, i.e., using only information about the primaries. We then followed the same procedure explained earlier for the SB1s to infer the mass ratios, and compared them with the  $q$  values directly measured for these systems. For this test we did not consider the triple-lined system HII 1338 because the photometry is contaminated by the light from the third star. Only one other SB2 (HII 1348) has a known close visual companion at about  $1''.1$ , but it is more than five magnitudes fainter in the  $K$  band, so its effect will be negligible. The result of the comparison is shown in Figure 14, along with a line representing the one-to-one relation. The average mass ratio difference in the sense  $q_{\text{model}} - q_{\text{obs}}$  is 0.04, with a scatter of 0.11. The median absolute deviation from the one-to-one relation is 0.076, which corresponds to about a 10% error for a typical mass ratio of  $\sim 0.8$  for this sample.

An additional check is available from the fact that one

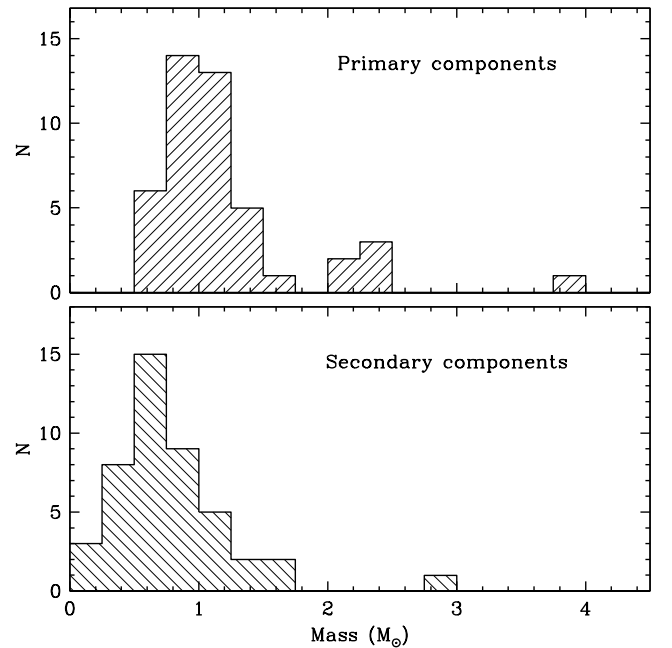


**Figure 13.** Distribution of the primary and secondary masses of our SB1 and SB2 binaries, derived from the dynamical information provided by our orbital solutions combined with photometric information from Gaia and 2MASS (see the text).

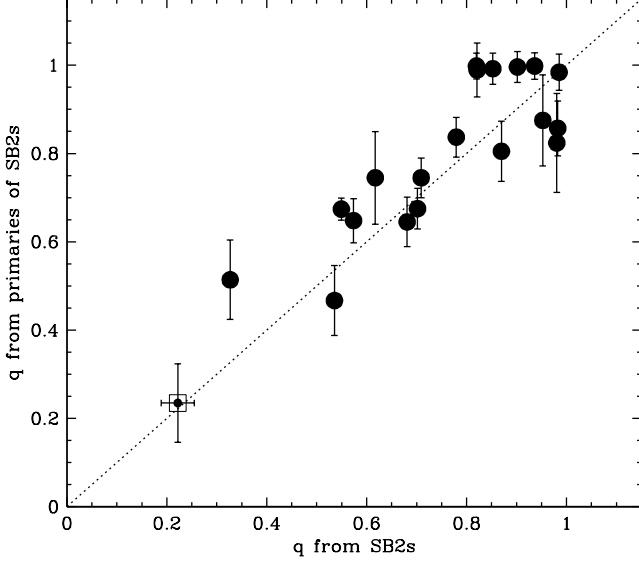


**Figure 14.** Comparison between inferred and measured mass ratios for 19 SB2s in the Pleiades, with HII 1338 excluded. The inferred values were derived by using the model isochrone shown in Figure 1, along with brightness measurements for the combined light from Gaia and 2MASS, and the measured minimum secondary masses calculated as if the system were single-lined. The dotted line represents the one-to-one relation. The smaller dot with a square corresponds to HII 2407, a single-lined eclipsing system used as a check (see the text).

of our SB1s, HII 2407, is an eclipsing binary discovered by David et al. (2016) based on Kepler/K2 photometry. The individual masses we derive using our  $M_2 \sin i$  value, the Gaia and 2MASS magnitudes, and the isochrone, are  $M_1 = 0.80 \pm 0.04 M_\odot$  and  $M_2 = 0.19 \pm 0.07 M_\odot$ , giving a ratio of  $q = 0.24 \pm 0.09$ . These agree well with the values  $M_1 = 0.81 \pm 0.08 M_\odot$ ,  $M_2 = 0.18 \pm 0.02 M_\odot$ , and  $q = 0.22 \pm 0.03$  reported by David et al. (2016), supporting the accuracy of our procedures at the low end of the distribution. We represent our mass ratio for this system along with theirs as a small dot and a square in Figure 14. Another consistency check is provided by HII 2147, for which Torres et al. (2020) determined individual masses from a combination of astrometric observations from VLBI and radial velocities for the secondary only. They reported primary and secondary masses of  $0.978 \pm 0.024 M_\odot$  and  $0.897 \pm 0.022 M_\odot$ , giving  $q = 0.917 \pm 0.004$ . We obtained  $0.946 \pm 0.049 M_\odot$ ,  $0.918 \pm 0.049 M_\odot$ , and  $0.969 \pm 0.073$ , respectively, which are within 3% for the masses and within 6% for  $q$ .

These tests suggest that, while not perfect, our inferred mass ratios for the SB1s in the sample are sufficiently accurate for our statistical purposes. The distribution of the  $q$  values is displayed in histogram form in the top panel of Figure 15. Because of the relatively small number of SB1s (23), we have chosen a bin size of 0.2, equivalent to about twice the scatter in  $q_{\text{model}} - q_{\text{obs}}$  mentioned earlier. The gray histogram includes the corrections for incompleteness from Section 9. As expected for SB1s, the distribution rises toward smaller values, although the leftmost bin should be interpreted with caution as the incompleteness corrections are a factor of four larger than the actual number of binaries in that range. A somewhat surprising feature of this distribution, however, is that the rightmost bin is not empty, as would be expected for SB1s, but in fact contains three binaries with mass ra-

tios larger than 0.8, which are more typical of SB2s. The three systems are AK II-346, HII 1762, and HII 2147. In all three cases (and no others) there is evidence that the star whose velocities we measured is the secondary rather than the primary. This was confirmed for HII 2147 by Torres et al. (2020). For the other two, the evidence is based on the appearance of the cross-correlation profiles, which display broad wings suggesting the presence of a much more rapidly rotating star that we presume to be the (more massive) primary, in addition to the narrow(er) peak that we are able to measure. The fact that we detect both stars is then an indication of similar brightness, and therefore of similar mass.

The second panel of Figure 15 shows the distribution of measured mass ratios for the 20 SB2s. In this case it is not obvious that corrections for incompleteness should be applied, because double-lined systems are often detectable from a single exposure, and are then immediately placed on higher observing priority than stars that only show single lines. We therefore present the distribution without any corrections. The preference for higher mass ratios is typical of SB2s in other populations, and responds to the fact that companions are more easily detected when they are similar to the primary in mass, and therefore in brightness.

The sum of the SB1 and SB2 histograms is shown in the third panel of Figure 15, with error bars added to indicate formal uncertainties from counting statistics. The distribution is consistent with being flat, as indicated by the dashed line, with the caveat mentioned above about the smallest bin. The cumulative distribution of mass ratios, measured directly for the SB2s and inferred as explained above for the SB1s, is shown in the bottom panel of the same figure. The dashed line corresponds to the flat distribution modified as we described previously for the period and eccentricity distributions, to reflect the same level of incompleteness as the observations. There is no distinction between the two based on the Anderson-Darling test.

An earlier study of the mass-ratio distribution in the Pleiades by Goldberg & Mazeh (1994) was based on a sample of only 9 spectroscopic binaries, more than four times smaller than ours, but also found it to be essentially flat, or perhaps rising slightly toward  $q = 1$ . A comparison between the mass-ratio distribution in the Pleiades and in other populations suggests there may be some differences. In NGC 188, for example, Geller & Mathieu (2012) found a distribution that rises toward lower mass ratios, along with a slight excess of binaries with  $q > 0.9$ . The distribution for M67 was also found to be rising toward small mass ratios (Geller et al. 2021), but without an excess of equal-mass binaries. For solar-type binaries in the field, Raghavan et al. (2010) reported a roughly flat distribution in the range  $0.2 < q < 0.95$ , with some evidence for an excess of equal-mass pairs. A study of a sample of high proper motion field stars by Goldberg et al. (2003) found a rise down to  $q \sim 0.2$ , a drop below that, and a peak near  $q = 0.8$ . A similar sample with a higher fraction of SB2s was investigated by Mazeh et al. (2003), and their results indicated the mass ratios follow a uniform distribution between 0.3 and 1.0, with an apparent rise toward lower values down to 0.1. It is unclear to what extent these differences may depend on the analysis methodologies, or on the details of the

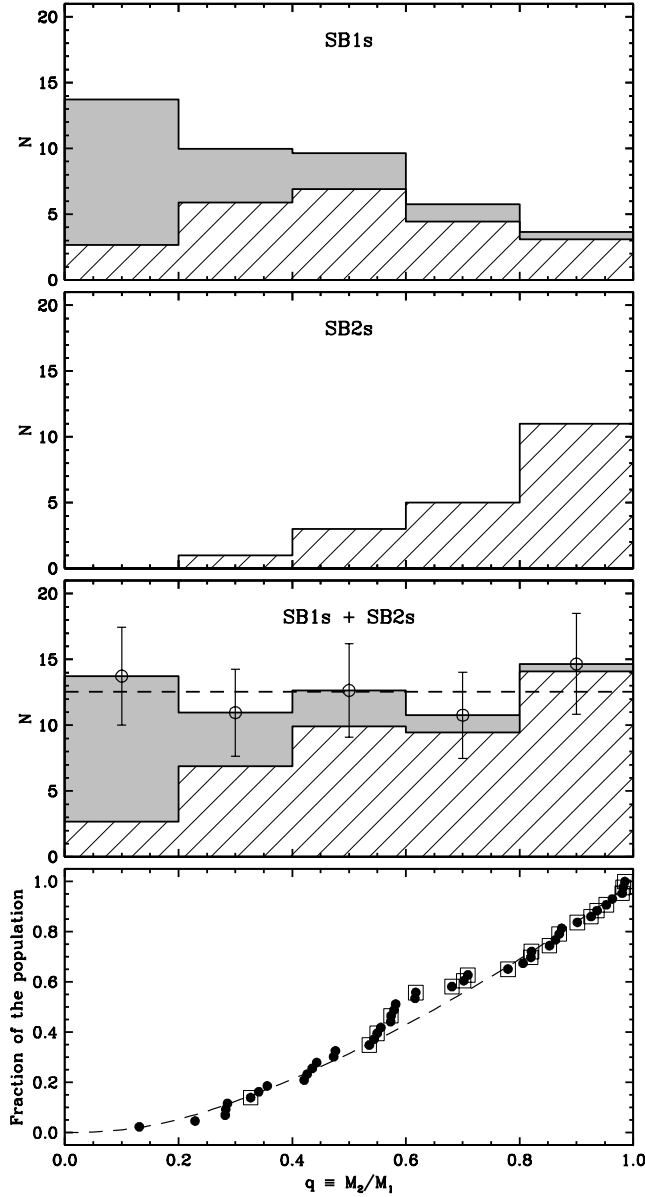


**Figure 15.** Mass ratio distribution for the SB1s and SB2s (top two panels) with periods  $P < 10^4$  days, along with the merged samples (third panel). Hatched histograms correspond to the observed distributions, and the gray histograms add the incompleteness corrections from Section 9. For the SB1s the observed distribution is based on estimates of the individual mass ratios using brightness measurements from Gaia and 2MASS, the measured minimum secondary masses, and a model isochrone for the Pleiades (see the text). Note that the smallest bin for the SB1s may be unreliable as the incompleteness corrections are four times larger than the number of observed binaries. Error bars in the third panel are based on counting statistics, and the dashed line represents a flat distribution. The bottom panel shows the cumulative distribution function for the SB1s (dots) and SB2s (dots with squares), along with the curve corresponding to the flat distribution modified to have the same incompleteness as the observations.

sample selection, including the mass and period ranges.

#### 11. THE SPECTROSCOPIC BINARY FREQUENCY IN THE PLEIADES

As indicated earlier, only two of the objects in our sample with known orbits have periods approaching the duration of our survey, which is  $\sim 15,000$  days, or  $\sim 40$  yr: HII 3197 ( $P \approx 11,100$  days), and the triple system

**Table 13**  
Binary Frequency in the Pleiades Compared with Other Populations.

Population	Age (Gyr)	Frequency (%)	Source
Blanco 1	0.1	$20 \pm 6$	1
Pleiades	0.125	$25 \pm 3$	This paper
M35	0.15	$24 \pm 3$	2
NGC 7789	1.6	$31 \pm 4$	3
NGC 6819	2.5	$22 \pm 3$	4
M67	4	$34 \pm 3$	5
NGC 188	7	$29 \pm 3$	6
Field	...	$14 \pm 2$	7
Halo	$\sim 10$	$15 \pm 2$	8

**Note.** — Binary frequencies for solar-type stars in different populations up to orbital periods of  $10^4$  days, corrected for incompleteness. Sources are: (1) Mermilliod et al. (2008); (2) Leiner et al. (2015); (3) Nine et al. (2020); (4) Milliman et al. (2014); (5) Geller et al. (2021); (6) Geller & Mathieu (2012) (7) Raghavan et al. (2010); (8) Latham et al. (2002). The estimate for Blanco 1 did not specify an upper limit to the period, but is presumed to be similar to the others (see Geller & Mathieu 2012), and is not corrected for incompleteness. Similarly for the halo sample. For Blanco 1 we have added an uncertainty based on the number of binaries discovered in that survey.

HII 2027 ( $P \approx 13,400$  days for the outer orbit). We do not consider the former because its binary nature was discovered astrometrically rather than spectroscopically (see Schaefer et al. 2014). All other systems have periods roughly half that of the outer orbit of HII 2027, or shorter. As for our studies of the distribution of orbital properties, we therefore chose here to adopt a cutoff period of  $10^4$  days for computing the multiplicity frequency, which we define as the fraction of targets in our sample that are in multiple systems, including triples. We refer to it in the following simply as the binary frequency. Our detection completeness in this period range is 67% (Section 9).

Of the 289 objects in our survey that we consider to be Pleiades members and have three or more observations, we have identified 25 SB1s and 21 SB2s (we include here the inner binary of the triple system HII 2027). Two additional objects have variable radial velocities ( $e/i > 2$ ), but we lack sufficient observations or coverage to determine a period; we will assume here that both periods are shorter than  $10^4$  days. The raw binary frequency is then 17% (48/289), which after correction for incompleteness becomes  $25 \pm 3\%$ . While this binary fraction includes stars of all spectral types (from B to M), restricting the sample to just the “solar-type” stars of spectral type FGK does not change the result.

Table 13 lists determinations of the binary fraction up to the same orbital period for solar-type (FGK) stars in six other open clusters, and in two field samples in the solar neighborhood (disk stars in the field, and halo stars). Interestingly, we find that within the uncertainties, our estimate for the Pleiades is quite consistent with what has been found in a variety of other populations spanning nearly two orders of magnitude in age, except perhaps for the field and halo samples. We note that the latter has not been corrected for incompleteness, so it is only a lower limit. The binary frequency for solar-type field stars appears decidedly smaller than in several of the clusters, particularly NGC 7789, M67, and NGC 188. Geller & Mathieu (2012) had already pointed this out for NGC 188, and suggested it may be a dynam-



ical signature, as  $N$ -body simulations predict single stars are preferentially lost from a cluster through evaporation because they are generally lighter than binaries.

Even though our sensitivity to binaries drops for longer periods, the fact that we have uncovered about a dozen systems with long-term velocity trends shows that we can still detect binaries with periods that are longer than the duration of the survey. These systems are valuable because they begin to bridge the gap between spectroscopic and astrometric binaries, and provide useful information on the multiplicity fraction out to much larger binary separations. While their orbital periods are not known, they are likely to be a few times longer than the span of our observations, perhaps of order a century or two. Circumstantial evidence for this is given by the case of HII 717, which shows a monotonically decreasing velocity drift (Figure 24) and has a visual companion at  $0''.213$  (Mason et al. 1993) that is almost certainly the same as the companion we detect spectroscopically. At the distance to the Pleiades, this separation corresponds to a period of roughly a century, or perhaps slightly longer. A few other objects with long-term RV drifts also have visual companions, but they are much wider and are unlikely to be the ones responsible for the RV variations.

If we then adopt a new period cutoff of  $10^5$  days, corresponding to about 270 yr, we find that our completeness is reduced to 49%. Including now in the tally the 12 systems with long-term drifts, the raw multiplicity frequency out to this period is  $60/289 = 21\%$ , or  $42 \pm 4\%$  once the correction for undetected binaries is applied. Based on the study of Raghavan et al. (2010), solar-type binary systems in the field occur with a frequency of about  $22 \pm 3\%$  up to the same period of  $10^5$  days, which is significantly lower than in the Pleiades. These wider binaries are more susceptible to ejection from a cluster, so it is possible that this difference is in fact a signature of ongoing evaporation in the Pleiades, as proposed above for NGC 188 by Geller & Mathieu (2012).

If the period distribution in the Pleiades is assumed to be consistent with that of solar-type binaries in the field, an extrapolation of our binary frequency from a cutoff of  $10^4$  days to orbits of any period results in a total fraction of  $76 \pm 5\%$ , again significantly higher than the rate in the field (44%; Raghavan et al. 2010). Studies by others of the total binary frequency in the Pleiades using the distribution of stars in the color-magnitude diagram have produced similarly high estimates: Kähler (1999) reported 60–70%, and Converse & Stahler (2008) obtained 68–76%. We note, however, that the extrapolation mentioned above may not be valid, as Deacon & Kraus (2020) have concluded that the wide binary fraction in the Pleiades (and also in other clusters) is low: approximately 2% between 300–3000 au, corresponding to a range of  $\log P$  in days of about 6.3–7.8.

## 12. ASTROMETRIC BINARIES

Much wider binaries than we can detect spectroscopically in the Pleiades have been found by adaptive optics, speckle interferometry, and lunar occultation techniques. The most extensive and systematic surveys (excluding those for substellar companions) have been carried out by Bouvier et al. (1997), Richichi et al. (2012), and Hillenbrand et al. (2018), and resulted in the discovery of several dozen visual companions to our targets.

Many others have been found serendipitously by other investigators. Most of these companions are within a few arc seconds of the primaries, and are likely physically associated with them.

Cross-matching our target list against the Gaia EDR3 catalog revealed companions to another dozen or so objects, some much wider and fainter than reported by others. Many of these have been announced previously by Deacon & Kraus (2020). In several cases the companions are also on our target list, and therefore have measured velocities. For many of them Gaia also lists the proper motion and parallax, so it is possible to confirm the physical association, or at least membership in the cluster. We have ignored any Gaia companions failing this check.

Table 14 is a compilation of 75 of our targets with companions listed in the Washington Double Star Catalog (WDS; Hartkopf et al. 2001) separated by less than  $20''$ , supplemented with other discoveries from the literature. We restrict the list to members of the cluster, and omit companions that have been shown to be background stars. Targets with notes of interest in the Appendix are flagged in the last column of the table. Three of the companions are reported to be substellar: those around HII 1348 (Geißler et al. 2012), AK I-2-199 (Konishi et al. 2016), and HII 1132 (Rodríguez et al. 2012).

There are 58 objects in our sample that have one or more visual companions that are *not* also spectroscopic binaries, i.e., that represent new multiple systems not considered previously. This list is likely incomplete, however, in part because of the intrinsic sensitivities of the various astrometric surveys. For example, the Gaia EDR3 catalog is known to be missing many close pairs within about  $1''.5$  due to instrumental limitations, and many more below  $0''.7$  (Fabricius et al. 2020). Furthermore, not all our targets have been examined for close companions.

If the total binary fraction in the Pleiades is as high as our estimate of 76% in the previous section, which assumes the same period distribution as in the field, it would mean there should be a total of 220 binary or multiple systems in our sample. The number of spectroscopic binaries uncovered by our survey up to periods of  $10^5$  days is 60, which after correction for incompleteness becomes 122 (60/49%). This period cutoff corresponds to an angular separation of  $\sim 0''.3$  at the distance to the Pleiades, and most of the astrometric binaries in Table 14 (43 out of the 58 that represent additional multiples) are indeed wider than this, so they complement the spectroscopic observations well by sampling the regime to which we have no sensitivity. We would therefore expect a total of  $220 - 122 = 98$  binaries wider than about  $0''.3$ , whereas we find only 43.<sup>7</sup> This would imply a total binary frequency of  $(122 + 43)/289 = 57\%$ , which is independent of any assumption on the shape of the period distribution, yet is still higher than in the field. It is only a lower limit, however, as we have excluded lunar occultation pairs that may actually be wider than  $0''.3$ , and some number of astrometric companions to our targets

<sup>7</sup> Note that the majority of the separations under  $0''.3$  are from lunar occultations, which are only lower limits because they represent the angular separation projected in the direction of the motion of the Moon during the event. Their true separations are unknown.

**Table 14**  
Astrometric Companions to our Target Stars.

	Name	WDS ID	Discov.	$\rho$ (")	Mag. diff. (mag)
7	AK III-153	03313+2515	A 1825	2.9	4.86( <i>G</i> )
56*	HCG 65	...	...	1.3	0.08( <i>G</i> )
69*	HII 102	03434+2314	BOV 2 AB	3.6	3.12( <i>K</i> ), 5.34( <i>G</i> )
70	HII 97	03434+2500	BOV 1	0.7	1.62( <i>K</i> )
72*	TRU S45	03435+2244	OCC 97 Aa,Ab	0.1	0.0
72*	TRU S45	03435+2244	STF 438 AB	1.7	1.0( <i>V</i> ), 0.88( <i>G</i> )

**Note.** — Companions are mostly from the Washington Double Star Catalog (WDS), and are listed only for cluster members. Columns after the target name give the WDS identifier, the discoverer code and component designations as listed in the WDS, the angular separation from the most recent measurement available, and magnitude differences from the WDS or other sources, including Gaia. Bandpasses are indicated in parentheses, when available. An asterisk after the running number calls attention to notes in the Appendix. (This table is available in its entirety in machine-readable form.)

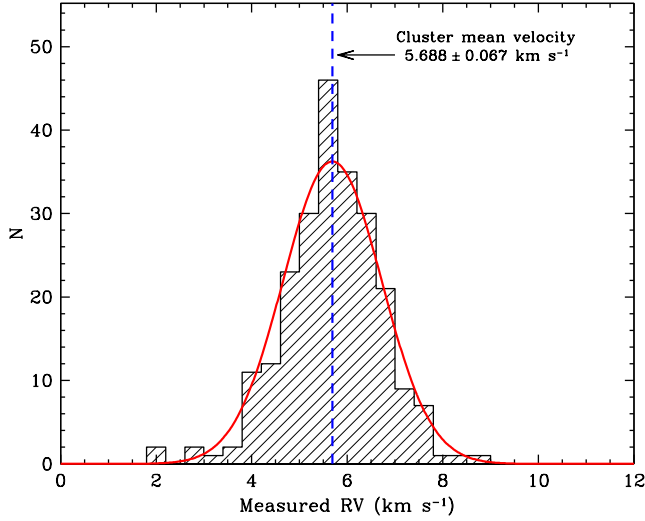


**Figure 16.** Histogram of the weighted mean radial velocities for 234 members of the Pleiades cluster. Binaries for which we only see long-term trends are excluded, as are the early-type stars reported by Torres (2020) (see the text). For binaries with orbits, we used their center-of-mass velocities.

have likely gone undetected.

### 13. MEAN CLUSTER VELOCITY AND INTERNAL VELOCITY DISPERSION

A histogram of the weighted mean velocities for 234 cluster members is shown in Figure 16. It includes all objects with at least three RV observations, but excludes the early-type stars published earlier (Torres 2020) because their velocities were measured in a different way that makes it difficult to place them on the same reference system as the ones in this paper. Objects with long-term trends have also been excluded, along with a few with very large velocity uncertainties that make them unreliable. For binaries with orbital solutions, we used the center-of-mass velocity rather than the mean RV. We left out six of the binaries with orbital fits (HII 164, HII 605, HCG 495, AK V-198, HII 1392, and HII 1431) because our solutions in Table 7 show a significant primary/secondary velocity offset of more than  $0.5 \text{ km s}^{-1}$ , which can potentially bias the center-of-mass velocity (see Section 5).

The mean radial velocity,  $5.688 \pm 0.067 \text{ km s}^{-1}$ , is very close to the result from the Gaia mission (DR2), which is  $5.65 \pm 0.09 \text{ km s}^{-1}$  (Gaia Collaboration et al.

2018b). The standard deviation of the 234 measurements is  $1.03 \text{ km s}^{-1}$ , although this does not represent the true velocity dispersion of the cluster in the radial direction. Observational errors will tend to inflate the scatter, as will the presence of unrecognized binaries and any unrecognized non-members there may still be in the sample. Furthermore, because of the large angular extent of the Pleiades on the plane of the sky, there is a radial velocity gradient of several  $\text{km s}^{-1}$  across the cluster due to changes in the projection of the mean space velocity along the line of sight. Additionally, the measured radial velocities do not reflect the true motion of a star's center of mass, as they are affected by the gravitational redshift and convective blueshift, which depend on spectral type. This can cause extra scatter in the measured velocities.

The projection effect dominates the scatter of the raw velocities. We removed this bias by subtracting from each star the radial velocity predicted using the object's coordinates and the space velocity vector of the center of the cluster, determined on the basis of the proper motions and parallaxes of member stars (see, e.g., Gaia Collaboration et al. 2017, eq. A.13). These predicted velocities, which range between  $3.5$  and  $8.2 \text{ km s}^{-1}$ , are referred to as astrometric radial velocities. The components of the velocity vector in the equatorial system, adopted from the latest determination from Gaia DR2 (Gaia Collaboration et al. 2018b), are:

$$\begin{aligned} V_x &= -1.311 \pm 0.070 \text{ km s}^{-1} \\ V_y &= +21.390 \pm 0.105 \text{ km s}^{-1} \\ V_z &= -24.457 \pm 0.057 \text{ km s}^{-1}. \end{aligned}$$

The mean residual velocity for the 234 stars (observed minus predicted) is  $\Delta = +0.015 \pm 0.050 \text{ km s}^{-1}$ , indicating excellent agreement between the spectroscopic and astrometric velocities, on average. The scatter around this value is reduced to  $0.77 \text{ km s}^{-1}$ .

Observational errors in our sample depend quite strongly on the projected rotational velocity, among other factors. A histogram of the errors of the mean velocities is seen in Figure 17. To ensure that we use the most precise measurements for the estimate of the velocity dispersion in the Pleiades, we restricted the analysis to the 157 objects with errors smaller than  $0.5 \text{ km s}^{-1}$ . The standard deviation of the mean velocities for these objects, with the projection effect removed,

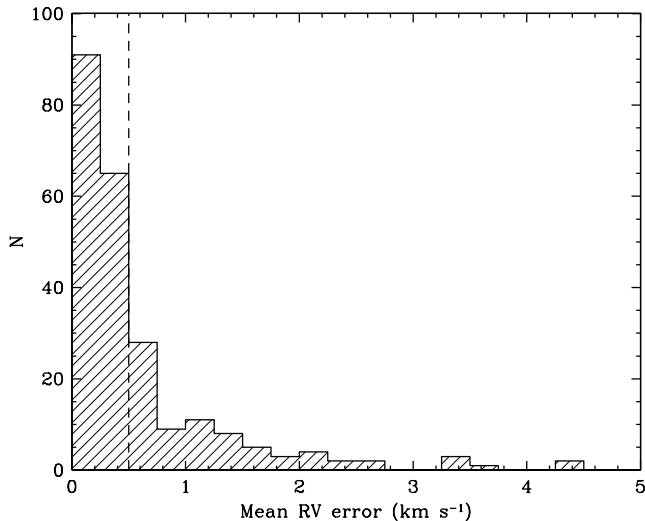


**Figure 17.** Histogram of the errors of the weighted mean radial velocities for 234 members of the Pleiades cluster (see the text). Only objects with errors smaller than  $0.5 \text{ km s}^{-1}$  (dotted line) have been used for the calculation of the true velocity dispersion in the cluster.

is  $0.62 \text{ km s}^{-1}$ . After correction for observational errors following McNamara & Sekiguchi (1986), we obtained a preliminary estimate of the dispersion within the cluster of  $0.56 \pm 0.04 \text{ km s}^{-1}$ .

This still contains the effect of undetected binaries, mostly with very long periods. These systems will show constant velocities over the duration of our survey, but their average RV may be slightly offset from the expected radial motion in the cluster. To account for this bias as much as possible, we removed from the above set of 157 targets the 21 stars that have astrometric companions reported in Section 12, leaving 136 objects. The dispersion is reduced to  $0.50 \pm 0.04 \text{ km s}^{-1}$ , showing that astrometric binaries do, in fact, contribute to the scatter.

Closer examination of the RVs with the projection effect removed revealed a monotonically decreasing trend with effective temperature. Dividing the sample into three bins (4000–5000 K, 5000–6000 K, 6000–7000 K), we obtained average differences between the spectroscopic and astrometric velocities of  $\Delta_1 = +0.440 \pm 0.073 \text{ km s}^{-1}$ ,  $\Delta_2 = +0.113 \pm 0.060 \text{ km s}^{-1}$ , and  $\Delta_3 = -0.175 \pm 0.090 \text{ km s}^{-1}$ , respectively. The difference between the first and last bins is significant at the  $5.3\sigma$  level.

The astrometric RVs measure the true motion of the center of mass of each star, while the spectroscopic RVs do not, as mentioned earlier. By construction, our RVs have the gravitational redshift of the Sun taken out ( $0.63 \text{ km s}^{-1}$ ), as well as its convective blueshift, because our velocity zero-point is based on observations of minor planets in the solar system, which represent reflected sunlight. Stars with different properties than the Sun will have their velocities affected differently by those two effects, and will therefore be biased to some degree. We illustrate the expected magnitude of these effects in Figure 18. The curve for the differential gravitational redshift is based on the masses and radii tabulated in the same Pleiades isochrone we have used throughout this paper, and is seen to vary relatively little over most of the temperature range shown. On the other hand, the convective blueshift has a steeper dependence on tem-

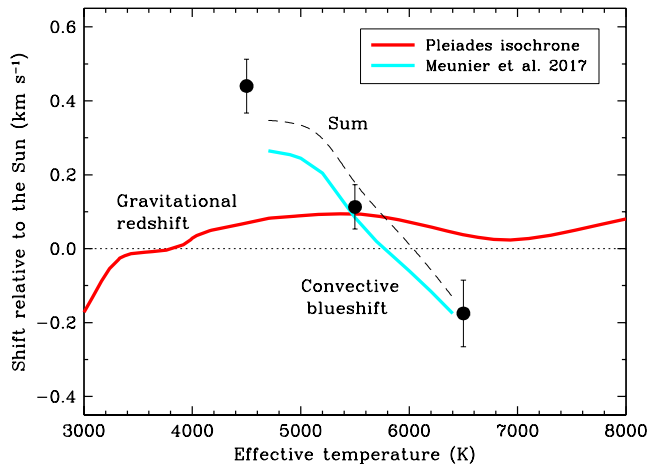


**Figure 18.** Astrophysical components of the measured RVs, relative to the effects in the Sun. The differential gravitational redshift curve is based on masses and radii from the Pleiades isochrone shown in Figure 1. The convective blueshift curve, with the value for the Sun subtracted out, is taken from Figure 3 of Meunier et al. (2017). Adding these two effects together results in the curve represented with a dashed line. Dots with error bars correspond to the measured differences ( $\Delta_1$ ,  $\Delta_2$ ,  $\Delta_3$ ) in three temperature bins between the spectroscopic and astrometric velocities for stars with mean RV errors smaller than  $0.5 \text{ km s}^{-1}$ , and shows rather good agreement with the dashed curve.

perature. The curve shown was derived from Figure 3 of Meunier et al. (2017), which is based on measurements in a sample of F7–K4 stars, after subtracting out the value for the Sun from the same figure ( $-0.34 \text{ km s}^{-1}$ ). The dashed line in our Figure 18 corresponds to the sum of the two effects, and is dominated by the convective blueshift. Our measurements of the difference between the spectroscopic and astrometric velocities as a function of temperature ( $\Delta_1$ ,  $\Delta_2$ ,  $\Delta_3$ ) also capture both effects, and are represented in the figure by the dots with error bars. The observations appear quite consistent with expectations, supporting the accuracy of our radial velocities, and showing they are precise enough to enable us to detect the dominant effects of varying convective blueshifts among solar-type stars in the Pleiades.

These systematic differences with spectral type make our earlier estimate of the cluster’s velocity dispersion slightly larger than it should be. To remove this bias, we performed a simple linear fit to the differences between the measured and predicted velocities as a function of temperature, and subtracted it from those differences. The resulting scatter is reduced slightly to  $0.48 \pm 0.04 \text{ km s}^{-1}$ . This represents our best estimate of the internal dispersion in the Pleiades cluster in the radial direction.

Earlier estimates of the one-dimensional (1D) dispersion in the cluster have varied significantly. Jones (1970) reported  $0.46 \text{ km s}^{-1}$  based on proper motions from photographic plates, while Makarov & Robichon (2001) obtained  $0.69 \text{ km s}^{-1}$  and  $0.22 \text{ km s}^{-1}$  for a sample of weak and strong X-ray sources, respectively, using proper motions from the Tycho-2 catalog (Høg et al. 2000). We have rescaled these three determinations here from their originally reported values in order to account for the difference between the adopted distance to the cluster in those studies and the current estimate of 136 pc from Gaia (Gaia Collaboration et al. 2018b). An additional

estimate by Galli et al. (2017) using proper motions from Bouy et al. (2015) and Tycho-2 gave a 1D dispersion of  $0.8 \text{ km s}^{-1}$ . Rosvick et al. (1992) used radial velocity observations for 34 stars with the CORAVEL instrument, and reported an estimate of  $0.68 \text{ km s}^{-1}$ , which they noted was only an upper limit due to undetected long-period binaries. Raboud & Mermilliod (1998) also used CORAVEL, and obtained  $0.36 \text{ km s}^{-1}$  from a sample of 67 stars.

The Gaia mission now presents an opportunity to obtain high-precision estimates of the velocity dispersion in two directions orthogonal to our own determination. To perform this calculation, we used the membership list from Gaia Collaboration et al. (2018b), and filtered it using the quality criteria recommended by Arenou et al. (2018) (their eqs. 1 and 2) to retain only stars with good astrometric solutions. This still left many stars with statistically significant excess astrometric noise (Gaia parameter `astrometric_excess_noise_sig`  $> 2$ ), which we chose to also exclude as in some cases this may be caused by unrecognized binarity. We then removed projection and distance effects following Gaia Collaboration et al. (2017) (eq. A.13), using the same space velocity vector as above. Because the predicted p.m. components subtracted from the measurements to remove projection effects are directly proportional to the parallax, we applied the further condition that the relative errors in the parallaxes should be 2% or less. With this, and an adopted distance to the cluster of 136 pc, we obtained identical 1D velocity dispersions in the right ascension and declination directions of  $0.48 \pm 0.02 \text{ km s}^{-1}$  (corrected for observational errors), based on 292 stars. Some contamination by non-members and remaining long-period binaries affecting the Gaia proper motions is to be expected, so this may represent an upper limit. In any case, these determinations happen to agree with our value in the radial direction, strongly suggesting the velocity field is isotropic. Our best estimate of the 3D velocity dispersion in the Pleiades is then  $0.83 \pm 0.03 \text{ km s}^{-1}$ .

Our determination of the internal dispersion enables an estimate of the total mass of the Pleiades through the virial theorem, on the assumption that the cluster is in dynamical equilibrium. Following Geller et al. (2015), the total mass can be expressed as  $M_{\text{tot}} = 10 r_{\text{hp}} \sigma_r^2 / G$ , where  $r_{\text{hp}}$  is the projected half-mass radius,  $\sigma_r^2$  is the velocity dispersion in the radial direction, and  $G$  is the gravitational constant. This relation assumes the velocity dispersion is isotropic, a conclusion our results above seem to support. Adopting a projected half-mass radius of  $53 \pm 10 \text{ arc min}$  from Raboud & Mermilliod (1998), which at the 136 pc distance to the cluster corresponds to  $2.1 \pm 0.4 \text{ pc}$ , we obtain  $M_{\text{tot}} = 840 \pm 200 M_{\odot}$ . This value is consistent with estimates by others done in different ways (e.g., Raboud & Mermilliod 1998; Pinfield et al. 1998; Adams et al. 2001; Converse & Stahler 2008; Danilov & Seleznev 2020).

#### 14. TIDAL CIRCULARIZATION

The eccentricity versus log period diagram is a valuable diagnostic tool to investigate the effectiveness of tidal forces in binary systems belonging to coeval populations. It relies on the fact that tidal forces tend to circularize the orbits through energy dissipation, although the pre-

cise mechanisms are still not well understood. As the strength of tidal forces is very sensitive to the orbital separation (e.g., Zahn 1975), coeval binaries of similar mass are observed to have circular orbits up to a certain orbital period, beyond which the orbits display a range of eccentricities. For older and older populations, the effects of tidal forces affect wider and wider binaries and the critical period separating circular from eccentric orbits increases.

The precise definition of this transition period has varied among different studies (see, e.g. Mazeh 2008). Nevertheless, estimates are now available in a variety of populations of different ages and different masses, including G-type stars in the solar neighborhood (Duquennoy & Mayor 1991; Raghavan et al. 2010), A-type stars (Matthews & Mathieu 1992), M67 (Latham et al. 1992b; Geller et al. 2021), NGC 188 (Mathieu et al. 2004; Geller & Mathieu 2012), M35 (Meibom & Mathieu 2005; Leiner et al. 2015), NGC 7789 (Nine et al. 2020), NGC 6819 (Milliman et al. 2014), Hyades/Praesepe (Meibom & Mathieu 2005), the Pleiades (Mermilliod et al. 1992a), and even among giants (Mermilliod & Mayor 1992b; Verbunt & Phinney 1995), halo stars (Latham et al. 2002), and pre-main-sequence stars (Melo et al. 2001). These studies have confirmed that the transition period, which we refer to here as the tidal circularization period  $P_{\text{circ}}$ , following Meibom & Mathieu (2005), varies as a function of age, and it has even been proposed as a clock to date coeval populations (Mathieu & Mazeh 1988). The trend with age has been shown most recently by Nine et al. (2020), compared against several theoretical predictions.

The latest study of tidal circularization in the Pleiades is that of Meibom & Mathieu (2005). These authors defined a procedure to determine the circularization period involving the fitting of a function dependent on several parameters that control its shape. They calibrated these parameters with binaries in several clusters as well as with numerical simulations. They then used a sample of 12 solar-type binaries in the Pleiades known at the time from the work of Mermilliod et al. (1992a, 1997), and reported a circularization period of  $7.2 \pm 1.9 \text{ days}$ .

There are now a total of 52 main-sequence binaries or triples in the cluster with well characterized orbital solutions, including several new systems near that critical orbital period. They range in spectral type from B to M, and they are shown in a diagram of eccentricity versus orbital period in Figure 19. The circularization period may depend on stellar mass to some degree (see, e.g., Mathieu & Mazeh 1988), and most studies of the  $e$ -log  $P$  diagram have focused on stars more or less similar to the Sun. We have therefore done the same, and restricted the sample to primaries of approximately solar type (filled circles), broadly defined here as those with spectral type FGK. As a precaution we have left out the triple system HII 2027 (with two entries), which may have suffered eccentricity changes due to internal dynamics between the inner binary and the outer perturber. We are left with 38 systems. Our fit of the circularization function of Meibom & Mathieu (2005) gives a circularization period of  $P_{\text{circ}} = 7.2 \pm 1.0 \text{ days}$ , which is identical to that of those authors, but about twice as precise.<sup>8</sup> Including

<sup>8</sup> As a check, we note that one of the fixed parameters of this



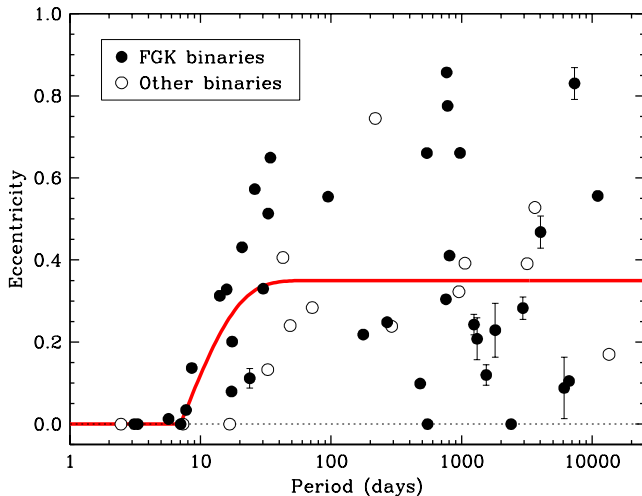


**Figure 19.** Eccentricity versus log period diagram for the 52 binaries in the Pleiades cluster with orbital solutions. The curve represents the circularization function of Meibom & Mathieu (2005) fitted to the 38 binaries of spectral type FGK (filled symbols), resulting in a circularization period  $P_{\text{circ}} = 7.2 \pm 1.0$  days. Open symbols represent binaries of spectral type B, A, and M.

the remaining twelve B, A, and M-type systems gives essentially the same value,  $P_{\text{circ}} = 7.3 \pm 1.0$  days.

We note that DH 794 has an orbital period of 5.69 days that is shorter than  $P_{\text{circ}}$ , yet the orbit appears to be slightly eccentric ( $e = 0.0126 \pm 0.0022$ ). A possible explanation is the presence of a tertiary component, given that dynamical interactions with the inner pair can pump up the eccentricity in a short-period system that normally would have already been circularized (Mazeh 1990). While no such companions have been directly imaged around DH 794, the Gaia EDR3 catalog indicates excess astrometric noise that is statistically significant, and which could be due to an unresolved companion, although there may be other causes. It is also possible that DH 794 was formed with a very high eccentricity, which would delay circularization.

#### 15. PROSPECTS FOR ABSOLUTE MASS DETERMINATIONS FROM GAIA

With its long observational history and close distance to the Earth, the Pleiades cluster would seem like an ideal place to test models of stellar evolution using well measured properties of stars. The most fundamental of these is the mass. As of this writing, however, model-independent absolute mass determinations have only been made for four binary systems in the Pleiades. One is the B-type spectroscopic-interferometric binary Atlas (27 Tau; Zvahlen et al. 2004), which has formal fractional errors for the masses of 5–7%, making the measurements only marginally useful. Another is the A-type eclipsing system HII 1431 (HD 23642; Munari et al. 2004; Southworth et al. 2005; Groenewegen et al. 2007; David et al. 2016), which is in our sample. A third system is HCG 76 (V612 Tau; David et al. 2016), also an

function, the average eccentricity of binaries with periods longer than 50 days, was set by Meibom & Mathieu (2005) to a value of 0.35 based on the mean eccentricity found for binaries in the Pleiades, M35, Hyades/Praesepe, M67, and NGC 188. We have verified for our expanded sample of 38 solar-type systems in the Pleiades that the average for  $P > 50$  days is indeed 0.35, with a formal uncertainty for the mean of 0.06.

eclipsing system with low-mass components of spectral type M. The last is HII 2147, a spatially resolved G-type binary on our target list that was studied separately by Torres et al. (2020).

The Gaia mission promises to provide many more examples. It will detect the orbital motion of virtually all binaries in the Pleiades astrometrically, even for periods longer than the duration of the observations. However, with the instrument’s angular resolution of  $\sim 0''.1$ , as currently stated in the mission’s online documentation<sup>9</sup> (see also Gaia Collaboration et al. 2016), the individual components will remain spatially unresolved at the 136 pc distance to the cluster for orbital periods shorter than 35 yr, if the total mass is  $2 M_{\odot}$ , or 50 yr, if it is  $1 M_{\odot}$ . Only the motion of the photocenter will be detected. Modeling this motion will provide in many cases the inclination angle of the orbit, along with the angular size of the photocentric ellipse ( $a''_{\text{phot}}$ ) and other shape and orientation elements, but not the true semimajor axis ( $a''$ ), without which the absolute masses cannot be determined. For this to be possible, the binaries must have SB2 orbits. The absolute masses of the components can then be calculated from the spectroscopic minimum masses  $M_{1,2} \sin^3 i$  and the inclination angle  $i$ .

For the most stringent tests of models, the fractional mass errors (and therefore also those of the minimum masses from spectroscopy) should be smaller than about 3% (see, e.g., Andersen 1991; Torres et al. 2010). Not counting the eclipsing system HII 1431 mentioned above, there are 14 SB2s in Table 8 that satisfy this requirement, and should therefore yield high-quality masses at the conclusion of the Gaia mission. This will more than quadruple the number of current systems with absolute mass determinations.

In addition to the masses, it will also be possible to derive the individual brightness (absolute magnitude) of each component in the Gaia  $G$  band, even if the pair is not resolved. This can be done by combining the Gaia parallax and inclination angle with the total projected semimajor axis in linear units from spectroscopy ( $a_{\text{tot}} \sin i$ ; Table 8) to give  $a''$ , and then using the photocenter semimajor axis  $a''_{\text{phot}}$ , also from Gaia. These last two quantities are related by the classical expression  $a''_{\text{phot}} = a''(B - \beta)$  (e.g., Van De Kamp 1981). Here  $B \equiv M_2/(M_1 + M_2) = q/(1 + q)$  is the mass fraction, and  $\beta \equiv \ell_2/(\ell_1 + \ell_2) = 1/(1 + 10^{0.4\Delta G})$  is the fractional luminosity, with  $\Delta G$  being the magnitude difference in the Gaia bandpass. As the mass ratio  $q$  is known for SB2s, the brightness difference in the Gaia bandpass immediately follows. Finally, the measured combined-light  $G$ -band magnitude along with  $\Delta G$  and the parallax provide the absolute magnitude of each star. In this way it becomes possible to compare the measurements with the predicted  $G$ -band model fluxes at each mass. Our flux ratios from TODCOR near a wavelength of 5187 Å (Table 8) can be easily converted to  $V$ , providing another constraint on the model fluxes for the same masses.

Alternatively, if the binaries are only single-lined and are unresolved by Gaia, individual component masses can still be derived if the systems can be spatially re-

<sup>9</sup>

solved from the ground at least once using other techniques. Most of our SB1s are beyond the sensitivity limits of current long-baseline interferometers such as CHARA, but the ones with the longer periods should be reachable with adaptive optics observations on large telescopes.

## 16. SUMMARY AND CONCLUSIONS

In this paper we have derived key properties of the binary population in the Pleiades cluster based on more than 6100 radial velocity measurements for 377 stars, obtained over 39 years using four different telescope/spectrometer combinations at the CfA. We augmented this material with some 1150 other velocity measurements of similar precision obtained by the CORAVEL team, overlapping substantially in time with ours. The total duration of the observations is more than 43 years.

Nearly three dozen new spectroscopic binary and multiple systems have been identified, and their orbital solutions are presented here. The periods range from 3 days to more than 36 yr. The current tally of spectroscopic systems (binaries and triples) with orbital solutions in the Pleiades stands at 52, including systems reported by others. An additional 10 objects show long-term drifts in their radial velocities, implying periods longer than the duration of the survey.

With the enlarged sample of binaries, we have revisited the determination of the tidal circularization period and obtained  $P_{\text{circ}} = 7.2 \pm 1.0$  days for FGK stars, identical to the estimate of Meibom & Mathieu (2005), but with an uncertainty reduced by half. The binaries that carry the most weight for this determination are those with periods near  $P_{\text{circ}}$ . Given this, and because of the high degree of completeness of our binary survey for short periods (97% for periods up to 100 days), our  $P_{\text{circ}}$  result for FGK binaries seems unlikely to change much in the future.

An investigation of the binary orbital properties of the sample shows the distribution of orbital periods (up to  $10^4$  days) to be similar in shape to that of solar-type binaries in the field (Raghavan et al. 2010), after corrections for incompleteness. The eccentricity distribution for  $P > P_{\text{circ}}$ , on the other hand, is different (see Raghavan et al. 2010; Geller & Mathieu 2012) and is well represented by a Gaussian with a mean of  $e = 0.16$  and  $\sigma_e = 0.37$ . We find the distribution of mass ratios to be flat, again similar to that in the field, except that we do not find an excess of equal-mass pairs as Raghavan et al. (2010) proposed.

The fraction of binaries in the Pleiades up to periods of  $10^4$  days is  $25 \pm 3\%$ , which is nearly double that of solar-type binaries in the field and in the halo. This excess of binaries is similar to what has been found in several other open clusters (Blanco 1, M35, NGC 7789, NGC 6819, M67, NGC 188) and has been proposed as evidence that single stars have been preferentially lost to the clusters through dynamical interactions, consistent with results from  $N$ -body simulations. Accounting for the several dozen astrometric binaries in the cluster discovered in adaptive optics and lunar occultation surveys, as well as wide pairs identified by Gaia, we estimate the total binary fraction in the Pleiades to be

at least 57%. This lower limit is again higher than the multiplicity frequency of solar-type stars in the field (44%; Raghavan et al. 2010). Estimates of the total binary frequency by others are even higher (Kähler 1999; Converse & Stahler 2008).

Taking the average radial velocity of 234 member stars, we derive a mean RV for the cluster of  $5.688 \pm 0.067 \text{ km s}^{-1}$  on the velocity system defined by minor planets in the solar system, in excellent agreement with the result from Gaia DR2. The internal velocity dispersion in the radial direction is  $0.48 \pm 0.04 \text{ km s}^{-1}$ , after accounting for perspective effects, observational errors, and long-period (astrometric) binaries that we are not sensitive to. The precision of our velocities is high enough that we are able to detect and remove from the dispersion calculation a systematic change in the average velocity as a function of effective temperature over the range 4000–7000 K. We ascribe this effect mostly to changes in the strength of convective blueshifts affecting the Doppler measurements (Meunier et al. 2017), and to a lesser degree to variations in the gravitational redshift. The magnitude of the changes we measure agrees very well with expectations for these astrophysical effects. Proper motion measurements from Gaia result in new estimates of the velocity dispersions in the right ascension and declination directions of  $0.48 \pm 0.02 \text{ km s}^{-1}$  each, which are identical to our measurement in the radial direction, and support the conclusion that the velocity field is isotropic.

Finally, with our measure of the dispersion in the radial direction, we have used the virial theorem to estimate the total mass of the Pleiades. Our result,  $M_{\text{tot}} = 840 \pm 200 M_{\odot}$ , is in good agreement with earlier estimates using different methodologies.

This paper is dedicated to the memory of John R. Stauffer (1952–2021), who contributed so much to our knowledge of the Pleiades cluster. A large number of observers, students, and colleagues at the CfA have contributed to gathering the spectroscopic observations for this survey over the past four decades. We thank them all. We are also grateful to R. Davis and J. Mink for maintaining the CfA Digital Speedometer and TRES databases over the years. Helpful comments and suggestions by the anonymous referee and the statistics editor are appreciated. We acknowledge the long-term support from the Smithsonian Astrophysical Observatory that enabled this study, in the form of telescope time and instrumentation. The research has made extensive use of the SIMBAD and VizieR databases, operated at the CDS, Strasbourg, France, and of NASA’s Astrophysics Data System Abstract Service. We also acknowledge the use of the Fourth Catalog of Interferometric Measurements of Binary Stars (Hartkopf et al. 2001, and online updates), and of the Washington Double Star Catalog, maintained at the U.S. Naval Observatory. The work has used data from the European Space Agency (ESA) mission *Gaia* (<https://www.cosmos.esa.int/gaia>), processed by the *Gaia* Data Processing and Analysis Consortium (DPAC, <https://www.cosmos.esa.int/web/gaia/dpac/consortium>). Funding for the DPAC has been provided by national institutions, in particular the institutions participating in the *Gaia* Multilateral Agreement.

## APPENDIX

## 1. NOTES

Included below are notes of interest for many of the objects in our sample, concerning spectral peculiarities or issues with the radial velocity measurements, multiplicity, or comparison with RV measures by others in a few cases. To facilitate reference to the tables in the main text, we include the object number from Table 1 (in order of increasing right ascension) along with the SIMBAD name.

**1. AK III-31.** Mermilliod et al. (1997) found this star to be a 5 day SB1, and presented an orbit. A very faint secondary is seen in our spectra, making it an SB2. Independent estimates of the secondary temperature and rotational velocity were not possible from our observations. A template for that star for the TODCOR measurements was selected based on the primary temperature with the help of properties predicted from a model isochrone for the cluster. Although the center-of-mass velocity agrees with the cluster mean, Gaia EDR3 places the object in the foreground of the Pleiades at half the distance, so it is not a member. This explains its location far above the main-sequence.

**5. AK III-79.** Our mean RV and the Gaia p.m. indicate this is a non-member, even though the parallax agrees with the cluster mean.

**15. PELS 7.** Our measurements show the velocities to be clearly variable. A minimum occurred in September of 2017, and a handful of CORAVEL observations include another low point in October of 1995. An SB1 orbital solution with a period of 20 yr is presented in Table 6 and shown in Figure 20, but is only tentative due to poor phase coverage. The center-of-mass velocity is inconsistent with cluster membership, and the Gaia catalog indicates the parallax and p.m. are as well.

**21. AK III-419.** Our observations reveal this to be a 34 day SB2.

**22. AK III-416.** The Gaia EDR3 parallax and p.m., as well as its velocity, indicate this is a non-member. Mermilliod et al. (1997) found it to be a single-lined binary, and published an orbit with a 10.9 day period.

**26. AK II-346.** There is spectroscopic evidence for the presence of a narrow-lined star and a broad-lined star from the shape of the cross-correlation functions (CCFs), which show asymmetries. Queloz et al. (1998) also reported it to be an SB2. While we are not able to reliably detect the broad-lined star due to strong blending, the sharp-lined star (which we assume is the secondary) shows clear signs of long-term variability. However, our observations alone are not sufficient to determine an orbit unambiguously, due to a gap in the data between our Digital Speedometer and TRES measurements. The object was also observed by the CORAVEL group (Rosvick et al. 1992; Mermilliod et al. 2009), and fortunately those ten measurements fill the gap and point to a period of about 6100 days. Our orbital fit results in a large coefficient for the minimum mass of the companion of  $0.38 M_{\odot}$ , consistent with our presumption that it corresponds to the more massive primary star, and which we do not detect directly because of its rapid rotation. On one of their epochs, Mermilliod et al. (2009) claim to have resolved the companion and report for it a velocity measurement of  $+39.01 \text{ km s}^{-1}$  that seems much too large, if the orbit determined here is approximately correct, because it would imply unreasonable minimum masses for the components of 27 and 4 solar masses. We have chosen to disregard that measurement here, and use only their “primary” velocity at that epoch, which fits our orbit well. We consider our solution in Table 6 to be somewhat preliminary at this time, although we do note that an old Mt. Wilson velocity from 1921 reported by Abt (1970) is consistent with our model, and so is the median RV reported by Gaia (gathered over a timespan much shorter than the period of the orbit). The orbital period we determine corresponds to a semimajor axis of about 67 mas at the distance to the Pleiades. We are not aware of any visual companions reported for this object.

**32–33. TRU S25 A, TRU S25.** The similar SIMBAD names suggest an association, but the stars are nearly  $4^{\circ}$  apart on the sky. TRU S25 A is a non-member according to Gaia and our RV measurements. TRU S25 is listed in the WDS as a visual binary, but the accompanying note indicates this is dubious. Its velocities have been reported by Torres (2020).

**35. TRU S26.** RVs together with a 71 day SB1 orbit for this rapidly-rotating A star were reported by Torres (2020). A previously published 4.7 day orbit by Pearce & Hill (1975) is incorrect.

**43. PELS 25.** The mean RV is lower than the cluster mean, but the entry in the Gaia EDR3 catalog shows the parallax and p.m. to be consistent with membership.

**44. AK III-664.** Our observations show this to be a 14 day SB1.

**56. HCG 65.** A  $1''.3$  astrometric companion is listed in the Gaia EDR3 catalog.

**69. HII 102.** This was observed with the CORAVEL by Mermilliod et al. (1992a), but variability was not noticed. Our own velocities also show little change, but are  $2\text{--}3 \text{ km s}^{-1}$  higher. A time history of all the observations (Figure 24) indicates this is a very long period binary. Additional velocities by Soderblom et al. (1993) and White et al. (2007) fit the trend, as does the median value listed in the Gaia EDR3 catalog. A faint visual companion at  $3''.6$  is listed in the WDS and has an entry in the Gaia catalog, but seems too wide to be the spectroscopic secondary. The system may therefore be a hierarchical triple.

**72. TRU S45.** A close  $0''.1$  astrometric companion discovered by lunar occultations has been reported only once in 1930, and is unconfirmed. A wider,  $1''.7$  companion to the south is confirmed by Gaia to be physically associated. Our spectroscopic observations do not resolve it, but signs that this is a close binary are seen from the broad wings of the CCF and the impression that the spectral lines are diluted compared to those of other stars of similar spectral type. This suggests the presence of a very rapidly rotating star, in addition to the one we are able to measure velocities for. We presume the star we measure is the fainter secondary of the  $1''.7$  pair, from the fact that its spectroscopically determined temperature is consistent with the  $G_{BP} - G_{RP}$  color from Gaia, whereas the Gaia color of the primary star is much bluer.

**74. HII 120.** RV variability was first noticed by Raboud & Mermilliod (1998) based on 5 measurements. An 8 yr orbit is reported for the first time in the present paper. Bouvier et al. (1997) detected a close astrometric companion, but considered the target to be a non-member; Gaia confirms membership. No parallax or p.m. are listed in Gaia EDR3 for the  $3''.4$  astrometric companion listed in the WDS (Table 14). If the visual companion is physically associated, it would make the system a triple.

**80. MT 41.** The parallax and p.m. components are somewhat different than the cluster mean, but the very high value of  $RUWE = 10.146$  indicates the astrometry may be biased. The rotation period from Rebull et al. (2016a,b) is consistent with membership. We retain it as a possible member.

**81. HII 164.** The secondary is very faint, and is only seen in our TRES spectra. The best parameters for the corresponding template could not be determined independently, and are merely educated guesses. As different choices change the secondary velocities to some degree, we consider the orbit for that component (specifically,  $K_2$ ) to be preliminary.

**86. HII 173.** This SB2 was found by Mermilliod et al. (1992a), who published the first orbit with a period of 1.3 yr. We have combined all CORAVEL observations (including others by Mermilliod et al. 2009) with ours to update the orbital solution.

**89. HII 177.** Queloz et al. (1998) reported this as an SB2, but no orbit was presented. A single CORAVEL observation by Mermilliod et al. (2009) that resolves the components agrees with the 2280 day orbit we report here. This is a non-member based on the center-of-mass velocity, as well as information from the Gaia mission.

**93. HII 233.** Mermilliod et al. (1992a) reported a drift in their CORAVEL velocities suggesting a long orbital period. Our observations reveal it to be an SB1 with a period of 3.5 yr.

**98. HII 250.** We find this to be a 970 day SB1.

**100. HII 263.** RV variability was first noticed by Raboud & Mermilliod (1998). Merging the CORAVEL velocities with ours indeed shows this to be a binary with a period longer than the duration of our survey. No visual companions have been reported. Prosser & Stauffer (1993) reported an anomalous dip in brightness in late 1992, and speculated it might be an eclipse. However, the velocities now show that event to have occurred near the bottom of the RV curve, so an eclipse by this companion is ruled out. Spottedness on the primary seems like a natural explanation.

**103–104. HII 298, HII 299.** This is a  $5''.7$  pair with membership confirmed by Gaia EDR3. The brighter star is HII 299, which is slightly hotter than the companion, as expected. The velocities are similar.

**106–107. HII 303, HII 302.** This is a  $16''$  pair showing similar RVs. The northern (brighter) component, HII 303, is in turn a close  $1''.8$  visual binary that we have observed separately only once. We refer to it in this paper as HII 303 B. The CCFs for all other observations of HII 303 show variable widths, which may be caused by variable, seeing-dependent contamination from the close companion.

**112. HII 320.** This is an SB2. Mermilliod et al. (1992a) reported it as single-lined, and presented the first orbit with a period of 2 yr, but noted their suspicion that the companion is a rapidly-rotating star, which they could not measure. We confirm this, and are able to measure the secondary RVs in our TRES spectra. Application of TODCOR to our Digital Speedometer spectra shows hints of the secondary, but the velocities for that star are too poor to be useful. Nevertheless, the use of TODCOR has the benefit of avoiding “peak-pulling” for the primary velocities<sup>10</sup>. We find those primary velocities to be consistent with those from TRES, so they have been incorporated into our final solution. We have chosen not to use the CORAVEL velocities in our updated orbital solution because the semiamplitude of the primary from those velocities is significantly smaller than ours, compared to the errors, suggesting the CORAVEL measurements may be affected by peak-pulling. A  $v \sin i$  measurement for the primary star from CORAVEL ( $10.8 \pm 0.5 \text{ km s}^{-1}$ ; Queloz et al. 1998) agrees with our estimate of  $10 \pm 2 \text{ km s}^{-1}$ . For the secondary we measure  $v \sin i = 35 \pm 4 \text{ km s}^{-1}$ , and a cooler temperature than the primary.

**113. HII 338.** Our RVs show long-term variability, possibly associated with a  $3''.8$  visual companion listed in the WDS.

<sup>10</sup> “Peak-pulling” refers to a bias in the measured velocities for a star caused by blending with an unresolved companion. The 1D cross-correlation peak will have a (sometimes subtle) shoulder on the side of the companion, resulting in a RV for the visible

star shifted in the direction of the companion, i.e., in the direction of the center-of-mass velocity of the binary. Depending on the brightness of the companion, this will generally lead to a velocity semi-amplitude for the visible star that is too small.



- 119. PELS 38.** Rosvick et al. (1992) reported it as a spectroscopic binary, on the basis of three observations. We find it to be a 17 day SB2 with a faint secondary, and present the first orbit. The TODCOR template for the secondary is an educated guess.
- 123. AK I-2-199.** A  $0''.49$  visual companion was reported by Konishi et al. (2016), and is substellar.
- 127. HII 468.** This is Electra (17 Tau). The two astrometric companions discovered by lunar occultations may be one and the same (see Richichi et al. 1996). A 100 day spectroscopic orbit reported by Abt et al. (1965) is spurious (see Torres 2020). RV measurements were reported separately in the latter work.
- 129. HII 476.** Raboud & Mermilliod (1998) claimed their RVs indicated a drift. We do not see that in our measurements, and our  $e/i$  metric classifies the object as non-variable.
- 133. HII 522.** An SB1 orbit with a 23.8 day period was presented by Mermilliod et al. (1992a), which is consistent with ours. Those CORAVEL observations have been included with our own in an updated solution.
- 134. HII 514.** A  $0''.78$  astrometric companion was reported by Makarov & Robichon (2001) from a special reduction of the Tycho-2 observations.
- 138. HII 541.** An astrometric companion has been discovered by lunar occultations. See also Torres (2020).
- 140. HII 563.** This is Taygeta (19 Tau). RVs and a tentative 8.7 yr spectroscopic orbit for this object were reported by Torres (2020), who presented new velocities that are inconsistent with an earlier orbit (Abt et al. 1965). An astrometric companion is known from lunar occultations. The spectroscopic and astrometric companions may be the same.
- 144. HII 571.** A 15.9 day SB1 orbit was published by Mermilliod et al. (1992a) that is consistent with ours. We have combined the observations to update the solution. A  $3''.8$  visual companion is listed in the WDS, and has a separate entry in Gaia. This would make it a triple system.
- 145. HII 605.** Mermilliod et al. (1992a) reported not being able to measure this object with CORAVEL because of its rapid rotation. Our observations show instead that it is double-lined, with components of relatively sharp features. The secondary is too faint to determine its rotational velocity independently. We adopt for it  $v \sin i = 0 \text{ km s}^{-1}$ . Our SB2 orbital solution with a period of 21 days is presented in Tables 7–8 and shown in Figure 21.
- 156. HII 717.** A close visual companion is known at a separation of  $0''.2$ , corresponding to a period of roughly a century. The RVs show a slow downward drift consistent with this (see Figure 24). RVs by Liu et al. (1991) and Soderblom et al. (1993) agree with the trend. A wider, very faint, and physically associated  $5''.3$  companion is listed in the Gaia EDR3 catalog, which would make the system a triple.
- 158. HII 727** This is a long-period binary with incomplete phase coverage from our own observations, showing a single periastron passage in late 2019. By adding six CORAVEL observations from Mermilliod et al. (2009), two from Liu et al. (1991), and one from Soderblom et al. (1993), we are able to find a satisfactory orbital solution with a period of about 20 yr, and a high eccentricity of  $e = 0.83$ . The minimum secondary mass is fairly large, but we do not detect the companion in our spectra.
- 160. HII 745.** We find this to be a 4.2 yr SB1. Although the minimum secondary mass is quite large, we are not able to detect the secondary with confidence. Two measurements of the primary star by Liu et al. (1991) fit our orbit well. The Gaia catalog lists a very wide astrometric companion at  $15''.8$  that shares the parallax and p.m. of the primary. The system may thus be triple.
- 162. HII 739.** An astrometric companion was discovered by lunar occultations.
- 165. HII 761.** A 3.3 day SB1 orbit was reported by Mermilliod et al. (1992a). We have found it to be double-lined and measured the secondary’s velocities. However, the secondary is too faint to determine its temperature independently, so we have relied for that on an estimate from a model isochrone for the cluster.
- 169. HII 785.** This is Maia (20 Tau). An astrometric companion was discovered by lunar occultations.
- 172. HII 817.** This is Asterope (20 Tau). An astrometric companion is reported in the Gaia EDR3 catalog.
- 175–176. HII 879, HII 883.** The WDS lists this as a wide  $17''.5$  visual pair, the brighter primary being HII 879. Gaia EDR3 gives nearly identical parallaxes and p.m.
- 177. HII 890.** A visual companion discovered by Bouvier et al. (1997), currently at  $1''.2$ , is also listed in the Gaia EDR3 catalog, but the entry has no parallax or p.m.
- 178. HII 885.** A  $0''.9$  visual companion discovered by Bouvier et al. (1997) is also listed in the Gaia EDR3 catalog, but the entry has no parallax or p.m.
- 180. AK I-2-288.** Mermilliod et al. (1997) first reported this object as an SB2, but lacked sufficient observations to solve for the orbit. Their seven measurements are combined with ours for the new SB2 orbital solution presented in Tables 7–8.
- 182. HII 916.** RV variability was first noticed by Raboud & Mermilliod (1998). The combination of the CORAVEL

measurements with our own does seem to support a long-term trend (see Figure 24).

**185. HII 956.** Visual binary with a preliminary orbit by Popović & Pavlović (1995) giving an angular semimajor axis of  $a'' = 1''.9$  and a period of 1400 yr. Another determination by Malkov et al. (2012) reports  $a'' = 1''.2$  and  $P = 900$  yr. The star whose velocities we are able to measure has a line broadening corresponding to  $v \sin i = 55 \text{ km s}^{-1}$ , but the lines appear shallower than expected for its temperature, suggesting dilution by another star. Estimates in the literature of the rotational velocity of HII 956 are much higher than we measure: Smith & Struve (1944) reported  $v \sin i = 150 \text{ km s}^{-1}$ , Morse et al. (1991) gave  $200 \text{ km s}^{-1}$ , and Kounkel et al. (2019) estimated  $174 \text{ km s}^{-1}$ . We speculate these determinations correspond to the primary star of the pair, which would explain the dilution we see. The velocities we measure would therefore be for the secondary.

**199. HII 1084.** An astrometric companion was discovered by lunar occultations.

**201. TRU S93.** Our observations show this to be a single-lined binary with a period of 2.9 yr.

**203. HII 1100.** The Gaia EDR3 catalog reports that the  $0''.8$  visual companion listed in the WDS has a slightly different p.m. than the target, although the Gaia quality flags indicate the astrometric solutions were problematic (large RUWE values for both components).

**204. HII 1117.** An SB2 orbit with a period of 26 days was published by Mermilliod et al. (1992a). Additional velocities were reported by Mermilliod et al. (2009), though some of them have the primary and secondary interchanged. All of these CORAVEL observations have been incorporated into our updated orbital solution.

**206. HII 1132.** A  $2''.6$  astrometric companion reported by Geißler et al. (2012) and Yamamoto et al. (2013) is substellar.

**218. HII 1284.** RVs have been reported by Torres (2020). Our new effective temperature estimate is  $7740 \pm 200 \text{ K}$ .

**219. HII 1298.** The closer of two astrometric companions reported in the WDS ( $0''.6$ ) was discovered by lunar occultations. It may be the same as the  $1''.2$  companion.

**221. HII 1306.** An astrometric companion was discovered by lunar occultations.

**227. HII 1338.** See Section 5.2.

**228. HII 1348.** Queloz et al. (1998) reported this to be an SB2 based on three spectra from the ELODIE instrument, although no velocities were published. Our velocities yield the 95 day SB2 orbit presented in Tables 7–8. A visual companion at  $1''.1$  is known, which is substellar (see Geißler et al. 2012; Yamamoto et al. 2013). This would therefore be an interesting triple system with a circumbinary brown dwarf.

**232. HII 1375.** The astrometric companion listed in the WDS was discovered by lunar occultations.

**233. HII 1407.** Our observations show this to be a single-lined binary with a period of 2.6 yr.

**234–235. HII 1392, HII 1397.** This pair is separated by  $5''.7$ . The brighter star, HII 1397, is a metallic-line star, and an SB1 with a 7 day orbit that was first reported by Conti (1968). Our independent solution is consistent with theirs. The elements reported in Table 6 combine all observations together. We find HII 1392 to be an SB2 with a 2 yr period and a large eccentricity ( $e = 0.82$ ), which would make this a quadruple system. Raboud & Mermilliod (1998) reported four measurements of HII 1392 with CORAVEL, but they are all near times of conjunction so the double nature of the source was not detected. Queloz et al. (1998) measured a projected rotational velocity of  $15.7 \pm 1.6 \text{ km s}^{-1}$  that is larger than our values for the two components ( $10\text{--}12 \text{ km s}^{-1}$ ); this is likely the result of line blending.

**237. HII 1431.** This is a 2.5 day eclipsing binary (HD 23642) discovered independently by Miles (1999) and Torres (2003) using Hipparcos photometry. It has been used to address the controversy over the distance to the Pleiades, following the Hipparcos determination of a value smaller than the canonical one (see Munari et al. 2004; Southworth et al. 2005; Groenewegen et al. 2007). The secondary of this SB2 is a metallic-line A star. Consequently, we used a synthetic template with a metallicity of  $[\text{Fe}/\text{H}] = +0.5$  for that star, which provided better results. Nevertheless, a statistically significant primary/secondary velocity offset remains in our orbital solution, which we attribute to template mismatch stemming from the anomalous chemical composition of the secondary.

**245. TRU S115.** Our RVs for this rapid rotator show a hint of a downward trend (about  $2 \text{ km s}^{-1}$  over 6000 days), which may or may not be significant. The  $e/i$  value is smaller than our threshold for variability.

**249. HII 1645.** This is a non-member, and appears to have variable RV.

**251. HII 1653.** Our RVs show this to be a single-lined binary with a period of 1.5 yr.

**254. HII 1762.** The 10.7 yr spectroscopic orbit reported here has a very large minimum secondary mass. The RVs measured are believed to be for the secondary component. This is based on the broad wings seen in the CCF, and the unexpectedly shallow spectral lines for a star of near-solar temperature as determined from our spectra, corresponding to a spectral type of G1. This suggests dilution of the lines from the presence of a much more rapidly rotating star. This interpretation is supported by the large  $v \sin i$  of  $180 \text{ km s}^{-1}$  reported for HII 1762 by Uesugi & Fukuda (1970), and the combined color index from Gaia EDR3, which, after correction for reddening, corresponds to an early F star

(consistent with the A9 V classification given in SIMBAD). The pair was resolved once by speckle interferometry, and found unresolved on two other occasions. The companion may be the same one detected spectroscopically. Liu et al. (1991) reported double lines in one of their two observations, but the velocity difference they measured is far too large to correspond to the 10.7 yr period.

**261. HII 1823.** The astrometric companion listed in the WDS was discovered by lunar occultations.

**264. HII 1876.** The astrometric companion listed in the WDS was discovered by lunar occultations. A new effective temperature estimate from this paper gives  $9580 \pm 200$  K. RVs have been published by Torres (2020).

**266. HII 1912.** This target has no parallax or p.m. from Gaia EDR3, and is listed as having a highly significant excess astrometric noise. A poorly determined p.m. from the Gaia DR2 catalog does appear consistent with membership, while the (also poor) parallax is smaller than expected. It has been considered a cluster member by some authors (e.g., Schilbach et al. 1995; Belikov et al. 1998; Sampedro et al. 2017), and more doubtful by others (Olivares et al. 2018). A rotation period of 3.17 days by Oelkers et al. (2018) seems to agree with the rotational sequence for the Pleiades, arguing for membership. A close ( $0''.2$ ) visual companion is listed in the WDS, and a wider one at  $0''.85$  was reported by Makarov & Robichon (2001) from a special reduction of Tycho-2 observations. The latter measurement is uncertain, and it is unclear whether it corresponds to a different companion. In any case, one or both of these companions probably explain the difficulty with Gaia’s astrometric solution. Our spectra suggest a blend of broad and narrow lines. We report velocities for the narrow-lined star only, which are constant and agree with the cluster mean.

**267. TRU S127.** Our velocities indicate this very rapid rotator ( $v \sin i = 175 \text{ km s}^{-1}$ ) is a long-period binary (see Figure 24), but the orbit is as yet undetermined. As the center-of-mass is not yet known, we have retained it as a possible Pleiades member even though the Gaia parallax is formally different from the cluster mean (but the p.m. is consistent with membership). The Gaia EDR3 quality flags indicate the astrometric solution was problematic, which may have affected the parallax.

**269. HII 2027.** See Section 5.2.

**274. HII 2147.** Single-lined binary with an 18 yr orbit and absolute mass determinations from Torres et al. (2020), from a combination of astrometric and spectroscopic observations. The star seen spectroscopically is the secondary.

**277. HII 2172.** A 30.2 day SB1 orbit was presented by Mermilliod et al. (1992a). We have combined their observations with ours to update the solution. We see no sign of the secondary in our spectra.

**278. HII 2195.** The astrometric companion listed in the WDS was discovered by lunar occultations.

**282. HII 2284.** Raboud & Mermilliod (1998) reported this object as a spectroscopic binary based on eight CORAVEL measurements, but did not have enough velocities for an orbit. We confirm it to be a single-lined binary with a period of 807 days.

**283. HII 2278.** A  $0''.4$  visual companion discovered by Bouvier et al. (1997) is also listed in the Gaia EDR3 catalog, but has no parallax or p.m.

**290. HII 2406.** A 33 day single-lined orbit was reported by Mermilliod et al. (1992a). We have detected the secondary in our TRES spectra, and updated the solution using all measurements.

**291. HII 2407.** Mermilliod et al. (1992a) reported the first orbit for this SB1 with a 7 day period. It was recently discovered by David et al. (2015) to be an eclipsing binary based on observations from NASA’s K2 mission. We combine the original CORAVEL velocities (as transformed to the IAU system by Mermilliod et al. 2009) with our own, more numerous measurements, to provide an improved solution. The secondary is very faint and is not seen in our spectra.

**297–299. HII 2500, HII 2503, HII 2507.** These three objects may well form a multiple system. The brighter star, HII 2507, is an SB2 ( $P = 16.7$  days) first announced as an SB1 by Abt et al. (1965) and later by Pearce & Hill (1975). The secondary has been detected here for the first time. The two astrometric companions to HII 2507 reported in the WDS correspond to HII 2503 ( $3''.3$ ) and HII 2500 ( $10''.1$ ). The latter is itself a close visual binary ( $0''.3$ ), and also an SB1 with a period of about 6.5 yr, although these two companions cannot be the same, making the object at least a triple. The variability of HII 2500 was first noticed by Raboud & Mermilliod (1998), who did not have enough observations for an orbit. There is no indication of a change in the width of the CCF for HII 2500, as might be expected from the  $0''.3$  companion. If all of these stars are physically bound, this would be a sextuple system.

**300. HCG 384.** This is a 542 day SB2 with a faint secondary, for which we report an orbit here. A wide  $13''.9$  companion listed in Gaia EDR3 may not be physical: its parallax and p.m. are somewhat different from those of the target.

**303. HII 2601.** A  $1''.9$  companion is listed in the Gaia EDR3 catalog.

**316. HII 2881.** Queloz et al. (1998) reported this as a suspected long-period double-lined binary. Our velocities show no significant change, and the  $e/i$  diagnostic incorporating the CORAVEL measurements is below our threshold for variability.

**328. HII 3104.** Our RVs show this to be a 3.6 yr SB1. The declination component of the p.m. from Gaia EDR3 is rather different from the mean for the cluster, suggesting the object may not be a member. However, the quality flags indicate the astrometric solution may be severely disturbed by the companion, so membership cannot yet be ruled out. The center-of-mass velocity is not far from the expected value.

**330. HII 3097.** A 2 yr SB1 orbit was published by Mermilliod et al. (1992a) with a very high eccentricity of  $e = 0.78$ . The better phase coverage of our observations improves the solution significantly. Table 6 and Figure 22 present the combined fit using both data sets, augmented with additional CORAVEL measures by Mermilliod et al. (2009).

**332. HII 3163.** The shape of the CCF suggests a blend of a broad and narrow peak. Our RVs correspond to the narrow peak. No astrometric companions have been reported.

**338. HII 3197.** This is a close visual binary with a 30.2 yr astrometric orbit reported by Schaefer et al. (2014). The semimajor axis is  $0''.08$ . A wider companion at  $0''.5$  has also been found, making this a triple system. Our spectroscopic measurements correspond to the combined light.

**342. PELS 69.** This is a non-member according to Gaia. We find it to be an SB1 with a period of 3.6 yr. Our solution combines our own measurements with about a dozen older ones from the CORAVEL (Mermilliod et al. 2009).

**348. AK IV-287.** Our observations show that this is an SB1 with a 5 yr period.

**349. TRU S177.** The parallax and p.m. information in the Gaia EDR3 catalog casts doubt on the membership of this object. However, there are indications that the astrometric solution may have been disturbed. Our RVs display a slow downward drift of  $4 \text{ km s}^{-1}$  indicating binarity, which may be the cause of the excess astrometric noise. We retain it as a possible member.

**351. DH 794.** We find this to be a 5.7 day SB2, with a secondary that is too faint for us to establish its temperature and  $v \sin i$  independently from our spectra. The corresponding template was selected with help from the cluster isochrone.

**352. AK IV-314.** The  $1''.0$  astrometric companion listed in the WDS has an entry in the Gaia EDR3 catalog, but no parallax or p.m. are reported.

**356. HCG 489.** We find this to be a 3 day double-lined binary.

**358. HCG 495.** Our observations show this is an 8.5 day SB2.

**359. AK V-151.** We find this to be an 8.4 yr SB2, in which the rapidly rotating primary is only detectable in our TRES spectra. Gaia EDR3 indicates this is a background object; the center-of-mass velocity from our orbital solution is far from the cluster mean.

**366. AK V-198.** Mermilliod et al. (1997) reported this as a double-lined binary, but lacked enough observations for an orbit. We now report an SB2 orbit with a period of 176 days. The parallax and p.m. information in the Gaia EDR3 catalog are somewhat different than the cluster mean, although evidence from a statistically significant excess astrometric noise and a large value of 2.797 for the RUWE parameter indicate the astrometric solution may have been affected. The rotation period measured by Rebull et al. (2016a,b) is consistent with membership. We retain it as a possible member.

**367. TRU S184x.** This is a non-member according to Gaia. It was observed 25 times with the CORAVEL by Rosvick et al. (1992), and although the measurements show considerable scatter, the authors were unable to decide whether it is a binary. The effective temperature and projected rotational velocity of the object are near the limit of the instrumental capabilities of northern CORAVEL. Our own observations show less scatter, but have not clarified the picture. Using only our TRES measurements, which have higher precision (except for the first, with an uncertainty twice as large as the others), we are able to obtain a marginally significant orbital solution with a period of about 6 yr and a semi-amplitude of only  $1.5 \text{ km s}^{-1}$ , which we consider too tentative to report. The apparent variability could simply be due to stellar activity.

**369. TRU S185.** The Gaia EDR3 catalog lists a companion at  $7''.4$  with similar parallax and p.m. as the target.

**372. TRU S194.** RVs along with a 10 yr SB1 orbit have been reported by Torres (2020) for this rapidly rotating B star. Our new effective temperature estimate is  $10500 \pm 300 \text{ K}$ .

**375. PELS 173.** Information from Gaia EDR3 indicates this is a non-member. Adding the CORAVEL observations to ours, there is a hint of an upward drift in the velocities. The median RV from Gaia is consistent with this.



## 2. GRAPHICAL REPRESENTATIONS OF THE BINARY ORBITAL SOLUTIONS AND LONG-TERM TRENDS

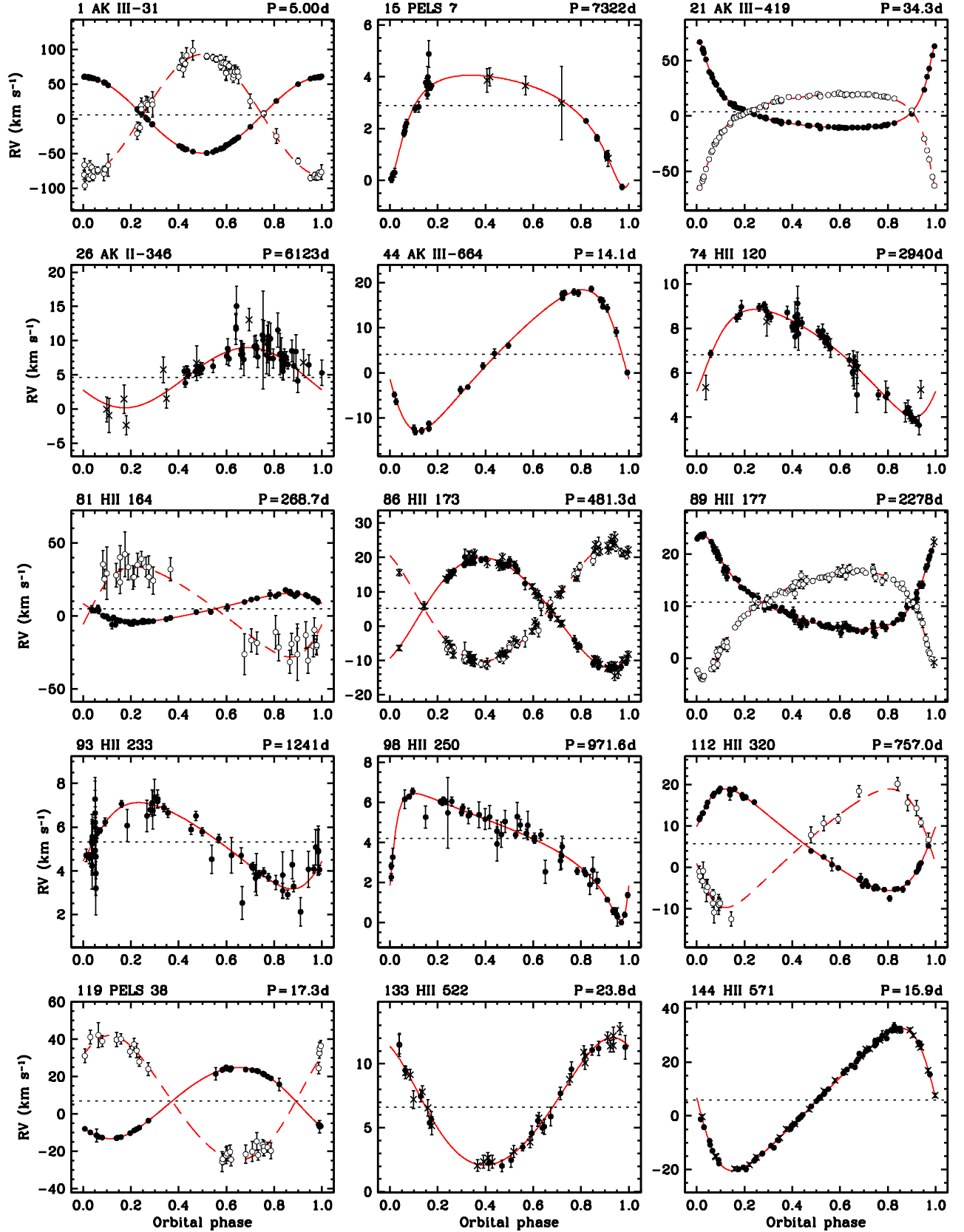


Figure 20. Plots of orbital solutions. Solid symbols are used for the primary velocities, open symbols for the secondary, and crosses for velocities from CORAVEL or other sources. The dotted line represents the center-of-mass velocity.

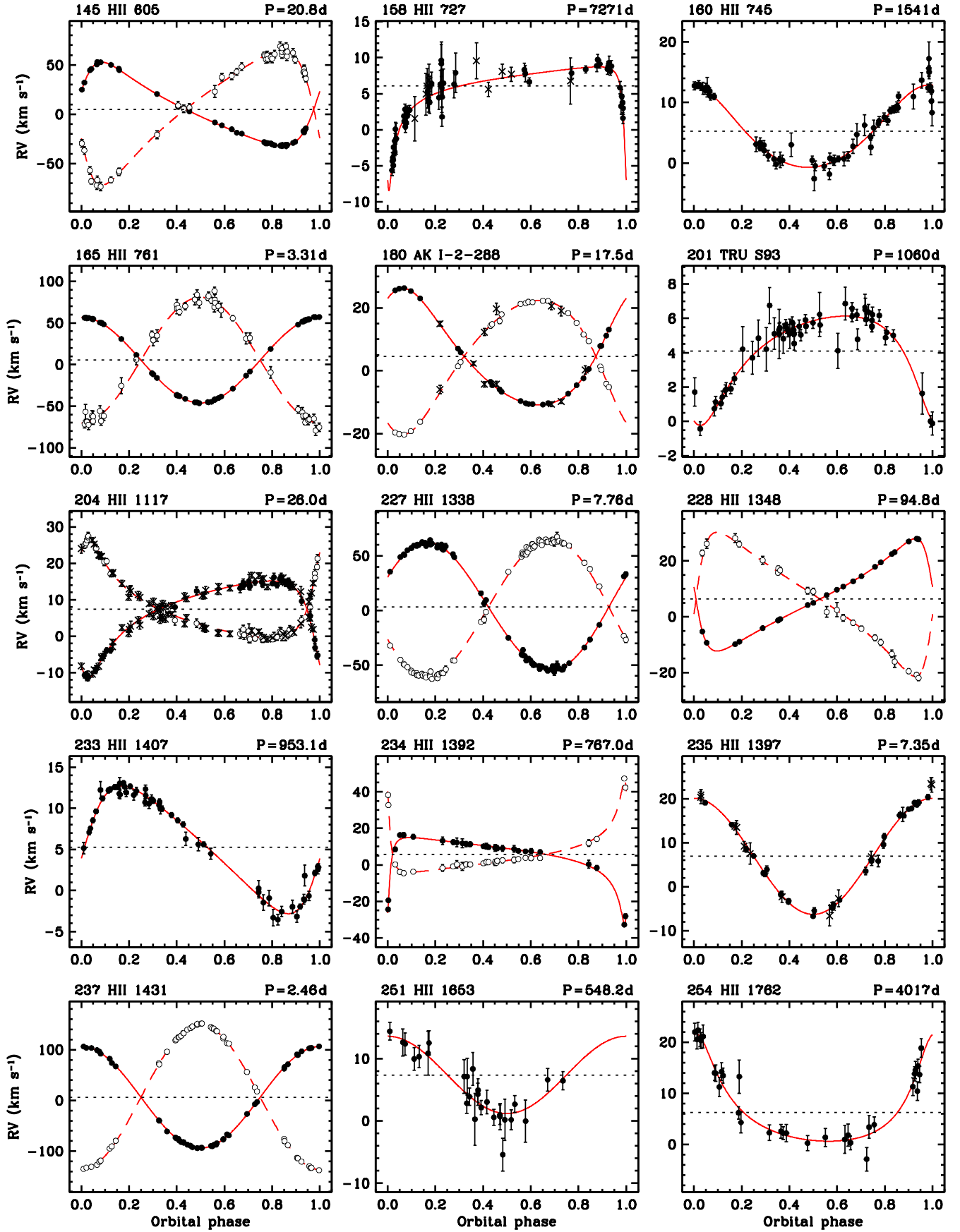


Figure 21. Plots of orbital solutions (continued).

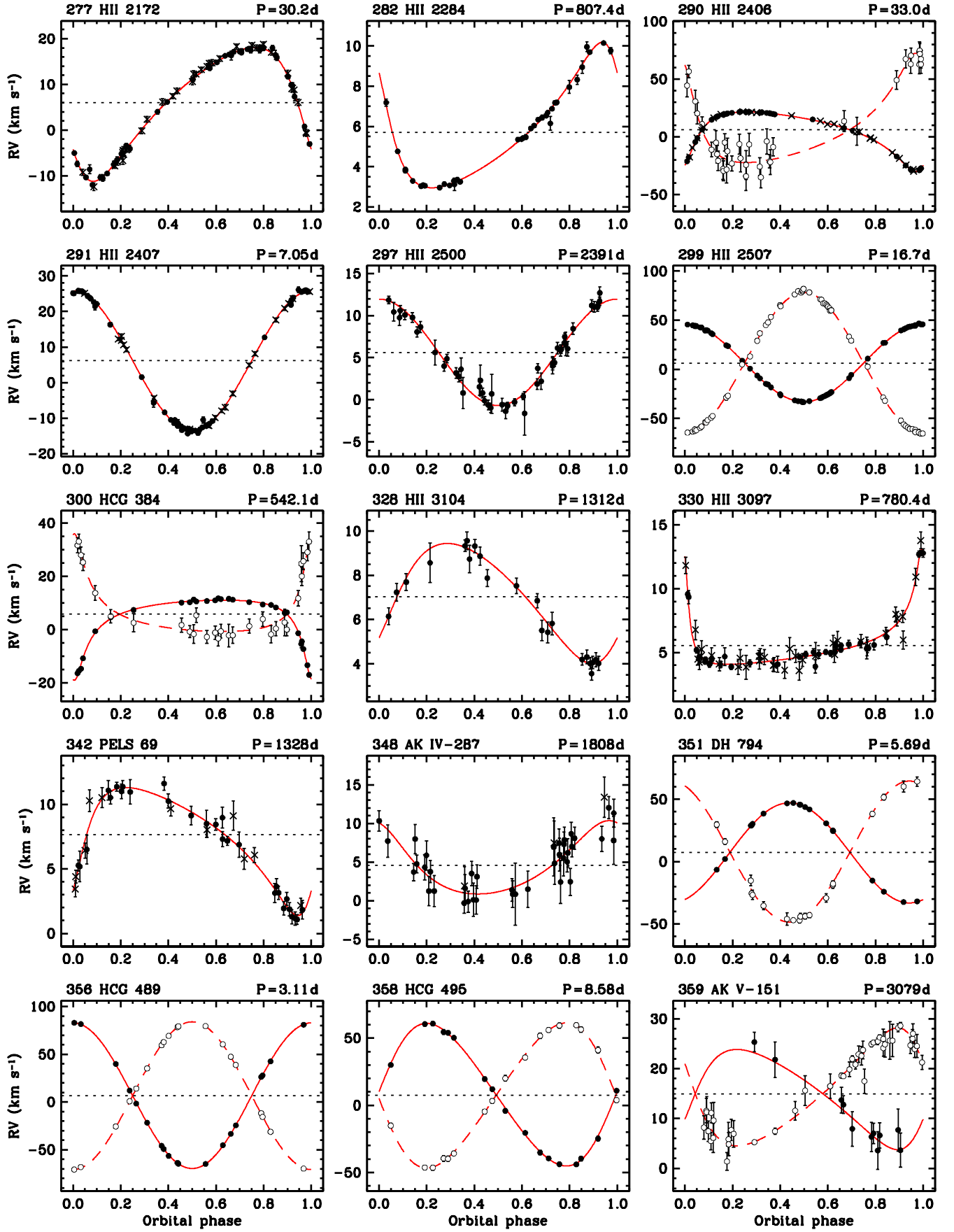


Figure 22. Plots of orbital solutions (continued).

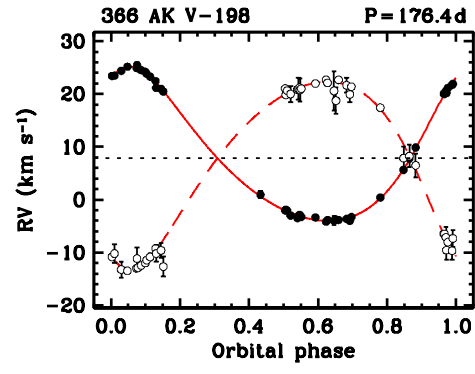


Figure 23. Plots of orbital solutions (continued).



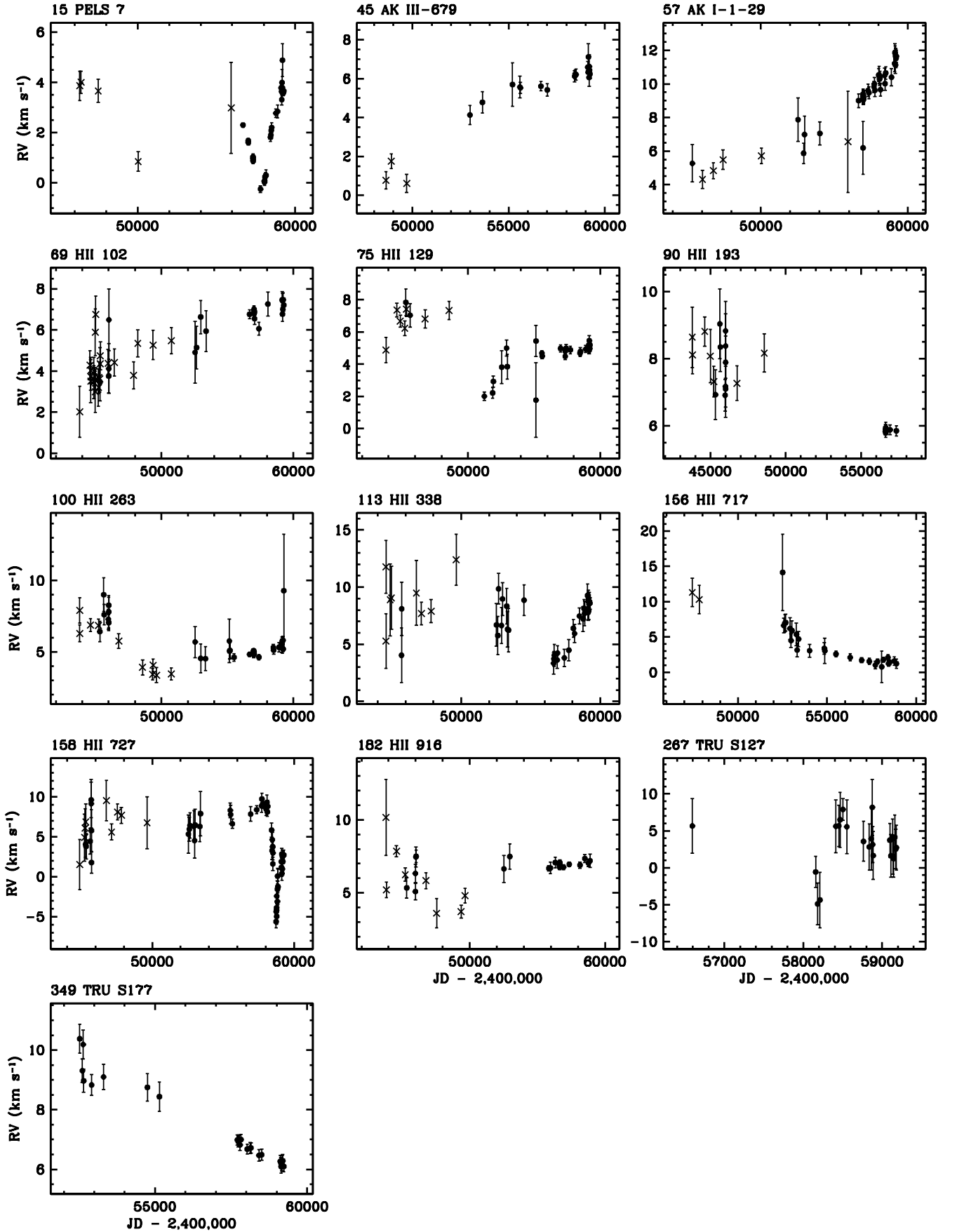


Figure 24. Plots for objects with long-term RV trends. Filled circles are used for CfA measurements, and crosses for velocities from CORAVEL or other sources..

## REFERENCES

- Abt, H. A. 1958, *ApJ*, 128, 139
- Abt, H. A. 1970, *ApJS*, 19, 387
- Abt, H. A., Barnes, R. C., Biggs, E. S., et al. 1965, *ApJ*, 142, 1604
- Abt, H. A., Levato, H., & Grosso, M. 2002, *ApJ*, 573, 359
- Adams, W. S. 1904, *ApJ*, 19, 338
- Adams, J. D., Stauffer, J. R., Monet, D. G., et al. 2001, *AJ*, 121, 2053
- Andersen, J. 1991, *A&A Rev.*, 3, 91
- Andersen, J. & Nordström, B. 1983, *A&A*, 122, 23
- Anderson, C. M., Stoeckly, R., & Kraft, R. P. 1966, *ApJ*, 143, 299
- Arenou, F., Luri, X., Babusiaux, C., et al. 2018, *A&A*, 616, A17
- Artyukhina, N. M. 1969, *Soviet Ast.*, 12, 987
- Baranne, A., Mayor, M., & Poncet, J. L. 1979, *Vistas in Astron.* 23, 279
- Baranne, A., Queloz, D., Mayor, M., et al. 1996, *A&AS*, 119, 373
- Barrado y Navascués, D., Stauffer, J. R., & Randich, S. 1998, *ApJ*, 506, 347
- Basri, G. & Martín, E. L. 1999, *AJ*, 118, 2460
- Bate, M. R. & Bonnell, I. A. 1997, *MNRAS*, 285, 33
- Beardsley, W. R. 1969, *Publications of the Allegheny Observatory of the University of Pittsburgh*, 7, 91
- Belikov, A. N., Hirte, S., Meusinger, H., et al. 1998, *A&A*, 332, 575
- Benacquista, M. J. & Downing, J. M. B. 2013, *Living Reviews in Relativity*, 16, 4
- Bodenheimer, P., Ruzmajkina, T., & Mathieu, R. D. 1993, *Protostars and Planets III*, 367
- Boffin, H. M. J. 2010, *A&A*, 524, A14
- Bouvier, J., Rigaut, F., & Nadeau, D. 1997, *A&A*, 323, 139
- Breger, M. 1986, *ApJ*, 309, 311
- Buchhave, L. A., Latham, D. W., Johansen, A., et al. 2012, *Nature*, 486, 375
- Bouy, H., Bertin, E., Sarro, L. M., et al. 2015, *A&A*, 577, A148
- Campbell, W. W., & Moore, J. H. 1928, *Publications of Lick Observatory*, 16, 1
- Cardelli, J. A., Clayton, G. C., & Mathis, J. S. 1989, *ApJ*, 345, 245
- Carquillat, J.-M. & Prieur, J.-L. 2007, *MNRAS*, 380, 1064
- Chen, Y., Girardi, L., Bressan, A., et al. 2014, *MNRAS*, 444, 2525
- Chini, R., Hoffmeister, V. H., Nasser, A. et al. 2012, *MNRAS*, 424, 1925
- Clarke, C. J. 2001, in *IAU Symposium No. 200, The Formation of Binary Stars*, eds. H. Zinnecker & R. D. Mathieu (San Francisco, CA: ASP), 346
- Conti, P. S. 1968, *AJ*, 73, 348
- Converse, J. M. & Stahler, S. W. 2008, *ApJ*, 678, 431
- Curé, M., Rial, D. F., Cassetti, J., et al. 2015, *A&A*, 573, A86
- Cutri, R. M., Skrutskie, M. F., van Dyk, S., et al. 2003, *The IRSA 2MASS All-Sky Point Source Catalog*, NASA/IPAC Infrared Science Archive, <http://irsa.ipac.caltech.edu/applications/Gator>
- Danilov, V. M. & Seleznev, A. F. 2020, *Astrophysical Bulletin*, 75, 407
- David, T. J., Conroy, K. E., Hillenbrand, L. A., et al. 2016, *AJ*, 151, 112
- David, T. J., Stauffer, J., Hillenbrand, L. A., et al. 2015, *ApJ*, 814, 62
- Deacon, N. R. & Kraus, A. L. 2020, *MNRAS*, 496, 5176
- Duchêne, G., & Kraus, A. 2013, *ARA&A*, 51, 269
- Duquenois, A. & Mayor, M. 1991, *A&A*, 500, 337
- ESA 1997, *The Hipparcos and Tycho Catalogues*, Vol. 1200 (Noordwijk:ESA)
- Fabrigius, C., Luri, X., Arenou, F., et al. 2020, *arXiv:2012.06242*
- Frémat, Y., Zorec, J., Hubert, A.-M., et al. 2005, *A&A*, 440, 305
- Frost, E. B., Barrett, S. B., & Struve, O. 1926, *ApJ*, 64, 1
- Fűrész, G. 2008, PhD thesis, Univ. Szeged, Hungary
- Gaia Collaboration, Brown, A. G. A., Vallenari, A. et al. 2018a, *A&A*, 616, 1
- Gaia Collaboration, Babusiaux, C., van Leeuwen, F., Barstow, M. A. et al. 2018b, *A&A*, 616, A10
- Gaia Collaboration, Prusti, T., de Bruijne, J. H. J. et al. 2016, *A&A*, 595, A1
- Gaia Collaboration, van Leeuwen, F., Vallenari, A., et al. 2017, *A&A*, 601, A19
- Galli, P. A. B., Moraux, E., Bouy, H., et al. 2017, *A&A*, 598, A48
- Gao, X.-h., 2019, *PASP*, 131, 044101
- Geißler, K., Metchev, S. A., Pham, A., et al. 2012, *ApJ*, 746, 44
- Geller, A. M., Latham, D. W., & Mathieu, R. D. 2015, *AJ*, 150, 97
- Geller, A. M. & Mathieu, R. D. 2012, *AJ*, 144, 54
- Geller, A. M., Mathieu, R. D., Latham, D. W. et al. 2021, *ApJ*, in press (arXiv:2101.07883)
- Głębocki, R., & Gnaniński, P. 2005, in *ESA SP-560, 13th Cambridge Workshop on Cool Stars, Stellar Systems and the Sun*, ed. F. Favata, G. A. J. Hussain & B. Battrock (Noordwijk, Netherlands: ESA), 571
- Goldberg, D. & Mazeh, T. 1994, *A&A*, 282, 801
- Goldberg, D., Mazeh, T., & Latham, D. W. 2003, *ApJ*, 591, 397
- Goldberg, D., Mazeh, T., Latham, D. W., et al. 2002, *AJ*, 124, 1132
- Gray, R. O., & Corbally, C. J. 1994, *AJ*, 107, 742
- Groenewegen, M. A. T., Decin, L., Salaris, M., et al. 2007, *A&A*, 463, 579
- Guerrero, C. A., Rosales-Ortega, F. F., Escobedo, G., et al. 2020, *MNRAS*, 495, 806
- Halbwachs, J. L., Mayor, M., Udry, S., et al. 2003, *A&A*, 397, 159
- Haro, G., Chavira, E., & Gonzalez, G. 1982, *Boletín del Instituto de Tonantzintla*, 3, 3
- Hartkopf, W. I., McAlister, H. A., & Mason, B. D. 2001, *AJ*, 122, 3480
- Hartmann, J. 1914, *Astronomische Nachrichten*, 199, 305
- Heacox, W. D. 1995, *AJ*, 109, 2670
- Hertzsprung, E. 1947, *Annalen van de Sterrewacht te Leiden*, 19, A1
- Hillenbrand, L. A., Zhang, C., Riddle, R. L., et al. 2018, *AJ*, 155, 51
- Høg, E., Fabricius, C., Makarov, V. V., et al. 2000, *A&A*, 355, L27
- Hole, K. T., Geller, A. M., Mathieu, R. D., et al. 2009, *AJ*, 138, 159
- Hube, D. P. 1970, *MmRAS*, 72, 233
- Hut, P., McMillan, S., Goodman, J., et al. 1992, *PASP*, 104, 981
- Jarad, M. M., Hilditch, R. W., & Skillen, I. 1989, *MNRAS*, 238, 1085
- Jones, B. F. 1970, *AJ*, 75, 563
- Jones, B. F. 1981, *AJ*, 86, 290
- Jung, J. 1914, *Astronomische Mitteilungen der Universitaets-Sternwarte zu Goettingen*, 17, 1
- Kähler, H. 1999, *A&A*, 346, 67
- Kahraman Aliçavuş, F., Niemczura, E., De Cat, P., et al. 2016, *MNRAS*, 458, 2307
- Kamai, B. L., Vrba, F. J., Stauffer, J. R., et al. 2014, *AJ*, 148, 30
- Katahira, J.-I., Hirata, R., Ito, M., et al. 1996, *PASJ*, 48, 317
- Kervella, P., Arenou, F., Mignard, F., et al. 2019, *A&A*, 623, A72
- Kochukhov, O., Makaganiuk, V., & Piskunov, N. 2010, *A&A*, 524, A5
- Konishi, M., Matsuo, T., Yamamoto, K., et al. 2016, *PASJ*, 68, 92
- Kounkel, M., Covey, K., Moe, M., et al. 2019, *AJ*, 157, 196
- Kunder, A., Kordopatis, G., Steinmetz, M., et al. 2017, *AJ*, 153, 75
- Kurtz, M. J. & Mink, D. J. 1998, *PASP*, 110, 934
- Latham, D. W. 1985, in *Proc. IAU Coll. 88, Stellar Radial Velocities*, ed. A. G. Philip & D. W. Latham (Schenectady, NY: L. Davis Press), 21
- Latham, D. W. 1992a, in *ASP Conf. Ser. 32, IAU Coll. 135, Complementary Approaches to Double and Multiple Star Research*, ed. H. A. McAlister & W. I. Hartkopf (San Francisco, CA: ASP), 110
- Latham, D. W., Mathieu, R. D., Milone, A. A. E., et al. 1992b, in *ASP Conf. Ser. 32, IAU Colloq. 135, Complementary Approaches to Double and Multiple Star Research*, ed. H. A. McAlister and W. I. Hartkopf (San Francisco, CA: ASP), 152
- Latham, D. W., Nordstroem, B., Andersen, J., et al. 1996, *A&A*, 314, 864
- Latham, D. W., Stefanik, R. P., Torres, G., et al. 2002, *AJ*, 124, 1144
- Leiner, E. M., Mathieu, R. D., Gosnell, N. M., et al. 2015, *AJ*, 150, 10
- Lindgren, L., 2018, Re-normalising the astrometric chi-square in Gaia DR2, [https://dms.cosmos.esa.int/COSMOS/doc\\_fetch.php?id=3757412](https://dms.cosmos.esa.int/COSMOS/doc_fetch.php?id=3757412)
- Liu, T., Janes, K. A., & Bania, T. M. 1991, *ApJ*, 377, 141
- Loader, B., Asada, Y., Bradshaw, J. et al. 2012, *JDSO*, 8, 313

- Lucy, L. B. & Ricco, E. 1979, *AJ*, 84, 401
- Luthardt, R. & Menchenkova, E. V. 1994, *A&A*, 284, 118
- Madsen, S., Dravins, D., & Lindegren, L. 2002, *A&A*, 381, 446
- Makarov, V. V., & Kaplan, G. H. 2005, *AJ*, 129, 2420
- Makarov, V. V., & Robichon, N. 2001, *A&A*, 368, 873
- Malkov, O. Y., Tamazian, V. S., Docobo, J. A., et al. 2012, *A&A*, 546, A69
- Margheim, S. J. 2007, PhD thesis, Indiana Univ.
- Mason, B. D., Hartkopf, W. I., Gies, D. R., et al. 2009, *AJ*, 137, 3358
- Mason, B. D., Hartkopf, W. I., McAlister, H. A., et al. 1993, *AJ*, 106, 637
- Mason, B. D., Wycoff, G. L., Hartkopf, W. I., et al. 2001, *AJ*, 122, 3466
- Mathieu, R. D. 1985, in *IAU Symp. 113, Dynamics of Star Clusters*, eds. J. Goodman & P. Hut (Dordrecht, The Netherlands: Reidel), 113, 427
- Mathieu, R. D. & Mazeh, T. 1988, *ApJ*, 326, 256
- Mathieu, R. D., Meibom, S., & Dolan, C. J. 2004, *ApJ*, 602, L121
- Mathews, L. D. & Mathieu, R. D. 1992, in *ASP Conf. Ser. 32, IAU Colloq. 135, Complementary Approaches to Double and Multiple Star Research*, ed. H. A. McAlister and W. I. Hartkopf (San Francisco, CA: ASP), 244
- Mayor, M. & Maurice, E. 1985, in *IAU Coll. 88, Stellar Radial Velocities*, ed. A. G. D. Philip & D. W. Latham (Philadelphia, PA: Davis Press), 299
- Mazeh, T. 2008, *EAS Publications Series*, 29, 1
- Mazeh, T. 1990, *AJ*, 99, 675
- Mazeh, T. & Goldberg, D. 1992, *ApJ*, 394, 592
- Mazeh, T., Simon, M., Prato, L., et al. 2003, *ApJ*, 599, 1344
- McGraw, J. T., Dunham, D. W., Evans, D. S. et al. 1974, *AJ*, 79, 1299
- McNamara, B. J. & Sekiguchi, K. 1986, *ApJ*, 310, 613
- Melo, C. H. F., Covino, E., Alcalá, J. M., et al. 2001, *A&A*, 378, 898
- Meibom, S. & Mathieu, R. D. 2005, *ApJ*, 620, 970
- Melis, C., Reid, M. J., Mioduszewski, A. J., et al. 2014, *Science*, 345, 1029
- Mermilliod, J.-C., Bratschi, P., & Mayor, M. 1997, *A&A*, 320, 74
- Mermilliod, J.-C. & Mayor, M. 1992b, in *Binaries as Tracers of Star Formation*, ed. A. Duquennoy & M. Mayor (Cambridge, UK: Cambridge Univ. Press), 183
- Mermilliod, J.-C., Mayor, M., & Udry, S. 2009, *A&A*, 498, 949
- Mermilliod, J.-C., Platais, I., James, D. J., et al. 2008, *A&A*, 485, 95
- Mermilliod, J.-C., Rosvick, J. M., Duquennoy, A., et al. 1992a, *A&A*, 265, 513
- Meunier, N., Mignon, L., & Lagrange, A.-M. 2017, *A&A*, 607, A124
- Miles, R. 1999, *Journal of the British Astronomical Association*, 109, 106
- Milliman, K. E., Mathieu, R. D., Geller, A. M., et al. 2014, *AJ*, 148, 38
- Moe, M., & Di Stefano, R. 2017, *ApJS*, 230, 15
- Morse, J. A., Mathieu, R. D., & Levine, S. E. 1991, *AJ*, 101, 1495
- Munari, U., Dallaporta, S., Siviero, A., et al. 2004, *A&A*, 418, L31
- Nemravová, J., Harmanec, P., Kubát, J., et al. 2010, *A&A*, 516, A80
- Netopil, M., Paunzen, E., Heiter, U., et al. 2016, *A&A*, 585, A150
- Nine, A. C., Milliman, K. E., Mathieu, R. D., et al. 2020, *AJ*, 160, 169
- Nordström, B., Latham, D. W., Morse, J. A., et al. 1994, *A&A*, 287, 338
- Ochsenbein, F., Bauer, P., & Marcout, J. 2000, *A&AS*, 143, 23
- Oelkers, R. J., Rodriguez, J. E., Stassun, K. G., et al. 2018, *AJ*, 155, 39
- Olivares, J., Sarro, L. M., Moraux, E., et al. 2018, *VizieR Online Data Catalog*, J/A+A/617/A15
- Pearce, J. A., 1958, *PDAO*, 10, 435
- Pearce, J. A., & Hill, G. 1971, *PASP*, 83, 493
- Pearce, J. A., & Hill, G. 1975, *PDAO*, 14, 319
- Pickering, E. C. 1896, *ApJ*, 4, 370
- Pinfield, D. J., Jameson, R. F., & Hodgkin, S. T. 1998, *MNRAS*, 299, 955
- Popović, G. M. & Pavlović, R. 1995, *Bulletin Astronomique de Belgrade*, 151, 45
- Prosser, C. F. & Stauffer, J. R. 1993, *Information Bulletin on Variable Stars*, 3826, 1
- Prosser, C. F., Stauffer, J., & Kraft, R. P. 1991, *AJ*, 101, 1361
- Qian, B.-C. & Fan, Q.-Y. 1991, *Acta Astronomica Sinica*, 15, 336
- Queloz, D., Allain, S., Mermilliod, J.-C., et al. 1998, *A&A*, 335, 183
- Raboud, D., & Mermilliod, J.-C. 1998, *A&A*, 329, 101
- Raghavan, D., McAlister, H. A., Henry, T. J., et al. 2010, *ApJS*, 190, 1
- Rebull, L. M., Stauffer, J. R., Bouvier, J., et al. 2016a, *AJ*, 152, 114
- Rebull, L. M., Stauffer, J. R., Bouvier, J., et al. 2016b, *AJ*, 152, 113
- Richichi, A., Calamai, G., & Leinert, Ch. 1994, *A&A*, 286, 829
- Richichi, A., Calamai, G., Leinert, Ch. et al. 1996, *A&A*, 309, 163
- Richichi, A., Calamai, G., & Stecklun, B. 2002, *A&A*, 382, 178
- Richichi, A., Chen, W. P., Cusano, F., et al. 2012, *A&A*, 541, A96
- Rosvick, J. M., Mermilliod, J.-C., & Mayor, M. 1992, *A&A*, 255, 130
- Rodríguez, E., López-González, M. J., & López de Coca, P. 2000, *A&AS*, 144, 469
- Rodriguez, D. R., Marois, C., Zuckerman, B., et al. 2012, *ApJ*, 748, 30
- Royer, F., Grenier, S., Baylac, M.-O., et al. 2002, *A&A*, 393, 897
- Sampedro, L., Dias, W. S., Alfaro, E. J., et al. 2017, *MNRAS*, 470, 3937
- Schaefer, G. H., Prato, L., Simon, M., et al. 2014, *AJ*, 147, 157
- Schilbach, E., Robichon, N., Souchay, J., et al. 1995, *A&A*, 299, 696
- Schuler, S. C., Plunkett, A. L., King, J. R., & Pinsonneault, M. H. 2010, *PASP*, 122, 76
- Shahaf, S., Mazeh, T., & Faigler, S. 2017, *MNRAS*, 472, 4497
- Simón-Díaz, S., Godart, M., Castro, N., et al. 2017, *A&A*, 597, A22
- Smith, B., & Struve, O. 1944, *ApJ*, 100, 360
- Soderblom, D. R., Laskar, T., Valenti, J. A., et al. 2009, *AJ*, 138, 1292
- Soderblom, D. R., Stauffer, J. R., Hudon, J. D., et al. 1993, *ApJS*, 85, 315
- Southworth, J., Maxted, P. F. L., & Smalley, B. 2005, *A&A*, 429, 645
- Stauffer, J., Hartmann, L. W., Fazio, G. G. et al. 2007, *ApJS*, 172, 663
- Stauffer, J., Klemola, A., Prosser, C., & Probst, R. 1991, *AJ*, 101, 980
- Stefanik, R. P., Latham, D. W., & Torres, G. 1999, in *ASP Conf. Ser. 185, IAU Coll. 170, Precise Stellar Radial Velocities*, ed. J. B. Hearnshaw & C. D. Scarfe (San Francisco, CA: ASP), 354
- Szentgyorgyi, A. H., & Fűrész, G. 2007, *RMxAC*, 28, 129
- Taylor, B. J. 2008, *AJ*, 136, 1388
- Torres, G. 2003, *Information Bulletin on Variable Stars*, 5402, 1
- Torres, G., Andersen, J., & Giménez, A. 2010, *A&A Rev.*, 18, 67
- Torres, G. 2020, *ApJ*, 901, 91
- Torres, G., Melis, C., Kraus, A. L., et al. 2020, *ApJ*, 898, 2
- Torres, G., Neuhäuser, R., & Guenther, E. W. 2002, *AJ*, 123, 1701
- Torres, G., Stefanik, R. P., Andersen, J., et al. 1997, *AJ*, 114, 2764
- Trumpler, R. J. 1921, *Lick Observatory Bulletin*, 333, 110
- Udry, S., Mayor, M., & Queloz, D. 1999, in *ASP Conf. Ser. 185, IAU Coll. 170, Precise Stellar Radial Velocities*, ed. J. B. Hearnshaw & C. D. Scarfe (San Francisco, CA: ASP), 367
- Uesugi, A., & Fukuda, I. 1970, *Catalogue of rotational velocities of the stars*, *Contr. Astroph. Kwasan Obs., Univ. Kyoto*, 189
- van Belle, G. T. 2012, *A&A Rev.*, 20, 51
- Van De Kamp, P. 1981, *Stellar Paths. Photographic astrometry with long-focus instruments*, *Astrophysics and Space Science Library*, Vol. 85, (Dordrecht: Reidel), p. 82
- van Leeuwen, F., Alphenaar, P., & Brand, J. 1986, *A&AS*, 65, 309
- Verbunt, F. & Phinney, E. S. 1995, *A&A*, 296, 709
- White, R. J., Gabor, J. M., & Hillenbrand, L. A. 2007, *AJ*, 133, 2524
- Yamamoto, K., Matsuo, T., Shibai, H., et al. 2013, *PASJ*, 65, 90
- Yudin, R. V. 2001, *A&A*, 368, 912
- Zahn, J.-P. 1975, *A&A*, 41, 329
- Zorec, J., & Royer, F. 2012, *A&A*, 537, A120
- Zorec, J., Frémat, Y., Domiciano de Souza, A., et al. 2016, *A&A*, 595, A132
- Zucker, S., & Mazeh, T. 1994, *ApJ*, 420, 806

Zucker, S., Torres, G., & Mazeh, T. 1995, ApJ, 452, 863

Zwahlen, N., North, P., Debernardi, Y., et al. 2004, A&A, 425,  
L45